Medizinische Fakultät
der
Universität Duisburg-Essen

Aus dem Institut für Transfusionsmedizin

Cell cycle-dependent gene expression by Mybl2 - a tumor suppressor in MDS

I n a u g u r a l - D i s s e r t a t i o n
zur
Erlangung des Doktorgrades der Medizin
durch die Medizinische Fakultät
der Universität Duisburg-Essen

Vorgelegt von
Julia Severmann
aus Ahlen (Westf.)
1991

Dekan: Herr Univ.-Prof. Dr. med. J. Buer

1. Gutachter: Herr Univ.-Prof. Dr. med. P. Horn

2. Gutachter: Herr Priv.-Doz. Dr. med. A. Röth

3. Gutachter: Herr Univ.-Prof. Dr. med. W. Schmiegel, Bochum

Tag der mündlichen Prüfung: 3. Mai 2018

Publikationen:

Ein Teil der Ergebnisse dieser Arbeit wurde als Poster oder Vortrag auf Kongressen veröffentlicht und mit Preisen ausgezeichnet.

Julia Severmann, Peter A. Horn and Stefan Heinrichs (2015): Cell cycle-dependent gene expression by Mybl2, a tumor suppressor in MDS. *Abstract und Postervorstellung auf dem 8th International Meeting of the Stem Cell Network NRW in Bonn. Der Beitrag wurde mit einem Posterpreis ausgezeichnet.*

Julia Severmann, Peter A. Horn and Stefan Heinrichs (2015): Cell cycle-dependent gene expression by Mybl2, a tumor suppressor in MDS. *Abstract und Konferenzvortrag auf der Essen Conference for Hematology and Oncology in Essen. Der Vortrag wurde mit dem "1st Oral Presentation Award" ausgezeichnet.*

Abstract und Postervorstellung auf dem Forschungstag der Medizinischen Fakultät der Universität Duisburg Essen in den Jahren 2013 und 2014.

Table of content

1. Introduction

1.1 Myelodysplastic syndromes

Myelodysplastic syndromes (MDS) are a heterogeneous group of clonal bone marrow diseases originating from a malignant transformation of multipotent hematopoietic stem or progenitor cells (HSPCs). They are characterized by an impaired hematopoiesis leading to peripheral blood cytopenia and morphologic dysplasia of hematopoietic cells. Of note, patients suffering from MDS have a high risk of disease transformation to acute myeloid leukemia (AML) (Arber et al., 2016; Vardiman et al., 2009).

1.1.1 Epidemiology

MDS are a common hematologic malignant disease, especially in the elderly with a median age at diagnosis of 71 - 76 years (Ma et al., 2007). Considering all ages, in Germany the incidence of MDS is about 4 cases per 100,000 persons per year with a prevalence of 7 in 100,000 (Neukirchen et al., 2011). The incidence increases rapidly with advancing age, reaching more than 15 - 50 cases per 100,000 in the age group older than 70 years (Aul et al., 2001). New data estimate the incidence of MDS in the United States between 5.3 and 13.1 cases per 100,000, reaching between 75 and 162 cases per 100,000 in the age group above 65 years (Cogle, 2015). The incidence and prevalence is higher among men than women (Aul et al., 2001; Neukirchen et al., 2011). Most likely, the incidence of MDS will rise further due to the increasing life expectancy, a greater awareness of MDS among physicians, and longer survival of patients with other neoplasms after initial treatment placing them at risk for therapy-related MDS (Corey et al., 2007; Greenberg et al., 2012; Sperling et al., 2016). Very rarely, pediatric patients are affected, most often in association with inherited familial syndromes predisposing to MDS and AML, e.g. Fanconi anemia, familial platelet disorder with propensity to myeloid malignancy, Shwachman-Diamond syndrome, dyskeratosis congenita or severe congenital neutropenia (Corey et al., 2007; Liew and Owen, 2011).

1.1.2 Pathogenesis and clinical presentation

In the pathogenesis of MDS recurrent initiating mutations in HSPCs give rise to myelodysplastic stem cells (MSCs). MSCs possess increased self-renewal leading to clonal expansion and dominance over normal hematopoietic stem cells (HSCs). The acquisition of further cooperating mutations leads to an impairment of terminal maturation resulting in an aberrant differentiation process and morphological abnormalities of the myeloid hematopoietic cells in the bone marrow, two key characteristics of MDS. Consequently, despite an often hyper- or normocellular bone marrow, increased apoptosis

of differentiating cells results in an ineffective hematopoiesis with peripheral blood cytopenia. Unaffected HSCs can only partially compensate this dysfunction. Thus, MDS patients suffer from cytopenia of one or more myeloid lineages. They often present with clinical symptoms related to their peripheral cytopenia. For instance, anemia can result in symptoms such as fatigue, weakness or angina. Recurrent infections originate from neutropenia, while a history of bleeding is common when suffering from thrombocytopenia (Corey et al., 2007; Sperling et al., 2016). The peripheral cytopenia can progressively worsen during the course of the disease due to the mutation-driven evolution of the MSCs. For the individual patient, symptoms strongly depend on the types of mutations and the affected myeloid lineages as well as the speed of disease progression (Corey et al., 2007).

1.1.3 Diagnosis and classification

Patients can develop MDS either *de novo* (primary MDS) or therapy-related to potentially mutagenic therapy, such as chemo- or radiotherapy (tMDS/secondary MDS), then often showing a shorter time to leukemic transformation (Corey et al., 2007). According to the World Health Organization (WHO), the diagnosis of MDS requires three main criteria: otherwise unexplained cytopenia in one or more myeloid lineages, significant morphologic dysplasia and a blast count below 20 % of the total nucleated cells in the peripheral blood and bone marrow (Arber et al., 2016). MDS has to be carefully distinguished from differential diagnosis that may present with cytopenia and/or dysplasia, for instance megaloblastic anemia, aplastic anemia, MDS/MPN overlap syndromes, and AML. AML can also develop *de novo* or on top of a pre-existing hematologic disease, then termed secondary AML (sAML), showing a poor therapy response and a worse prognosis. MDS and sAML lie along a disease continuum and are mainly separated by the blast count. Currently, cases with blast counts above 20 % are defined as AML (WHO classification 2008 and 2016). The transformation from MDS to secondary AML is caused by clonal evolution of MSCs by accumulation of additional genetic lesions (Sperling et al., 2016). This development is encountered in about 30 % of MDS patients and severely worsens their prognosis (Greenberg et al., 2012).

Two prominent classification systems are used to determine the sub-types of MDS: the French-American-British (FAB) system, using cytomorphological abnormalities and blast percentage (Bennett et al., 1982), and the WHO classification of myeloid neoplasms and acute leukemia (Arber et al., 2016). The latter includes important decision criteria such as signs of dysplasia and cytopenia, blast proliferation as well as presence of a deletion of the long arm of chromosome 5 (Germing et al., 2013). MDS with an isolated

deletion of 5q is a separate entity in the WHO classification, termed the “5q - Syndrome”. It was first described in 1974 with distinct morphologic features and a rather favorable prognosis (Van den Berghe et al., 1974). The revised WHO classification from 2016 introduces refinements to morphologic criteria and cytopenia assessments. Also, it addresses newly described genetic information in MDS diagnosis and classification (Arber et al., 2016). In addition, the international prognostic scoring system (IPSS) (Greenberg et al., 1997) and the recently revised version (IPSS-R) (Greenberg et al., 2012) are widely used for estimation of survival and risk stratification of progression to AML. In the IPSS-R a prognostic score ranging from ≤ 1.5 to > 6 is defined according to the cytogenetic risk group, blast percentage in the bone marrow, and depth of cytopenia. The prognostic score stratifies patients into five different risk groups: very low, low, intermediate, high and very high risk. The median survival times range from 8.8 years (very low risk) to 0.8 years (very high risk), and the time for progression to sAML for 25 % of the patients from not reached (very low risk) to 0.73 years (very high risk) (Greenberg et al., 2012). The discoveries of recurrently mutated genes in MDS refine prognostic and diagnostic approaches, thus, many medical centers include detailed genetic analysis in their diagnostics to optimize their treatment according to the individual patient (Gangat et al., 2016). Recently, large scale sequencing studies have revealed that even asymptomatic individuals with a normal blood cell count have somatic mutations in MDS-associated genes, leading to a predisposition for myeloid malignancies such as MDS, AML or other myeloid neoplasms. This disease state has been termed clonal hematopoiesis of indeterminate potential (CHIP). It seems comparable to other known clonal pre-malignant disorders such as the monoclonal gammopathy of undetermined significance (MGUS) with a risk of progression to multiple myeloma. The annual risk for disease progression in the presence of CHIP is low at 0.5 to 1 %. Patients can present with cytopenia or without any symptoms at all, but they are lacking the morphological criteria for MDS. To date, the significance of screening patients for CHIP in order to prevent a possible disease progression remains to be determined in further research (Sperling et al., 2016; Steensma et al., 2015).

1.1.4 Therapy

Treatment options for MDS patients are risk-adapted and vary according to the clinical problems and the severity of the disease. Low risk patients are observed until symptoms appear, followed by best supportive care, treating the leading complaints to maintain a good quality of life. This includes blood transfusions, anti-infective therapy and stimulation with hematopoietic growth factors. Also, two approved drugs for MDS treatment, azacitidine and decitabine, both hypomethylating agents, and enrollment in clinical trials using novel drugs are treatment options, if clinical symptoms cannot be

controlled. MDS patients with an isolated 5q deletion benefit from a treatment with lenalidomide (List et al., 2006), a drug that targets the multifunctional protein cereblon (CRBN), an E3 ubiquitin ligase. Lenalidomide increases the CRBN affinity for casein kinase 1α (CK1α), resulting in degradation of CK1α. Cells with a 5q deletion have a lower level of CK1α than normal HSCs. Thus, the increased degradation by lenalidomide pushes CK1α below a certain level inducing cell death by a TP53-dependent mechanism. Consequently, TP53 mutations in 5q - Syndromes are an indicator for lenalidomide therapy resistance (Kronke et al., 2015). Patients with a higher risk MDS should be directly considered for high-dose chemotherapy followed by hematopoietic stem cell transplantation (HSCT) for long term remission. In fact, allogeneic HSCT is the only available cure for MDS. Unfortunately, due to the high age at diagnosis, associated co-morbidities and the risks of HSCT itself (e.g. infections, graft versus host disease, disease relapse), this treatment can only be offered to few (Gangat et al., 2016). Nevertheless, if low risk patients show progression to a higher risk group, e.g. by new cytogenetic lesions or severe symptom aggravation, a delayed transplantation approach should be considered. Another option for patients not eligible for HSCT is the enrollment in clinical trials using novel agents such as inhibitors of histone deacetylases (mocetinostat, pracinostat) or kinases (rigosertib, volasertib), rather than treatment with hypomethylating agents showing only limited survival benefit (Gangat et al., 2016).

1.2 Genetics in MDS

In contrast to the genomes of other neoplasms, the MDS genome is known to be karyotypically normal in about 50 % of all cases. However, chromosomal abnormalities have been detected in 50 % of *de novo* MDS cases using metaphase cytogenetic analysis (Haase et al., 2007; Schanz et al., 2012). More sensitive techniques such as single nucleotide polymorphism microarrays increased the sensitivity of detection of abnormalities up to 80 % (Heinrichs et al., 2009; Tiu et al., 2011). Notably, cytogenetic abnormalities in MDS are mostly deletions (Haase et al., 2007), suggesting a frequent deletion of tumor suppressor genes rather than oncogene activation. The most frequent recurrent isolated cytogenetic deletions in MDS involve deletions of chromosome 5q, 7q and 20q (Figure 1).

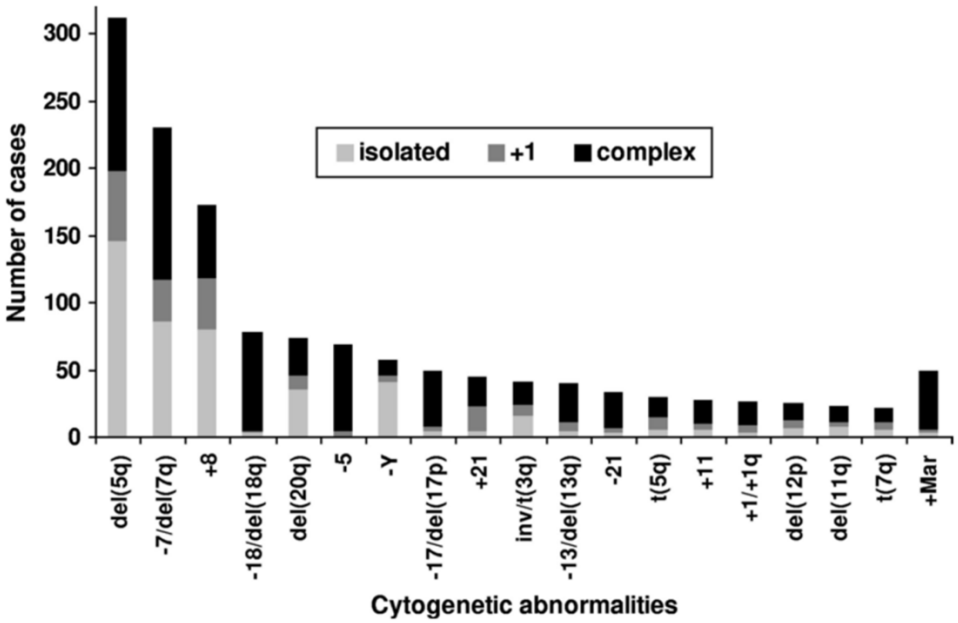

Figure 1: Recurrent cytogenetic abnormalities in MDS. Frequencies of most common cytogenetic aberrations in 1084 MDS cases with clonal cytogenetic abnormalities (52 %) from 2072 MDS cases in total, subdivided into isolated cases with only one anomaly, with one additional anomaly or as part of complex anomalies. *Figure taken from (Haase et al., 2007).*

Over the past ten years, technical and scientific advance such as next generation sequencing, has led to identification of new molecular abnormalities in MDS (Sperling et al., 2016). Recurrent somatic mutations have been identified in over 90 % of patients with MDS, including those with a normal karyotype. The most frequently mutated genes are involved in RNA splicing (SF3B1, SRSF2, U2AF1, ZRSR2) or epigenetic regulation of gene expression (TET2, ASXL1, EZH2, DNMT3A, IDH2). In addition, transcription factors such as RUNX1 or TP53 are among the most commonly mutated genes in MDS. Six particular genes - TET2, SF3B1, ASXL1, SRSF2, DNMT3A, and RUNX1 - are mutated with a frequency of more than 10 % (Figure 2). While many genes have been described to be recurrently mutated in MDS, most show a very low mutation frequency (<5 %, Figure 2) (Haferlach et al., 2014; Papaemmanuil et al., 2013).

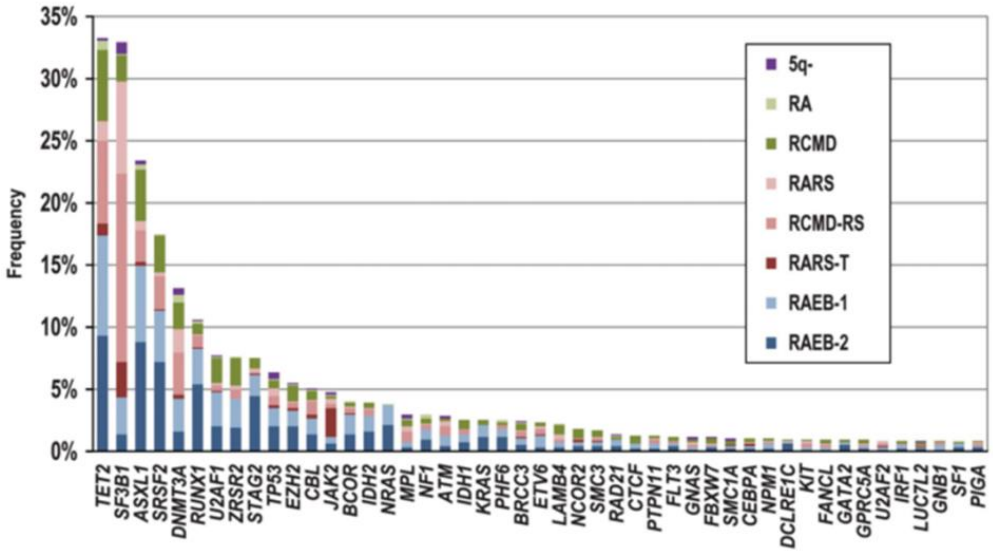

Figure 2: Significantly mutated genes in MDS. Frequency of mutations in recurrently mutated genes, colors indicating MDS subtype according to the WHO classification of 2008. *Figure taken form (Haferlach et al., 2014).*

Interestingly, many of these mutations dictate a specific morphological and clinical phenotype (Papaemmanuil et al., 2013). For instance, the SF3B1 mutation status has been shown to predict the presence of ringed sideroblasts in the bone marrow and is associated with a better overall survival (Malcovati et al., 2011). This finding has recently been included into the 2016 revision of the WHO classification of MDS (Arber et al., 2016). Of note, the described mutations do not occur in an isolated fashion; cells rather successively acquire mutations causing disease progression and potentially leukemic transformation. In this process, mutations in genes encoding for splicing factors, e.g. SF3B1 and SRSF2, and involved in DNA methylation, e.g. DNMT3A and TET2, occur very early, whereas mutations in genes for histone modification or signaling occur later (Papaemmanuil et al., 2013). Interestingly, the most common mutations in CHIP affect DNMT3A and TET2, as well. This might indicate, that some mutations primarily lead to CHIP and only after acquisition of additional mutations to MDS, while other initially acquired mutations, e.g. in splicing factor genes, directly cause morphologic dysplasia, and thus MDS onset (Sperling et al., 2016). The current understanding of cancer development suggests that patients with CHIP, showing recurrent MDS-associated mutations, represent the initial step of a continuous path of evolution of myeloid malignancies, depending on the time of occurrence and frequency of acquired cooperative mutations. Early mutations lead to a clonal advantage of malignant hematopoiesis, and further accumulation of mutations can lead to the development of dysplasia, low-risk and high-risk MDS, and eventually sAML. Consequently, the hierarchy, in which mutations

occur, might be useful to predict and monitor progression of the disease (Haferlach et al., 2014; Papaemmanuil et al., 2013; Sperling et al., 2016).

The combination of cytogenetic abnormalities and somatic mutations most likely causes the great clinicopathological heterogeneity of MDS (Lindsley and Ebert, 2013) represented in the great variety of clinical symptoms and genetic lesions. As a result, the number of genetic lesions - cytogenetic aberrations and somatic mutations - correlates strongly with the prognosis of the disease and the determination of the exact mutations of a patient could allow for more individualized treatment decisions (Haase et al., 2007; Haferlach et al., 2014; Papaemmanuil et al., 2013).

1.2.1 MDS with 20q deletion

Cytogenetic abnormalities in MDS are mostly deletions. The long arm of chromosome 20 contains a commonly deleted region (CDR) in myeloid malignancies, including 2 - 4 % of MDS cases (Figure 1) (Haase et al., 2007)). In MDS an isolated del(20q) is associated with fewer bone marrow blasts and a longer survival compared to other MDS patients (Braun et al., 2011; Schanz et al., 2012).

Certainly, the 20q CDR has been proposed to harbor at least one tumor suppressor gene, and efforts have been made to define the CDR and the candidate genes within (Bench et al., 2000). Interestingly, the 20q deletion has only been described as heterozygous without any evidence for a small deletion within the remaining region of the other chromosome and copy neutral loss-of heterozygosity have not been found (Heinrichs et al., 2009; Huh et al., 2010). In addition, a point mutation of genes on the remaining allele has never been reported. This implicates that the presence of a classical tumor suppressor requiring bi-allelic inactivation is very unlikely. Rather, a haploinsufficient tumor suppressor gene has been postulated for the del(20q) region that is essential for cell viability but has a strongly dose-dependent tumor suppressor function. Recently, the transcription factor MYBL2 was identified as such a gene-dosage dependent tumor suppressor gene in MDS, located within the 20q CDR (Heinrichs et al., 2013). Transcription factors are known to be frequently mutated in myeloid malignancies, including MDS. They are proposed to drive the dominance of the mutated clone by allowing for aberrant self-renewal and disruption of differentiation in hematopoietic cells (Lindsley and Ebert, 2013). Notably, MYBL2 was not only expressed at low levels in del(20q) MDS cases but also in MDS cases with a normal karyotype, suggesting additional mechanisms of reduction of MYBL2 expression levels (Heinrichs et al., 2013). Thus, the downregulation of MYBL2 expression appears to be a more common driver of MSCs and is not restricted to patients with 20q deletions. In this context, a competitive

bone marrow transplantation assay in mice showed that primary murine bone marrow cells with sub-haploinsufficient expression levels of Mybl2 (20 - 30 %) – mediated by RNA interference – became clonally dominant and the mice developed myeloid disorders. These findings implicate that low levels of MYBL2 gene expression are a central mechanism in development of clonal dominance in MDS (Heinrichs et al., 2013). This notion is supported by a second independent study showing that classical Mybl2 haploinsufficiency increased susceptibility to age-related hematopoietic disorders in mice (Clarke et al., 2013).

1.3 MYBL2

MYBL2 is a member of the highly conserved vertebrate Myb transcription factor family, comprising MYBL1 (A-MYB), MYBL2 (B-MYB) and MYB (C-MYB). MYBL2 is ubiquitously expressed in all proliferating cells (Nomura et al., 1988), while MYB and MYBL1 show rather tissue-specific expression patterns. For instance, the expression of MYB is mainly restricted to the small intestine and to hematopoietic progenitor cells, playing an important role in the blood cell development (Joaquin and Watson, 2003; Westin et al., 1982). Of note, MYB has oncogenic potential (Graf and Beug, 1978). MYBL1 is mainly expressed in mitotically active cells during embryogenesis, such as the developing central nervous system or spermatogenesis (Joaquin and Watson, 2003; Trauth et al., 1994).

MYBL2 is an essential gene, as bi-allelic inactivation was shown to cause early embryonic lethality in mice due to a block in the inner cell mass formation of the blastocyst (Tanaka et al., 1999). Further, it is long known to be indispensible for the cell cycle progression and therefore its transcription is regulated very tightly. MYBL2 expression is upregulated by an E2F-dependent mechanism in the late G1 phase with a peak during the S phase of the cell cycle (Lam et al., 1995; Lam et al., 1992), where it regulates the transcription of genes required for the G2/M phase transition. Specifically, MYBL2 and the MuvB-protein complex, encompassing LIN9, LIN37, LIN52, LIN54 and RBBP4, were found to target gene promoters upon recruitment of FOXM1 during the late S phase, and thus activate the transcription of G2/M phase genes (Sadasivam et al., 2012). In detail, the DREAM complex, comprising the Rb-like protein p130, E2F4, DP1 and the MuvB-protein complex, represses gene expression of early and late cell cycle genes in the G0 phase of the cell cycle (Litovchick et al., 2007). Among these genes is MYBL2. Upon cell cycle entry, the MuvB-protein complex dissociates form p130/DREAM, resulting in the release of the DREAM-complex from cell cycle regulated promoters. Activator E2F proteins can then bind to the promoters of early cell cycle genes with a peak expression

during G1/S phase and, among others, MYBL2 transcription is initiated (Takahashi et al., 2000). During the S phase MYBL2 is bound by the MuvB-protein complex and together, as MYBL2-MuvB complex, they activate transcription, upon recruitment of FOXM1 to promoters of late cell cycle genes. Among these G2/M phase genes are long known MYBL2 target genes, such as CCNB1 and CDK1 (Zhu et al., 2004). Interestingly, MYBL2 and FOXM1 share several target genes, such as CCNB1, PLK1 and Aurora kinase A (AURKA), while FOXM1 itself is a target gene of MYBL2 (Sadasivam et al., 2012). The MYBL2 activity in the late G1/S phase is controlled by phosphorylation by the cyclin A/Cdk2 complex (Joaquin and Watson, 2003; Robinson et al., 1996). Also, poly ubiquitination and the subsequent proteasome-mediated degradation, responsible for the fast decrease of MYBL2, are regulated by phosphorylation (Charrasse et al., 2000). Due to the phosphorylation mediated proteasome degradation in the late S phase, MYBL2 dissociates from the complex with the MuvB-protein complex and FOXM1, while they in turn stay bound to the promoters until late G2 phase (Sadasivam et al., 2012). In addition, MYBL2 appears to play a role in the correct formation of the mitotic spindle (Yamauchi et al., 2008), and, it might be important for S phase promotion independent from its DNA-binding activity (Werwein et al., 2012).

Most recently, MYBL2 has been discovered as a sub-haploinsufficient tumor suppressor in MDS, promoting expansion of hematopoietic progenitors cells at a strangely reduced gene dosage (Heinrichs et al., 2013). This finding was independently confirmed using haploinsufficient, i.e. heterozygous knockout, mice. Specifically, Mybl2 expression levels of 50 % led to the occurrence of hematologic disorders, including MDS, in aged Mybl2 haploinsufficient mice (Clarke et al., 2013). Both studies supported early hints obtained in a zebrafish screen that a gene dosage reduction of Mybl2 results in the loss of a tumor suppressor function (Shepard et al., 2005). In contrast, previous studies reported high MYBL2 expression levels in solid tumors associated with poor prognosis (Thorner et al., 2009). However, an oncogenic role for MYBL2 has never been demonstrated in functional experiments. Thus, while its tumor suppressor activity has been shown in functional assays, MYBL2 upregulation appears to be rather a consequence of an enhanced proliferation due to unrelated oncogenic mutations.

1.3.1 Gene dosage insufficiency of tumor suppressor genes

In the pathogenesis of malignant neoplasms, partial and complete loss of tumor suppressor gene expression has been investigated for many years and different paradigms of inactivation have been identified. The classical “two-hit” model of tumorgenesis requires a bi-allelic inactivation of a tumor suppressor gene in order to allow

for a malignant transformation of a cell, i.e. a complete loss of the tumor suppressor function. This has been shown for one of the most well-known tumor suppressor genes: RB1. Thus, a homozygous inactivation of the RB1 gene is required for retinoblastoma development (Figure 3, left) (Berger et al., 2011; Friend et al., 1986; Knudson, 1971). However, in other instances a mono-allelic inactivation leading to haploinsufficiency of a tumor suppressor gene can also drive cells towards malignancy. A very prominent tumor suppressor gene, acting as a tumor suppressor with gene-dosage dependency starting at a haploinsufficient level, is TP53 (Figure 3, middle). A reduced TP53 gene dosage, due to germline mutations, is found in individuals with the inherited familial cancer syndrome Li-Fraumeni (Lynch and Milner, 2006). Other cancer susceptibility genes, such as BRCA1 in breast cancer (Bellacosa et al., 2010), PAX5 in acute lymphoblastic leukemia (Mullighan et al., 2007), APC in intestinal carcinoma (Amos-Landgraf et al., 2012), and RUNX1 in AML (Song et al., 1999), have been shown to support neoplastic transformation by their heterozygous inactivation. Only recently, the understanding of cancer initiation by loss of tumor suppressor function has extended from discrete changes to a continuum model of gene dosage dependency of tumor suppressor gene expression (Berger et al., 2011). In this model, subtle changes to the expression level of a tumor suppressor can support tumorgenesis. In special cases, a complete loss of the tumor suppressor is not compatible with cell survival (Figure 3, right), leading to a so-called obligate haploinsufficiency of the tumor suppressor gene. This has been exemplified for PTEN in breast cancer (Alimonti et al., 2010), and in myeloid malignancies it could be shown for MYBL2 (Figure 3, right) (Heinrichs et al., 2013), and SFPI1 (Rosenbauer et al., 2004).

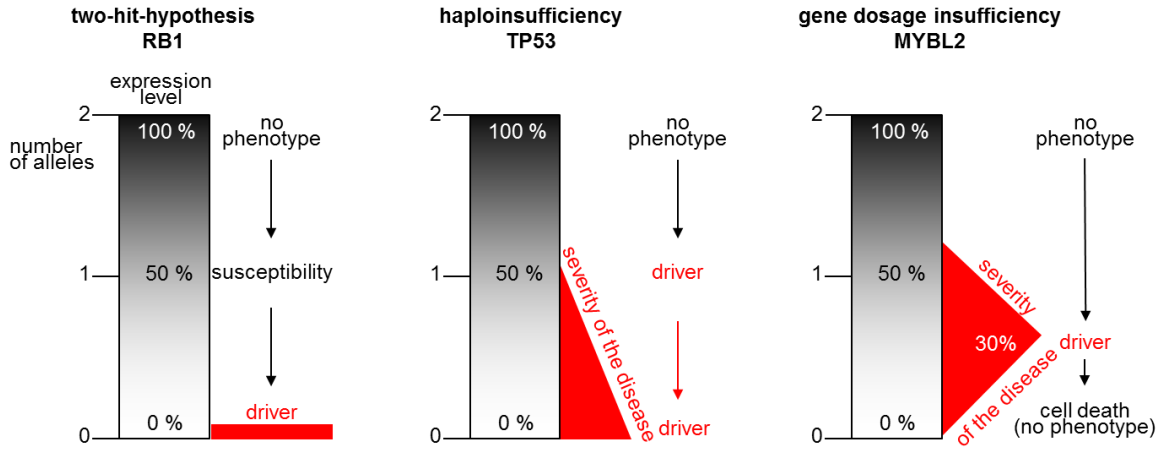

Figure 3: Concepts of tumor suppressor gene inactivation. *Left:* bi-allelic inactivation leads to loss of the tumor suppressor function, example RB1; *middle:* haploinsufficiency can drive cells towards malignancy, example TP53; *right:* gene dosage levels below haploinsufficiency increase tumor susceptibility, while bi-allelic inactivation leads to cell death, example MYBL2. *Figure adapted from (Berger et al., 2011), including results from (Heinrichs et al., 2013)*.

1.4 Fucci - Fluorescent ubiquitination-based cell cycle indicator

The Fucci technique marks cells according to their cell cycle phase in a different fluorescent color. It takes advantage of two anti-phase oscillating protein levels marking cell cycle transitions: Cdt1 and Gmnn (Geminin) (Sakaue-Sawano et al., 2008).

These two proteins are very important for the cell cycle regulation as they are involved in licensing the replication origin (Nishitani et al., 2000). Their levels oscillate reciprocally during the cell cycle due to proteolysis induced by the E3 ligase complexes APC^{Cdh1} and SCF^{Skp2}. SCF^{Skp2} is a substrate of APC^{Cdh1} but also a feedback inhibitor, thus their activities also oscillate reciprocally during the cell cycle (Nakayama and Nakayama, 2006). The APC^{Cdh1} complex is active in the M/G1 phase, while the SCF^{Skp1} complex is mostly active in the S/G2 phase. Consequently, protein levels of Cdt1, a direct target of the SCF^{Skp1} complex, are highest in the G1 phase, while Geminin, being controlled by the APC^{Cdh1} complex, accumulates in the S/G2/M phase (Figure 4 A) (Nishitani et al., 2004)). In the Fucci technique, a truncated version of the human cell cycle proteins Cdt1 and Geminin is fused to a fluorescent protein (Figure 4 C). In the original version, Fucci, Cdt1 is fused to mKO2 (mKO2-hCdt1(30/120)) and Geminin to mAG (Karasawa et al., 2003); mAG-hGem(1/110)), leading to a different fluorescence of cells depending on their cell cycle phase. Cells fluoresce red in the G1 phase and green in the S/G2/M phase of the cell cycle, while at the onset of S phase protein levels overlap and cells fluoresce yellow. After cell division a short time span without fluorescence can be observed (Figure 4 B) (Sakaue-Sawano et al., 2008).

These fluorescent cell cycle indicators, allow for the possibility of an unperturbed cell cycle phase detection by flow cytometry and separation by fluorescent activated cell sorting (FACS) (Figure 4, D and E). In an improved version, “Fucci2”, mKO2 and mAG were substituted by mCherry (Shaner et al., 2004), mCherry-CDT1(30/120), and Venus (Nagai et al., 2002), Venus-GMNN(1/110), marking cells bright red in the G1 phase and green in the S/G2/M phase of the cell cycle with an orange overlap at the onset of S phase (Figure 4 C) (Sakaue-Sawano et al., 2011).

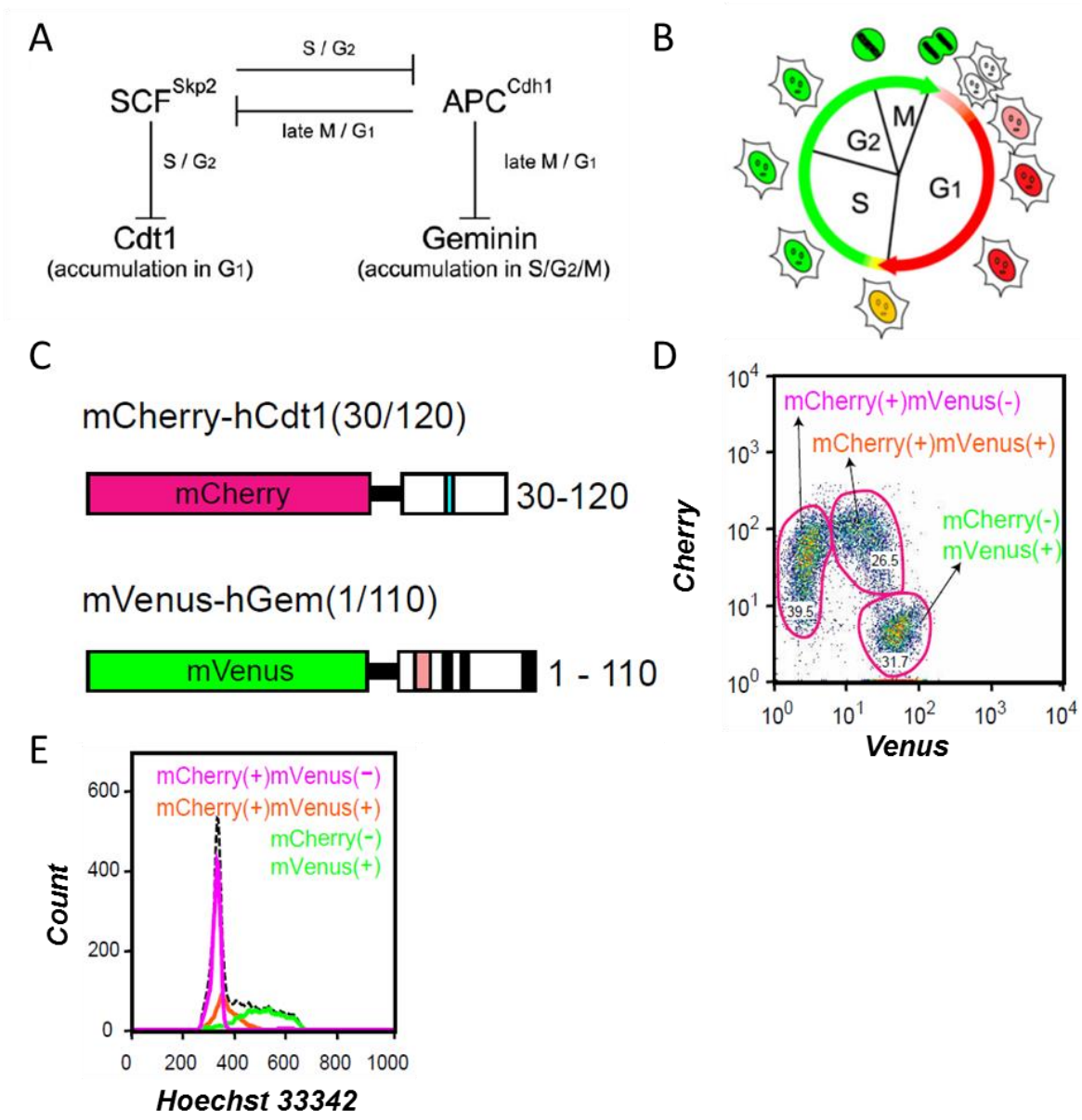

Figure 4: Fucci technique. (*A*) Cell cycle regulation by E3 ligases ACP^{Cdh1} and SCF^{Skp2}. ***(B)*** Cell cycle indicators label nuclei depending on their cell cycle phase. ***(C)*** Final constructs for Fucci2. ***(D)*** Flow cytometry of cells expressing Fucci2. **(E)** Flow cytometry analysis of Fucci2 expressing cells stained with Hoechst. (*A) and (B) taken from (Sakaue-Sawano et al., 2008), (C) to (E) taken from (Sakaue-Sawano et al., 2011)*.

1.5 Aim of this thesis

To date, the molecular mechanism of HSPC expansion by reduced MYBL2 levels is undiscovered. Interestingly, while a complete inactivation of Mybl2 leads to cell death (Tanaka et al., 1999), Mybl2 promotes cell expansion at an expression level of 30 - 50 % in a gene dosage dependent manner (Heinrichs et al., 2013). I propose that Mybl2 target genes are differentially affected by the downregulation of Mybl2 levels to sub-haploinsufficiency, possibly due to low and high affinity binding sites. Consequently, the expression of target genes with low affinity binding sites would be affected strongly by the downregulation of Mybl2, resulting in the loss of the tumor suppressor function of Mybl2 and allowing for clonal HSPC expansion. In contrast, the expression level of target genes with high affinity binding sites would be just marginally reduced, representing the subset of target genes required for cell cycle progression and cell survival. As Mybl2 is indispensible for the cell cycle progression and its activity strictly depends on the cell cycle phase, differences in target gene expression levels will also be cell cycle-dependent. Thus, to identify such differentially regulated genes, gene expression profiling with cell cycle phase-resolution would strongly improve the determination of significant Mybl2-dependent gene expression differences.

In order to test this hypothesis, I aimed to establish a system that allows for the analysis of cell cycle phase-dependent gene expression profiling in immortalized primary murine hematopoietic cells. I intended to implement a cell cycle analysis of murine HSPCs based on the Fucci2 technique. To modulate Mybl2 expression levels, I used RNA interference, a technique to knockdown expression of specific genes by expression of a short hairpin RNA (shRNA) via lentiviral vector transduction. Specifically, I introduced a Mybl2-targeting shRNA in an inducible expression vector system to reduce the Mybl2 expression level to sub-haploinsufficiency. In the described system, I sought to determine the expression differences of candidate target genes for the Mybl2 tumor suppressor function with cell cycle phase-resolution, comparing cells with regular Mybl2 levels to cells with an induced knockdown of Mybl2 expression to sub-haploinsufficiency.

2. Material and methods

2.1 Materials

2.1.1 Chemicals and reagents

All chemicals and reagents were purchased from Sigma Aldrich (St. Louis, MO, USA) and Carl Roth (Karlsruhe), if not stated otherwise.

2.1.2 Enzymes and standards

All enzymes and their buffers were purchased from Thermo Fisher Scientific (Waltham, MA, USA), if not stated otherwise. RNase A (100 mg/ml) and Proteinase K solution were purchased from Qiagen (Hilden); rAPid Alkaline Phosphatase was purchased from Roche (Basel, Switzerland); AmpliTaqGold DNA Polymerase, LifeTechnologies (Carlsbad, CA, USA); GeneRuler 1 kb and 100 bp, Thermo Fisher Scientific (Waltham, MA, USA).

2.1.3 Reagent systems (kits)

The QIAquick Gel Extraction kit, the QIAquick PCR Purification kit, the QIAprep Spin Miniprep kit, the QIAamp DNA Mini kit and the QuantiTect Reverse Transcription kit were purchased from Qiagen (Hilden); the Rapid DNA Ligation kit, Thermo Fisher Scientific Inc. (Waltham, MA, USA); CellTiter-Glo Luminescent Cell Viability assay, Promega (Fitchburg, WI, USA); Lineage Cell Depletion kit, mouse, Miltenyi Biotec (Bergisch Gladbach).

2.1.4 Antibodies

Lineage Cell Detection Cocktail - Biotin, mouse, Miltenyi Biotec (Bergisch Gladbach), containing biotin-conjugated monoclonal antibodies against CD5, CD11b, CD45R, Gr1 (Ly6G/C), and Terr-119.

Anti-mouse Ly-6A (Sca1) PE-Cy7 (clone D7), anti-mouse CD117 (c-Kit) APC (clone 2B8), anti-mouse CD11b APC (clone M1/70), anti-mouse Ly-6G eFluor 450 (clone RB6-8C5), anti-mouse CD45R (B220) PE-Cy 7(clone RA3-6B2), anti-mouse CD3e PerCP-Cy 5.5 (clone 145-2C11), anti-mouse CD34 FITC and Brilliant Violet (clone RAM34) were purchased from eBioscience (San Diego, CA, USA); BD Pharmingen anti-mouse CD16/32 PerCP-Cy 5.5 (clone 2.4G2) was ordered from BD Bioscience (San Jose, CA, USA); Anti-Biotin PE, Miltenyi Biotec (Bergisch Gladbach); Streptavidin APC-eFluor 780, eBioscience (San Diego, CA, USA).

2.1.5 Buffers and solutions

MACS buffer: PBS supplemented with 0.5 % BSA (bovine serum albumin) and 2 mM EDTA. The buffer was degassed and kept at 4 °C.

TAE buffer 50x: 24.2 % Tris, 5.71 % glacial acedtic acid, 0.05 M Na_2-EDTA; pH 8.5.

6x loading dye: 10 mM Tris-HCl, 0.005 % SDS, 60 mM EDTA, 60 % glycerol, 0.03 % xylene cyanol FF.

LB medium: 16 g tryptone, 8 g yeast extract, 8 g NaCl in 1 liter distilled water. The LB medium was used for agar plates as well and was prepared by adding 6 g agar and 300 ml water to 100 ml LB medium.

PBS: DPBS - Dulbecco's Phosphate-Buffered Saline (without $CaCl_2$ and $MgCl_2$), Life Technologies (Carlsbad, CA, USA).

PI staining solution: 0.2 % sodium citrate, 0.05 mg/ml propidium iodide, 0.1 % Triton X - 100 and 0.2 mg/ml RNase A.

2.1.6 Oligonucleotides

All oligonucleotides were ordered from Eurofins MWG Operon (Ebersberg). A detailed list of primer sequences is enclosed in the appendix.

2.1.7 Cell culture material

Cell culture material was purchased from Greiner Bio-One (Kremsmuenster), if not stated otherwise. Fetal Bovine Serum (Biochrome FBS Gold) was purchased from Biochrome (Berlin). Horse serum and Trypsin-EDTA Solution were purchased from Sigma Aldrich (St. Louis, MO, USA). HEPES Buffer Solution 1 M, Penicillin/Streptomycin 10,000 U/ml and L-glutamine 200 mM, all from LifeTechnologies (Carlsbad, CA, USA), were used in all cell culture experiments.

Cell culture media:

DMEM - Dulbecco's Modified Eagles Medium (1x) - high glucose (4,5 g/l D-Glucose) and RPMI Medium 1640 (1x) with L-glutamine were purchased from Life Technologies (Carlsbad, CA, USA); IMDM - Iscove's Modified Dulbecco's Medium - without L-glutamine, with 25 mM HEPES, and X-Vivo 15 chemically defined, serum-free hematopoietic cell medium without Gentamicin and Phenol Red, were purchased from Lonza (Basel, Switzerland).

Cytokines:

All cytokines used (recombinant murine IL-3, recombinant mFlt3 ligand, recombinant mTpo (murine thrombopoetin), recombinant mScf (murine stem cell factor)) were obtained from PeproTech GmbH (Hamburg).

2.1.8 Mice

Wild-type mice (C57BL/6) were provided by the animal facility of the University Hospital Essen. Transgenic mice expressing rtTA (reverse tetracycline-controlled transactivator) and a puromycin resistance gene were kindly provided by Prof. Dr. Andrea Vortkamp and were originally obtained from the Jackson Laboratory (R26 M2-rtTA) (Hochedlinger et al., 2005).

2.1.9 Laboratory material

Eukitt quick-hardening mounting medium (Fluka Analytical, St. Gallen, Switzerland); Syringe filters 0.2 µm (Minisart, Sartorius AG, Göttingen); Syringe 50 ml (Braun, Melsungen); 40 µm Cell Strainer (BIOLOGIX Research, Münster); ACK lysing buffer (Lonza, Basel, Switzerland); BD FACS Accudrop Beads (BD Bioscience, San Jose, CA, USA); Microscope slides (Marienfeld-Superior, Lauda Könighofen); Cover slips (Roth, Karlsruhe); Shandon EZ Single Cytofunnels (Thermo Fisher Scientific, Waltham, MA, USA); Sterile pipette tips (Biozym, Hessisch Oldendorf); Ultracentrifugation tubes (Beckman Coulter, Krefeld); Pipettes (Gilson Inc., Middleton, WI, USA); BD Falcon tubes (BD Bioscience, San Jose, CA, USA).

2.1.10 Laboratory devices

Flow cytometers:	FACS Aria I and III, BD Bioscience (San Jose, CA, USA); Cytomics FC 500 Flow Cytometer and Cytoflex, Beckman Coulter (Krefeld)
Luminometer:	Glomax Multi Detection System, Promega, (Fitchburg, WI, USA)
Spectophotometer:	Nano Drop 2000 Thermo Scientific (Waltham, MA, USA)
Agarose gel documentation system:	Biozym Scientific GmbH (Hessisch Oldendorf)
Centrifuges:	Eppendorf (Hamburg)
Ultracentrifuge:	Optima L-80XP Ultracentrifuge, Beckman Coulter (Krefeld)
Laminar flow hood:	HERAsafe HS12, Heraeus, Thermo Scientific (Waltham, MA, USA)

37 °C Incubator:	MaxQ 6000 Orbital Shaker, Thermo Scientific (Waltham, MA, USA)
CO_2 incubator:	HERAcell 240i, Thermo Scientific (Waltham, MA, USA)
Thermal Cycler:	CFX96 Real Time System C1000, Bio-Rad Laboratories, Inc. (Hercules, CA, USA); PTC 200 Thermal Cycler, MJ Research (Waltham, MA, USA)
Microscopes:	Olympus CKX41, Olympus Corporation (Shinjuku, Tokyo, Japan); Axio Vert.A1, Carl Zeiss GmbH (Jena)
Cytospin:	Shandon Cytospin II, Thermo Scientific (Waltham, MA, USA)
Cell Counter:	Sysmex XP-300 Automated Hematology Analyzer, Sysmex (Norderstedt); Neubauer counting chamber, Marienfeld-Superior (Lauda Königshofen)
Heating block:	Block Heater HX-1, Peqlab Biotechnologies (Erlangen)
Electrophoresis chamber:	Peqlab Biotechnologies (Erlangen)
Vortex-Schüttler:	VV 3,VWR (Darmstadt)

2.2 Methods

2.2.1 Flow cytometry

Flow cytometry allows the measurement and the analysis of molecular and physical properties of a large number of cells on a single cell basis. In the flow cytometer, cells separated by a fluidic stream pass a laser beam as single objects and the laser light is scattered. The cell size can be estimated by the light that scatters axial to the laser beam (forward scatter (FSC)), while the light that scatters perpendicular to the laser beam (side scatter (SSC)) allows an assessment of the cells granularity. Additional properties can be analyzed by staining the cells with fluorochrome-conjugated antibodies against surface antigens (e.g. immunophenotyping) or intracellular components. Also, the expression of fluorescent proteins (e.g. green fluorescent protein (GFP)) can be detected by the emitted fluorescence. Dyes that fluoresce upon DNA binding can be used to determine the DNA content of a cell for cell cycle analysis. Some flow cytometers can sort single cells and cell populations according to their properties as predefined by the user's sort criteria

(fluorescent activated cell sorting (FACS)). In the cell sorter, a droplet from the stream containing the cell of interest is electrostatically charged. This charged droplet is then deflected to the right or left by charged deflection plates into a collection tube or plate. Uncharged droplets are directed into the waste. The process of cell sorting allows a highly effective purification of cells and permits to further analyze the sorted subpopulations.

2.2.1.1 Immunophenotyping

Fluorochrome-conjugated antibodies directed against surface antigens were used to determine the phenotype of isolated murine bone marrow cells in culture (immunophenotyping). Based on expression of characteristic lineage markers, hematopoietic stem and progenitor cells (lineage-negative) can be distinguished from differentiated cells that are positive for at least one marker (lineage-positive). To discriminate lineage-positive from lineage-negative cells, cells were stained with a mixture of biotin-conjugated monoclonal antibodies against CD5, CD11b, CD45R, Gr1 (Ly6G/C), and Terr-119 (Lineage Cell Detection Cocktail - Biotin, mouse (Miltenyi Biotec, Bergisch Gladbach)). Labeling was performed in 100 µl MACS buffer for 20 min at 4 °C in the dark, using 10 µl cocktail per 10^6 cells. In a second step a streptavidin conjugated fluorochrome (Streptavidin APC-eFlour 780, eBioscience, San Diego, CA, USA) was used to detect the biotinylated antibodies. The cells were washed in MACS buffer after every step. To further identify specific cell populations, the following anti-mouse antibodies (eBioscience, San Diego, CA, USA) were used (clone in parentheses): Ly-6A/Sca1 (D7), CD117/Kit (2B8), CD11b/Mac1 (M1/70), Ly-6G/Gr1 (RB6-8C5), CD45R/B220 (RA3-6B2), CD3e (145-2C11), CD34 (RAM34) and CD16/32 (2.4G2; BD Bioscience, San Jose, CA, USA). If not stated otherwise, cells were stained in 100 µl MACS buffer for 30 min at 4 °C in the dark with a titrated amount of antibody and washed in MACS buffer afterwards. For flow cytometry measurements, the stained cells were re-suspended in 200 - 800 µl of MACS buffer.

2.2.1.2 Fluorescent activated cell sorting and single cell sorting

Cell sorting was performed on the FACS Aria I or III instrument (BD Bioscience). The instrument was calibrated with BD FACS Accudrop Beads (BD Bioscience, San Jose, CA, USA). All sort experiments were done with a 100 µm nozzle, and up to four different cell populations were sorted in parallel. After every sort, a re-analysis of an aliquot of the sorted cells was performed to ensure the purity of the sorted cell population. The cells were sorted into cell culture medium. For molecular analysis, they were spun down (300 g, 5 min) immediately after the sort and were either re-suspended in TRIzol (Life Technologies, Carlsbad, CA, USA) for subsequent RNA extraction or propidium iodide

staining solution for cell cycle analysis (2.2.1.3). Cells for cell culture experiments were also spun down but were re-suspended in freshly prepared cell culture medium. To generate clonal cell populations, single cells were sorted into 96-well plates. This special sort setting allows depositing only one cell into each well of the plate. To prevent bacterial contaminations, all media for cells used in further cell culture experiments were supplied with antibiotics (10,000 U/ml Pen/Strep, LifeTechnologies, Carlsbad, CA, USA).

2.2.1.3 Cell cycle analysis

The Cytomics FC 500 flow cytometer (Beckman Coulter) and the Cytoflex (Beckman Coulter) were used for cell cycle analysis measuring the cellular DNA content upon cell staining with propidium iodide staining solution. Propidium iodide (PI) is a DNA intercalating molecule that shows an increase in fluorescence upon binding to DNA. The amount of nucleic acid bound propidium iodide is proportional to the DNA content of a cell. As cells duplicate their DNA in the S phase of the cell cycle, a cell in the G2 phase contains a double amount of DNA compared to a cell in the G1 phase. Thus, the measurement of the propidium iodide intensity allows generating a cell cycle profile of cell populations. The PI staining solution (2.1.5) was freshly prepared prior to each cell cycle analysis. Before the measurement, 100,000 cells were centrifuged and re-suspended in 250 µl staining solution. Upon incubation for at least 45 min in the dark and at room temperature, flow cytometric analysis was performed. The recorded events were discriminated for cell doublets or clusters (Figure 5). The exclusion of doublets is important as for example two cells in the G1 phase have the same DNA content as one cell in the G2 phase of the cell cycle and if stuck together the recorded cell cycle profile would be falsified.

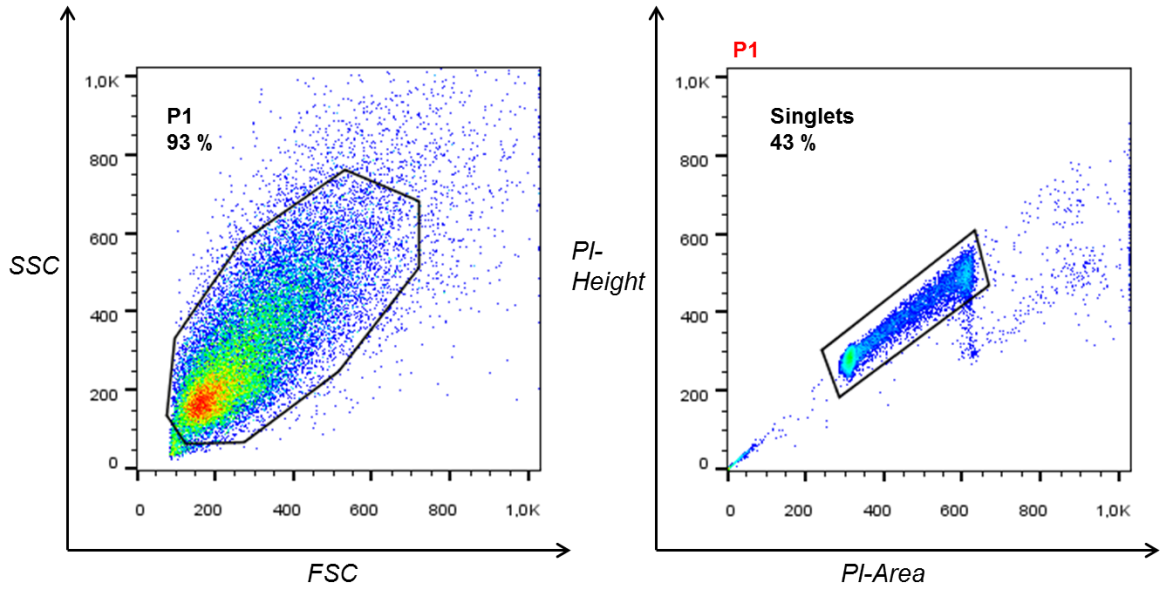

Figure 5: Flow cytometric gating strategy for the cell cycle analysis of cells stained with PI-staining solution. Discrimination of debris was performed according to FSC and SCC parameters, followed by fluorescence height (PI-height) and area (PI-area) analysis to discriminate doublets, as well. *In this example PI-stained EML cells were used.*

2.2.2 Preparation of murine bone marrow cells and lineage cell depletion

Mice were sacrificed, and femur and tibia were dissected. The bones were crushed in a mort after removing muscle and connective tissue. Bone marrow cells were suspended in MACS buffer and filtered to remove clumps and bone particles (40 µm cell strainer, BIOLOGIX Research, Münster). The erythrocytes were lysed with ACK lysing buffer (Lonza, Basel, Switzerland). The lineage-negative cells were enriched by magnetic cell sorting using the Lineage Cell Depletion kit, mouse (Miltenyi Biotec, Bergisch Gladbach). For the depletion of the mature hematopoietic cells, the isolated bone marrow cells were magnetically labeled with biotinylated antibodies against lineage markers (CD5, CD45R, CD11b, Gr1, Ter-119, 7-4) and with anti-biotin microbeads as a secondary labeling reagent. While the unlabeled lineage-negative cells can pass through a magnetic field, the magnetically labeled mature cells are retained. This procedure leads to an enrichment of “untouched” lineage-negative cells. All labeling and separation steps were performed according to the manufacturer’s protocol. The purity of the enriched lineage-negative cells was validated by flow cytometry using aliquots of the separated cell fractions stained with anti-biotin PE (Miltenyi Biotec, Bergisch Gladbach), 10 µl antibody for up to 10^7 cells (Figure 6, A to D). Thus, the relative amount of remaining mature hematopoietic cells (PE positive) in the enriched lineage-negative cell fraction could be determined (Figure 6, D). Usually, starting with about 5 to 10 % of lineage negative cells an enrichment up to 95 % was reached. After enrichment, lineage-negative cells were

cultivated in X-Vivo 15 medium supplemented with cytokines (80 ng/ml mScf, 40 ng/ml mTpo, 40 ng/ml mFlt3 ligand), 100 U/ml Pen/Strep, 2 mM L-glutamine and 10 % heat inactivated fetal bovine serum for 24 h.

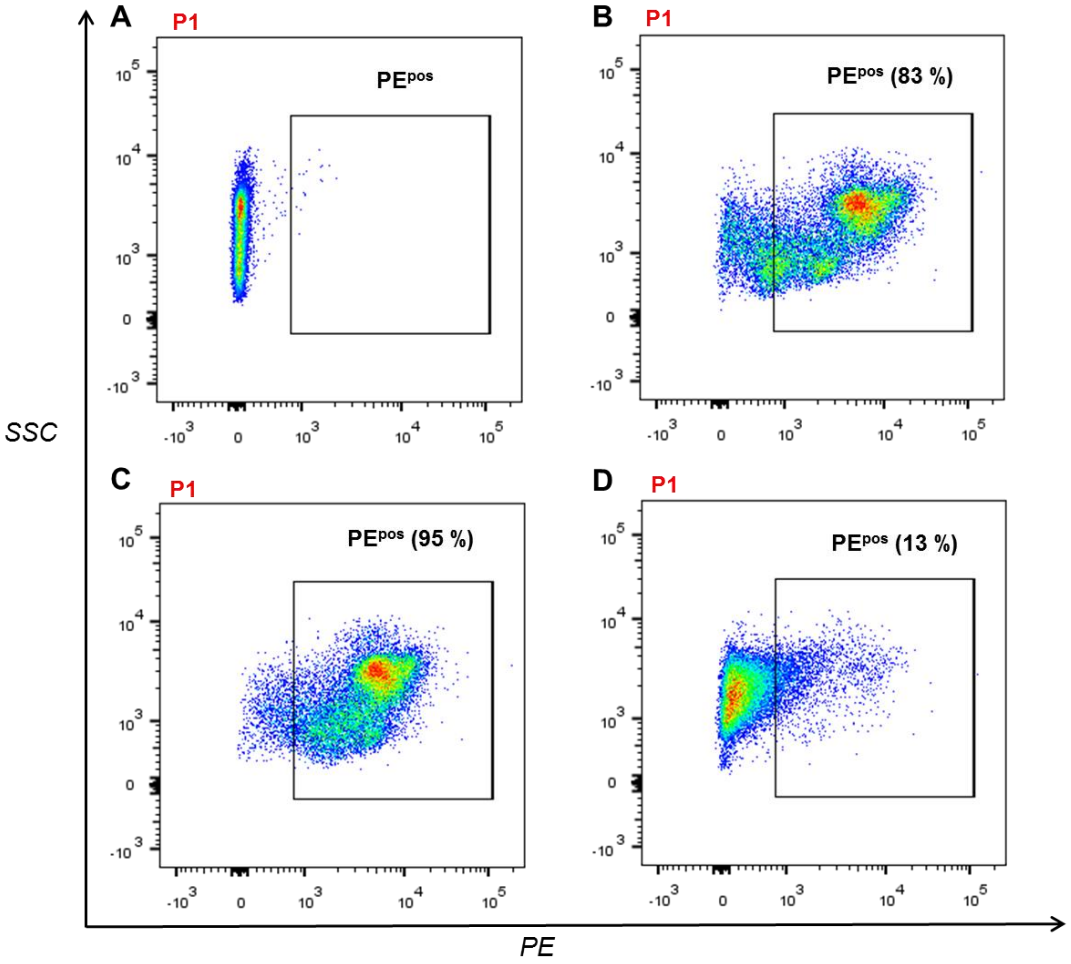

Figure 6: Analysis of the purity of the lineage-negative enriched bone marrow cells from mice (A) As a control isolated, unstained, full bone marrow cells were analyzed after erythrocyte lysis. **(B)** Control cells stained with anti-biotin PE to mark the mature cell fraction (83 %). **(C)** Depleted mature hematopoietic cells. **(D)** Lineage negative enriched bone marrow cells: 17 % of lineage negative cells (PE^{neg} in B) were enriched to 87 %. *In this example bone marrow cells isolated from M2-rtTA mice were analyzed.*

2.2.3 Polymerase Chain Reaction (PCR)

PCR is used to amplify a specific DNA sequence and allows for the introduction of new sequences, e.g. restriction sites and mutations, into the DNA of interest. A standard PCR includes the denaturation of the template DNA, the annealing of the primers (oligonucleotides that are complementary to one of the respective strands of the template DNA) and the extension of the primers at their 3' end by a heat-stable DNA Polymerase using deoxynucleoside triphosphates (dNTPs). These steps are repeated in cycles in

order to exponentially amplify the target sequence (amplicon) and to generate sufficient amounts of DNA for detection or cloning.

A standard PCR assay included 0.5 µM reverse and forward primer each (Eurofins Genomics, Ebersberg), 1 ng template (plasmid or PCR product), 0.2 mM dNTPs (Thermo Scientific, Waltham, MA, USA), 1x Phusion High-Fidelity buffer (Thermo Scientific, Waltham, MA, USA) and 1 U High-Fidelity Phusion Hot Start II DNA polymerase (Thermo Scientific, Waltham, MA, USA). Reactions were performed in 25 - 100 µl volume depending on the amount of product needed for subsequent experiments. A table of primer sequences is enclosed in the appendix.

If not stated otherwise, the standard PCR procedure was performed with a PTC-200 Thermal Cycler (MJ Research, Waltham) using the following program steps:

1. Initial denaturation 98 °C for 30 sec
2. Denaturation 98 °C for 10 sec
3. Annealing 50 °C to 65 °C for 30 sec (temperature depending on primer pair)
4. Extension 72 °C for 15 - 30 sec/1 kb of amplicon
5. *Repetition of step 2 to 4 between 25 to 35 cycles depending on amount of input DNA*
6. Final extension 72 °C for 10 min

2.2.3.1 Fusion PCR

This special type of PCR allows the fusion of two independent DNA fragments. First, the two DNA fragments of interest are amplified separately in two regular PCRs (Figure 7, 1. and 2.). However, the reverse primer of DNA fragment 1 and the forward primer of DNA fragment 2 are designed with an identical sequence that is introduced into both PCR products (Figure 7, red label). In a third PCR (Figure 7, 3.), these products are used as templates that are amplified with primers complimentary to the ends of the desired full-length product (forward primer of DNA fragment 1 and the reverse primer of DNA fragment 2; Figure 7, A and B), as the identical sequences of the two templates overlap in the annealing step. The product of this third PCR amplification is a fused DNA sequence that can be used for cloning. The program steps and the PCR reactions were performed as described above (2.2.3).

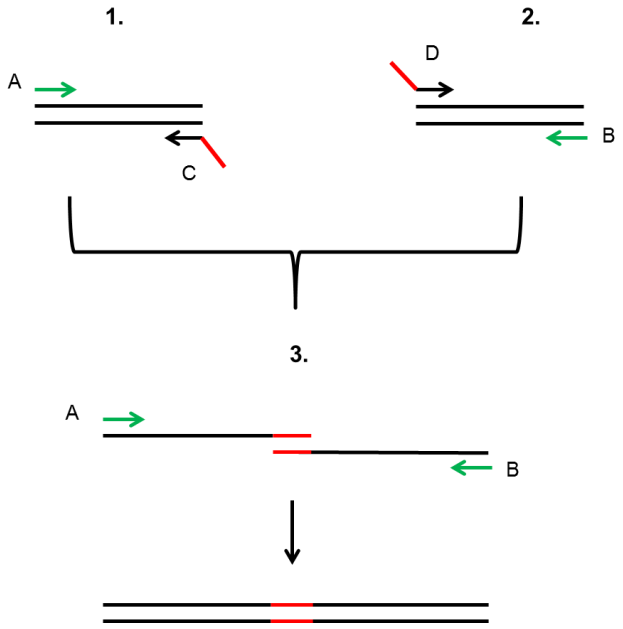

Figure 7: Fusion PCR. Two regular PCR amplifications (1. and 2.), primers C and D introduce an identical sequence (red) into both products. In a third PCR (3.), the identical sequences overlap, and the desired full-length product is amplified with primers A and B (green).

2.2.4 Agarose gel electrophoresis

Agarose gel electrophoresis was used to confirm a successful PCR amplification (analytical gel) or to purify DNA fragments (preparative gel). A 1 - 2 % agarose (Sigma Aldrich, St. Louis, MO, USA) gel was prepared depending on size of DNA fragments to be separated. The appropriate amount of agarose was heat-dissolved in 1x TAE buffer (2.1.5). After cooling to 50 - 60 °C, ethidium bromide (0.07 %, inno-train diagnostics GmbH, Kronberg), a DNA intercalator allowing the detection of DNA, was added and the gel was casted. Prior to loading the gel, DNA samples were mixed with a 6x DNA loading dye (2.1.5). A standard molecular weight marker (GeneRuler 1 kb or 100 bp, Thermo Scientific, Waltham, MA, USA) was loaded in parallel and used to estimate the size of DNA fragments. The gels were run in 1x TAE-buffer at 90 - 120 V for 45 - 60 min. In case of a preparative gel, the desired DNA gel fragments were cut out with a scalpel.

2.2.5 DNA purification

PCR products larger than 100 bp were purified using the silica-membrane-based column purification (QIAquick PCR Purification kit, Qiagen, Hilden). The nucleic acids are adsorbed to the silica membrane in presence of a high concentration of chaotropic salts allowing to remove unwanted contaminants. After several washing steps the pure DNA is eluted by a salt-free buffer (10 mM Tris-Cl, pH 8.5). All steps were performed according to the manufacturer's instructions. Purification of DNA bands in agarose gel was achieved using the QIAquick Gel Extraction Kit (Qiagen, Hilden). In a first step, the agarose block

containing the DNA was solubilized with an agarose-dissolving buffer (Qiagen, Hilden) at 50 °C for 10 min followed by the silica-based column purification as described.

2.2.6 Determination of nucleic acid concentration

The concentration and the purity of nucleic acids (RNA and DNA) were determined with a spectrophotometer (NanoDrop 2000, ThermoScientific, Waltham, MA, USA). Spectrophotometric quantitation of nucleic acids is based on the absorption of UV-light at 260 nm (absorption maxima). The Lambert Beer's law allows correlating the amount of absorbed UV-light to the concentration of nucleic acid in the sample. Thus, the more light is absorbed, the higher is the concentration of nucleic acids in the sample. The conversion factor for DNA is 50 µg/ml per absorption unit, for RNA this factor is 40 µg/ml. As proteins have their absorption maxima at 280 nm, the ratio of absorption at 260 nm to the absorption at 280 nm is used to assess contaminations of the nucleic acid samples. For pure DNA this ratio should be greater than 1.8 and for pure RNA greater than 2.0.

2.2.7 DNA digestion

Plasmids and PCR products were digested using FastDigest restriction enzymes (Thermo Scientific, Waltham) at 37 °C. The amount of enzyme and the time of incubation were adjusted to the amount of DNA to be digested. Digestion buffers were used according to the manufacturer's instructions. For analytical digestions, 0.5 to 2 µg DNA were used. Preparative digestions for cloning require a higher amount of DNA, 5 to 6 µg. Also, all preparative digestions providing the plasmid backbone in subsequent cloning reactions were treated with 1 U of phosphatase (rAPid Alkaline Phosphatase, Roche, Basel, Switzerland) for the last 10 min of the digestion reaction to remove 5'-phosphate groups preventing a re-ligation of the plasmid in the ligation reactions. Digested products were column-purified or separated by agarose gel electrophoresis and purified.

2.2.8 Ligation and transformation of bacteria

The desired insert and the dephosphorylated plasmid backbone were ligated using the T4 DNA ligase and a buffer allowing rapid ligation (Rapid DNA Ligation kit, Thermo Scientific). In a 10 µl reaction, 35 to 50 ng of plasmid were used with a three to four-fold molar excess of insert. As a control a ligation reaction without insert was prepared in parallel. Both were incubated at room temperature for 10 min. After incubation the ligation reaction was gently mixed with 50 - 100 µl of chemically competent bacteria that were thawed on ice. After 20 min incubation on ice, the bacteria were heat shocked at 42 °C for 45 sec followed by addition of 250 µl of LB medium (2.1.5) and incubation at 37 °C for 45 min. The bacteria suspensions were plated on agar plates containing ampicillin at

100 µg/ml as selective marker. The agar plates were incubated overnight at 37 °C. The next day, the number of colonies on the ligation plate was compared to that of the control plate allowing an estimation of the success rate.

2.2.9 Preparation of plasmid DNA

Individual bacterial colonies were picked and transferred to a liquid culture of 4 ml LB medium containing ampicillin (100 µg/ml). The cultures were incubated at 37 °C overnight while shaking at 150 rpm. Plasmid DNA was purified using the QIAprep Miniprep Kit (Qiagen, Hilden) according to the manufacturer's instructions. Taking advantage of the modified alkaline lyses by Birnboim and Doly (Birnboim and Doly, 1979), bacteria were lysed followed by a silica-based column purification of the plasmid DNA. The eluted DNA was sequenced at LCG genomics (Berlin) to validate the sequence of the new plasmid.

2.2.10 Lentiviral vectors

Genetic manipulations of cells were obtained with lentiviral particles derived from the human immunodeficiency virus 1 (HIV-1). Such particles are able to transduce dividing and non-dividing cells. In this study, a second generation packaging system was used to produce them. It consists of a packaging plasmid, an envelope plasmid and the transfer plasmid encoding the particle's genome including the transgene and an antibiotic resistance gene or a fluorescence reporter gene. Upon transduction the transgene RNA genome is reverse transcribed and integrated into the cells' genome leading to a stable expression. I used transfer plasmids encoding for the knockdown of mRNAs and the ectopic expression of protein-coding sequences. For antibiotic resistance blasticidin, puromycin or hygromycin were employed. As fluorescence reporter genes I used Venus (Nagai et al., 2002), DsRed2 (Strack et al., 2008), mTurquoise2 (Goedhart et al., 2012) and mTagBFP (Subach et al., 2011).

2.2.10.1 Production of lentiviral particles

Lentiviral particles were produced in HEK 293T cells. In order to reach a 50 - 80 % confluency $6x10^6$ cells were plated in 10 cm culture dishes 16 - 20 h prior to transfection. Each transfection was performed with 5 µg of the desired transfer plasmid, 1.8 µg of the envelope plasmid (pMD2G) and 5 µg of the packaging plasmid (pCMV-dR8.2). The plasmids were mixed into 600 µl of DMEM and 35 µl of transfection reagent were added (TransIT-LT1, Mirus Bio LLC, Madison, WI, USA). After 20 - 30 min of incubation at room temperature the mixture was spread evenly on the 293T cells. The supernatant was exchanged with fresh medium (DMEM, 10 % FBS) 24 h later. At 48 h, 60 h and 72 h post

transfection the supernatant containing lentiviral particles was collected and stored at 4 °C upon addition of HEPES-buffer (40 mM) to stabilize the pH (7.0). All supernatants were filtered after collection to remove cellular debris (0.2 µm Minisart, Sartorius AG, Göttingen). The filtered supernatant was aliquoted and stored at -80 °C. If required, e.g. for transduction of primary cells, it was concentrated by ultracentrifugation (4 °C, 100000 g, 90 min) before storage.

2.2.10.2 Transduction with lentiviral particles

All cells were spin-transduced at 25 °C, 1000 g for 90 min in presence of polybrene (4 µg/ml hexadimethine bromide, Sigma Aldrich, St. Louis, MO, USA). Subsequently, cells were washed and provided with fresh medium. The amount of cells to be transduced determined the volume of supernatant containing lentiviral particles and the plate size. A standard cell line transduction was done with $0.8x10^6$ cells in 1000 µl of the un-concentrated lentiviral-containing supernatant in a 12-well plate. After transduction the washed cells were transferred to a 6-well plate and supplied with fresh medium. If smaller or larger amounts of cells were transduced, volumes were adapted accordingly. 24 h after transduction the respective selection reagent was added (puromycin, blasticidin or hygromycin). Untransduced control cells were used to determine completion of the selection.

2.2.10.3 Determination of the efficiency of lentiviral particles

The efficiency of lentiviral particles was tested by a spin-transduction of $0.5x10^6$ K562 cells with 1/10 of the particle-containing supernatant that was used for a standard cell line transduction. As a control, pooled virus stocks with known efficiency were used for transduction in parallel. 2/3 of the cells were harvested after 48 h and genomic DNA was purified using the QIAmp DNA Mini Kit according to the manufacturer's instructions. Integration of the viral DNA into the genomic DNA was tested by quantitative PCR (qPCR). In addition, if the transfer plasmid encoded for a reporter fluorochrome, the remaining K562 were analyzed by flow cytometry. The expression level and the fluorescence intensity were used to predict the quality and the transduction rate of the particle-containing supernatant.

2.2.11 RNA extraction, cDNA synthesis and qPCR

RNA was extracted from TRIzol (Life Technologies, Carlsbad, CA, USA) according to the manufacturer's instructions. This procedure allows for a sequential isolation of RNA, DNA and proteins form the same sample and was first described by Chomczynski and Sacchi (Chomczynski and Sacchi, 1987). The TRIzol reagent is a monophasic solution

containing phenol and guanidine isothiocyanate. It dissolves all cell components during homogenization of the sample while maintaining the integrity of RNA due to RNAse inhibition. Upon addition of chloroform a phase separation is induced and the RNA can be precipitated from the aqueous phase with isopropanol. At least 200 ng of isolated RNA were used for cDNA synthesis with the QuantiTect Reverse Transcription Kit (Qiagen, Hilden). After elimination of potential traces of contaminating genomic DNA, the reverse transcription was performed using a mixture of Quantiscript reverse transcriptase (RT), Quantiscript RT buffer and RT primer mix. The reaction was performed according to the manufacturer's instructions. The cDNA was analyzed for gene expression with quantitative PCR (qPCR). A SYBR Green based assay was performed in triplicates on a CFX96 Real Time System (Bio-Rad Laboratories Inc., Hercules, CA, USA). Upon binding of double-stranded DNA, SYBR green fluoresces. The fluorescence intensity is measured after each PCR cycle and can be used to quantitate the amount of input DNA. Each reaction was prepared with 0.03 U AmpliTaqGold DNA Polymerase (LifeTechnologies, Carlsbad, CA, USA), 0.25 µM sequence-specific forward and reverse primer (see appendix) and 1x master mix containing SYBR green. Quantitative data were calculated with Ct-values from each reaction using mean primer pair efficiency. Data were normalized to at least two housekeeping genes, namely Vps39 and Ubqln1.

2.2.12 Monitoring cell growth

Cell growth was monitored using the CellTiter-Glo luminescent cell viability assay (Promega, Fitchburg, WI, USA). This assay quantifies the amount of ATP released from lysed cells by the oxidation of luciferin in presence of O_2, Mg^{2+} and ATP. Catalyzed by the Ultra-Glo recombinant luciferase, the oxidation results in oxyluciferin and thus in a stable luminescent signal that is proportional to the amount of viable cells. For growth monitoring of a standard cell line, 250,000 cells were plated in 2.5 ml medium in a 12-well plate. At each time point, 50 µl of each cell population plus 5 µl HEPES buffer (1 M) were thoroughly re-suspended with 100 µl of CellTiter-Glo Reagent. All cell populations were measured in triplicates in an opaque 96-well microplate suitable for luminescence measurement. The plate was incubated for 10 min at room temperature and luminescence was measured on the GloMax-Multi Detection System with 1 sec integration time in a predefined CellTiter-Glo protocol (Promega, Fitchburg, WI, USA). Growth was monitored every second day. All values of an individual cell suspension were normalized to its starting value. After the measurements, all cells were supplied with fresh medium including replacement of the medium taken for each measurement.

2.2.13 Cell culture

2.2.13.1 Cell lines

HEK 293T, a human embryonic kidney cell line used for production of lentiviral particles, were cultured in DMEM (DMEM high glucose, Life Technologies, Carlsbad, CA, USA) supplemented with 10 % heat-inactivated fetal bovine serum (FBS Gold, Biochrome, Berlin). Cells were trypsinized (1x Trypsin-EDTA solution) every second to third day and replated at a 1:3 to 1:5 dilution. K562 cells and OCI-AML2 cells, both human leukemic cell lines, were cultured in RPMI 1640 with L-glutamine (Life Technologies, Carlsbad, CA, USA) supplemented with 10 % FBS. For maintenance of 32D cells, a murine hematopoietic cell line, the same culture conditions were applied but in addition the media was supplemented with 5 ng/ml IL-3 (PeproTech, Hamburg).

EML cells, a murine multipotent hematopoietic progenitor cell line (Tsai et al., 1994) were cultured in IMDM (BioWhittaker's IMDM with HEPES (25 mM), without l-glutamine, Lonza, Basel, Switzerland) supplemented with 20 % heat-inactivated horse serum (Sigma Aldrich, St. Louis, MO, USA), 10 % SCF-conditioned medium from the BHK/MKL cell line (see below), 2 mM L-glutamine and 100 U/ml Pen/Strep. For selection after transduction, the EML medium was supplemented with 8 µg/ml blasticidin (AppliChem, Darmstadt), 1,5 µg/ml puromycin (SigmaAldrich, St. Louis, MO, USA) or 500 µg/ml hygromycin B (Life Technologies, Carlsbad, CA, USA). BHK/MKL cells (provided from S. Tsai, Utah) were cultured in DMEM supplemented with 10 % FBS. For passaging cells were trypsinized and replated at a 1:3 to 1:5 dilution.

All sera were heat-inactivated prior to use. All suspension cell lines were passaged every second or third day.

2.2.13.2 BHK/MKL stem cell factor conditioned medium

The BHK/MKL cells are genetically modified to express the secretory form of rat Scf. Their conditioned medium provides the stem cell factor for the EML cell line. In order to produce a conditioned medium of high quality, the cells have to reach 60 - 80 % confluency. 16 - 20 h prior to medium conditioning, $7x10^6$ cells were plated in a T75 flask in 25 ml DMEM supplemented with 10 % heat-inactivated FBS. As the desired confluency was reached, medium was replaced by 50 ml fresh DMEM supplemented with 10 % heat-inactivated FBS. The conditioned 50 ml of medium were collected after 48 h, and were replaced by additional 60 ml of fresh medium. Again 48 h later, the conditioned medium was collected. All collected media were pooled, centrifuged (300 g, 5 min, room temperature), filtered

(0.2 µm Minisart, Sartorius AG, Göttingen) and stored in aliquots at -20 °C.

2.2.13.3 Murine hematopoietic stem and progenitor cells

Murine hematopoietic stem and progenitor cells were cultured in X-Vivo medium (X-Vivo 15 without Gentamicin and Phenol Red, Lonza, Basel, Switzerland) supplemented with 10 % FBS, 2 mM L-glutamine, 100 U/ml Pen/Strep, 10 ng/ml mFlt3 ligand, 10 ng/ml mTpo and 20 ng/ml mScf. Cells were passaged every second day. For selection after transduction, the media was supplemented with 6 µg/ml blasticidin (AppliChem, Darmstadt), 1,5 µg/ml puromycin (SigmaAldrich, St. Louis, MO, USA) or 200 µg/ml hygromycin B (Life Technologies, Carlsbad, CA, USA). For the induction of tetracycline-regulated gene expression the medium was supplemented with titrated amounts of doxycycline (Sigma Aldrich, St. Louis, MO, USA).

2.2.14 Cytospins

150,000 cells were washed in 1 ml MACS buffer three times. For the spin funnel application, the cells were resuspended in 150 µl of MACS buffer and centrifuged on microscope slides (2 min, 800 rpm, Shandon Centrifuge Cytospin II). The resulting cytospins were air-dried for 30 min. Staining was performed with May-Grünwald-Giemsa solution for 20 min in 1x Giemsa (Sigma Aldrich, St. Louis, MO, USA) followed by a 2 sec distilled water wash, a 2 min May-Grünwald (Sigma Aldrich, St. Louis, MO, USA) solution incubation followed by a 1 sec distilled water wash step. Dried slides were mounted with coverslips (Roth, Karlsruhe) using Eukitt quick-hardening mounting medium (Fluka Analytical, St. Gallen, Switzerland).

2.2.15 Statistics

All graphs and statistics were obtained with GraphPad Prism (Graph Pad Software, San Diego, CA, USA; version 5.04 for Windows). Flow cytometry data was analyzed using FlowJo (Tree Star Inc., Ashland, OR, USA). All figures were prepared using Microsoft PowerPoint. Geneious (Biomatters, Auckland, New Zealand) was used for plasmid and primer design as well as determination of restriction sites.

3. Results

3.1 Establishment of a cell cycle-readout

The most precise gene expression profiling including a cell cycle phase-based resolution would ask for an undisturbed separation of cells according to their cell cycle phase. Classically, an enrichment of cells in a certain phase is achieved by chemical synchronization or, less common, by physical separation. Chemical synchronization is accomplished by a block of metabolic reactions leading to an arrest of all cells in the same cell cycle phase; upon release these cells undergo a synchronized division. Such an arrest can be provoked either by nutrition deprivation (e.g. serum starvation) or by inhibition of DNA synthesis and microtubule activity (e.g. aphidicolin, thymidine, nocodazole, etc.). Unfortunately, both methods disturb essential signaling pathways. Physical separation, for example mitotic shake off or centrifugal elutriation, requires special equipment and a large number of cells to obtain enough synchronized cells for further analysis (Davis et al., 2001). Thus, the analysis of cell cycle-dependent gene expression in primary murine hematopoietic stem and progenitor cells precludes classical cell cycle synchronization. In particular, an undisturbed cell cycle progression would allow for a highly accurate gene expression analysis of Mybl2, an essential cell cycle regulatory gene. I aimed to test whether the fluorescent ubiquitination-based cell cycle indicator (Fucci) technique (1.4) (Sakaue-Sawano et al., 2008), specifically the improved version Fucci2 (Sakaue-Sawano et al., 2011), could be used for an accurate separation of cell cycle phases in murine HSPCs. To date, the Fucci technique had not been used for analysis and separation of hematopoietic cell lines or cultured murine hematopoietic stem and progenitor cells.

3.1.1 Vector design and cloning

I implemented the Fucci2 technique (Sakaue-Sawano et al., 2011) with certain modifications. First, I replaced the fluorochrome mCherry by the tetrameric DsRed-Express2 (RFP) (Strack et al., 2008)), or alternatively mTurquoise2 (Tq) (Goedhart et al., 2012)) to enable measurements on flow cytometers not equipped with a 561 nm yellow-green laser. Second, instead of the Fucci2 ill-defined linker sequence that was designed to facilitate cloning steps, I introduced a defined glycine linker to fuse the fluorochrome protein to the cell cycle phase regulated protein domain. The glycine residues offer a high flexibility between the two protein domains. Further, I aimed to develop a single vector encoding both cell cycle indicators. This would facilitate the handling of vector transduction as well as the selection for transduced cells. Aiming to work with hematopoietic cells, I introduced the spleen focus-forming virus (SFFV) promoter to drive

expression of one of the fused proteins as it is one of the most potent promoters to drive gene expression in murine hematopoietic cells (Baum et al., 1995; Eckert et al., 1996). The other fusion protein was set up to be expressed under the control of the human phosphoglycerate kinase (hPGK) promoter.

To generate the vectors needed to implement the Fucci2 technique, I first PCR-amplified the RFP, the Tq and the Venus DNA sequences. In order to amplify the cell cycle gene-encoding DNA sequences and to introduce the glycine linker, I designed the forward primers for the $CDT1_{(30/120)}$ and the $GMNN_{(1/110)}$ DNA fragments with an overhang encoding the glycine sequence and part of the sequence encoding the fluorochrome to be linked. The cell cycle gene-encoding DNA sequences were then PCR-amplified. In a subsequent fusion PCR (2.2.3.1), the fluorochrome-encoding sequences were fused to the cell cycle gene-encoding sequences. Specifically, the amplified RFP- and Tq-encoding DNA sequences were fused to the amplified $CDT1_{(30/120)}$ DNA fragment and the Venus DNA sequence was fused to the amplified $GMNN_{(1/110)}$ DNA fragment. For cloning, I digested the fused PCR products (e.g. the Venus-$GMNN_{(1/110)}$ PCR product with the restriction enzymes BamHI and KpnI) before purification and ligation into a pRRL open vector backbone. The RFP-$CDT1_{(30/120)}$ and the Tq-$CDT1_{(30/120)}$ expression were each set up under the control of the SFFV promoter and the Venus-$GMNN_{(1/110)}$ expression was to be driven by the hPGK promoter. In total, I produced five plasmids, two encoding both, the $CDT1_{(30/120)}$ and the $GMNN_{(1/110)}$ cell cycle indicator fusion proteins (Figure 8, pVG7-RFPC, pVG7-TqC), and three plasmids encoding only one of the cell cycle indicator proteins (Figure 8, pVG, pRRL7-TqC, pRRL7-RFPC).

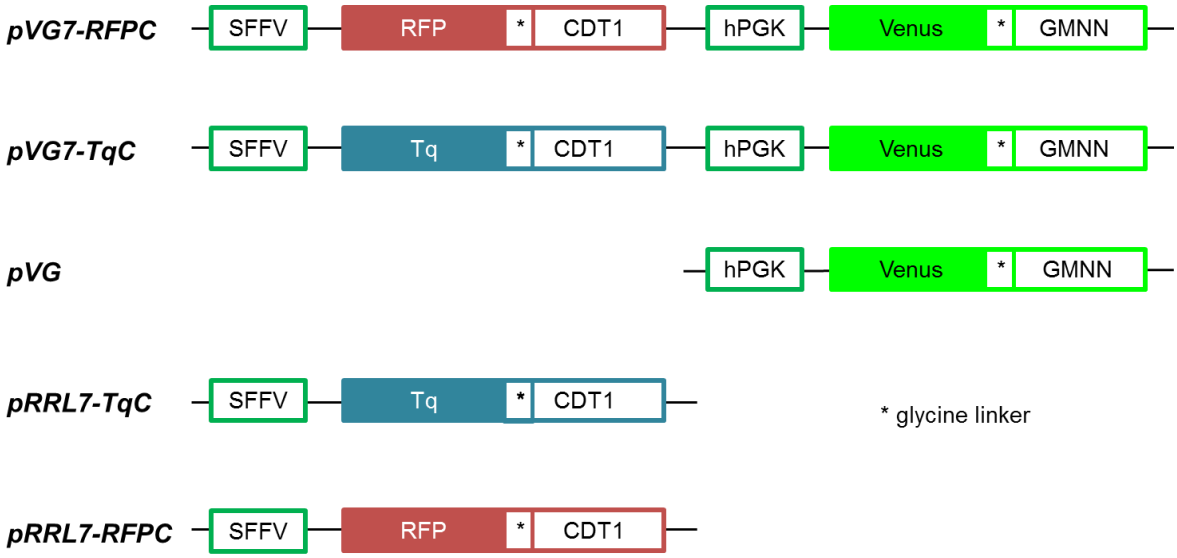

Figure 8: Modified Fucci vectors. Schematic outline of the expression cassettes of the modified Fucci vectors used in this study. *Open boxes in dark green represent the promoter sequences, colored boxes represent the indicated fluorochrome linked to the cell cycle indicator fragment by a glycine linker (*).*

3.1.2 Testing the modified Fucci vectors

I tested the Fucci vectors (Figure 8) by lentiviral vector transduction of the human leukemia cell line OCI-AML2. The transduced cells were analyzed for expression of the integrated vector cassette by flow cytometry. First, I established the flow cytometry protocol including the compensation using the vectors encoding only one fusion protein (single color). Prior to every analysis, a “live gate” determined by the forward scatter (FSC) and side scatter (SSC) parameters was defined to ensure exclusion of cellular debris for analysis (e.g. Figure 9 A, P1). I analyzed the cells for the expression of the cell cycle indicators and used fluorescence-activated cell sorting (FACS) to select for cells stably expressing the Fucci vector cassette. After expansion of the sorted cells, I tested the cell cycle-dependent expression of the cell cycle indicators by sorting cells according to the level of their fluorescence intensity. The sorted cells were re-analyzed using propidium iodide staining (PI staining) to confirm the anticipated cell cycle phase by DNA content analysis. The PI-based re-analysis was also performed by flow cytometry excluding debris, cell doublets and clusters (Figure 9 C) before the analysis of the PI fluorescence intensity, i.e. cell cycle profile.

3.1.2.1 Single vector strategy

First, I tested whether using a single vector encoding for both cell cycle indicator proteins would allow for the separation of cells according to specific cell cycle phases. I transduced one set of OCI-AML2 cells with the vector encoding for RFP-CDT1$_{(30/120)}$ and

Venus-GMNN$_{(1/110)}$ expression (Figure 8, pVG7-RFPC) and another set of cells with the vector encoding for Tq-CDT1$_{(30/120)}$ and Venus-GMNN$_{(1/110)}$ expression (Figure 8, pVG7-TqC). 48 h post transduction, I analyzed the cells expressing RFP-CDT1$_{(30/120)}$ and Venus-GMNN$_{(1/110)}$ for RFP and Venus expression by flow cytometry (Figure 9). A large amount of cells was neither positive for RFP nor for Venus expression (RFP^{neg}/Venus^{neg}: 45 %) comprising the untransduced cells. To select only those cells that stably expressed the cell cycle indicators, I sorted all cells that were either RFP^{pos}, Venus^{pos} or both using a NOT RFP^{neg}/Venus^{neg} gate (Figure 9 B). After expansion of the sorted cells stably expressing RFP-CDT1$_{(30/120)}$ and Venus-GMNN$_{(1/110)}$, they were analyzed a second time by flow cytometry (Figure 9 E). Surprisingly, again, a large fraction of RFP^{neg}/Venus^{neg} cells (25 %) appeared suggesting that the expression of the integrated vector cassette might not lead to sufficient expression levels of the fusion proteins in these cells. As a control for the following PI-based analysis, I chose to sort cells defined by the “live gate” (Figure 9 A, P1). Cells sorted for this gate have the advantage of representing a random sample of all transduced cells undergoing the same treatment, including FACS. The PI-based re-analysis of these control cells showed a regular cell cycle profile (Figure 9 D) when compared to non-modified OCI-AML2 cells, demonstrating that the expression of the fusion proteins did not disturb cell cycle progression (data not shown). Next, I tested the cell cycle-dependency of the fusion protein expression by sorting different cells positive for at least one cell cycle indicator. I sorted RFP^{pos}/Venus^{neg} cells (Figure 9 E) anticipating them to be in the G1 phase of the cell cycle when analyzed by PI-staining. In addition, I sorted RFP^{pos}/Venus^{pos} cells (Figure 9 E) anticipating these cells to be enriched in the S phase when analyzed by PI-staining. However, while PI-based re-analysis showed that as expected RFP^{pos}/Venus^{neg} cells were exclusively in the G1 phase, the double-positive cells contained cells in every phase of the cell cycle (Figure 9 E). In theory, only S phase cells should express both cell cycle indicators simultaneously (RFP^{pos}/Venus^{pos}), while cells in the G1 phase should be exclusively RFP^{pos}/Venus^{neg} and cells in the G2 phase exclusively RFP^{neg}/Venus^{pos}. This lead to the conclusion, that RFP^{pos}/Venus^{pos} cells that were not in the S phase when analyzed by PI-staining were “contaminants” suggesting that either the degradation of RFP-CDT1$_{(30/120)}$ or Venus-GMNN$_{(1/110)}$ did not work properly in the transduced cells. Thus the PI-based re-analysis demonstrated that lentiviral transduction of OCI-AML2 cells with a single vector encoding for RFP-CDT1$_{(30/120)}$ and Venus-GMNN$_{(1/110)}$ did not yield an optimal enrichment of S phase cells. Hence, one vector encoding for the expression of RFP-CDT1$_{(30/120)}$ and Venus-GMNN$_{(1/110)}$ did not allow for a successful cell cycle phase separation. The vector encoding for Tq-CDT1$_{(30/120)}$ and Venus-GMNN$_{(1/110)}$ – pVG-TqC – was tested in the same way as described for the vector encoding for RFP-CDT1$_{(30/120)}$ and Venus-GMNN$_{(1/110)}$ expression. However, the OCI-

AML2 cells showed neither Tq expression nor double-positive cells, only a weak Venus expression was measurable by flow cytometry (data not shown). This observation could be explained by the fact that both fluorochromes originate from GFP (Goedhart et al., 2012; Nagai et al., 2002). When Tq and Venus are encoded in the same vector, due to their high sequence homology, there is a tendency of recombination during reverse transcription in the transduction process, mostly resulting in expression of only one fluorescent protein (Aoki et al., 2012).

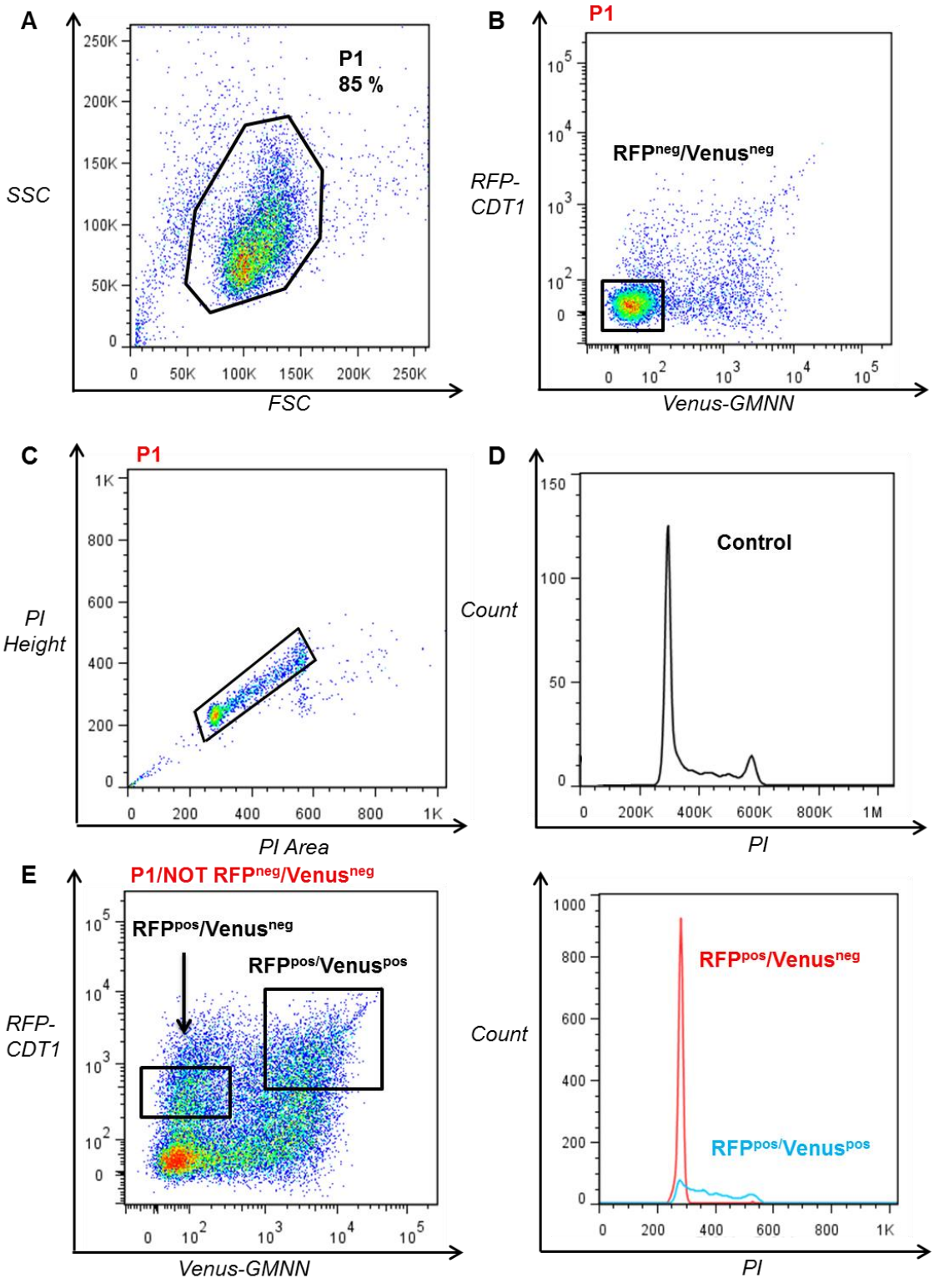

Figure 9: The "single vector strategy" did not lead to a successful cell cycle phase separation of OCI-AML2 cells. (A) Gate used to exclude cellular debris; "live gate" (P1). **(B)** Analysis of RFP-CDT1$_{(30/120)}$ and Venus-GMNN$_{(1/110)}$ expression in OCI-AML2 cells, all cells not RFP^{neg}/Venus^{neg} were sorted to select for the transduced cells. **(C)** Gate to exclude cell doublets for the cell cycle analysis of PI-stained cells. **(D)** PI-based re-analysis of the control, i.e. cells sorted for the "live gate" (P1, A) **(E)** *Left:* Analysis for RFP-CDT1$_{(30/120)}$ and Venus-GMNN$_{(1/110)}$ expression of the cells sorted in (B) and the sort gates for RFP^{pos}/Venus^{neg} and RFP^{pos}/Venus^{pos} cells; *right:* PI-based re-analysis of the RFP^{pos}/Venus^{neg} and RFP^{pos}/Venus^{pos} cells.

3.1.2.2 Dual vector strategy

As the single vector encoding both cell cycle indicator proteins did not lead to a complete cell cycle phase separation, I decided to use separate vectors each encoding only one cell cycle indicator as performed in the initial study (Sakaue-Sawano et al., 2008). Thus, I tested whether an appropriate cell cycle phase separation could be achieved in OCI-AML2 cells upon sequential transduction with two vectors. OCI-AML2 cells were separately transduced with the vectors encoding for RFP-CDT1$_{(30/120)}$ and Tq-CDT1$_{(30/120)}$ expression (Figure 8, pRRL7-RFPC, pRRL7-TqC). 48 h post transduction, I analyzed the cells for RFP and Tq expression by flow cytometry (Figure 10). Interestingly, the transduced cells showed a broad range of RFP and Tq fluorescence intensity (Figure 10), especially when compared to the fluorescence intensity measured testing the single vector strategy (Figure 9). For the selection of cells stably expressing the cell cycle indicators, I sorted the RFP^{pos} and Tq^{pos} cells. To reveal possible differences between cells having a high or low expression level of RFP and Tq, I sorted cells showing a high fluorescence intensity (Figure 10; A: RFP^{high}; B: Tq^{high}) and cells showing a low fluorescence intensity (Figure 10; A: RFP^{low}; B: Tq^{low}).

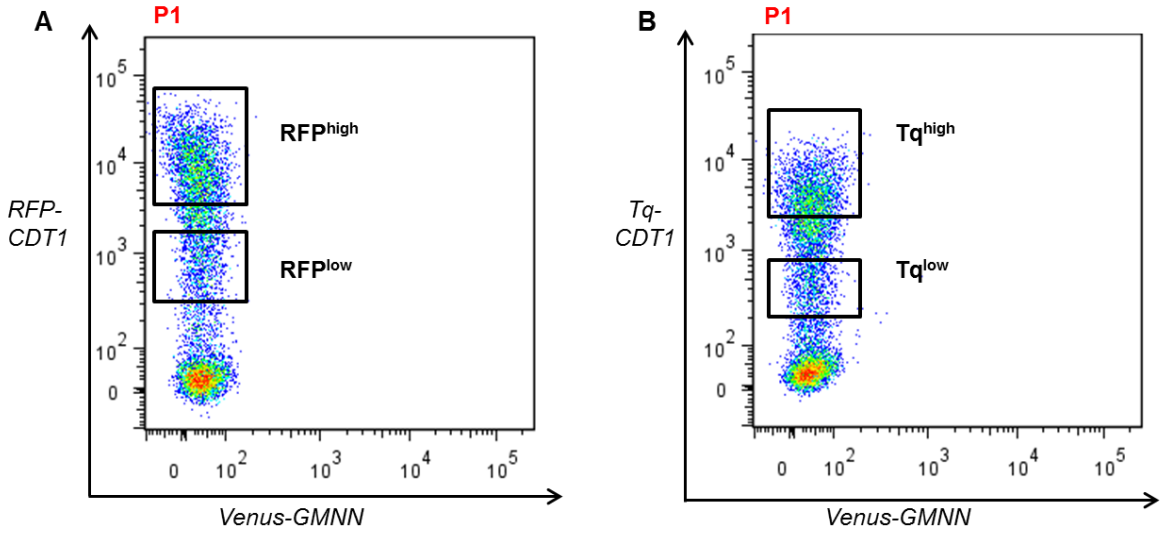

Figure 10: Flow cytometry analysis of OCI-AML2 cells expressing RFP-CDT1$_{(30/120)}$ or Tq-CDT1$_{(30/120)}$ showed a broad range of fluorescence intensity. (A) OCI-AML2 cells analyzed for RFP-CDT1$_{(30/120)}$ expression and the gates for sorting of RFP^{high} and RFP^{low} cells. **(B)** OCI-AML2 cells analyzed for Tq-CDT1$_{(30/120)}$ expression and the gates for sorting Tq^{high} and Tq^{low} cells.

Surprisingly, the RFP^{high} and Tq^{high} cells died within 48 h of further cultivation suggesting that high-level expression of the CDT1$_{(30/120)}$ fusion protein might not be tolerated by the cells. The cells with lower fluorescence intensity of the CDT1$_{(30/120)}$ fusion proteins, OCI-AML2 RFP^{low} and OCI-AML2 Tq^{low}, kept proliferating and could be transduced with the pVG vector (Figure 8) encoding for the expression of the Venus-

$GMNN_{(1/110)}$ fusion protein. Subsequently, the cells were sorted for the $Venus^{pos}$ cells using flow cytometry (Figure 11, A and B).

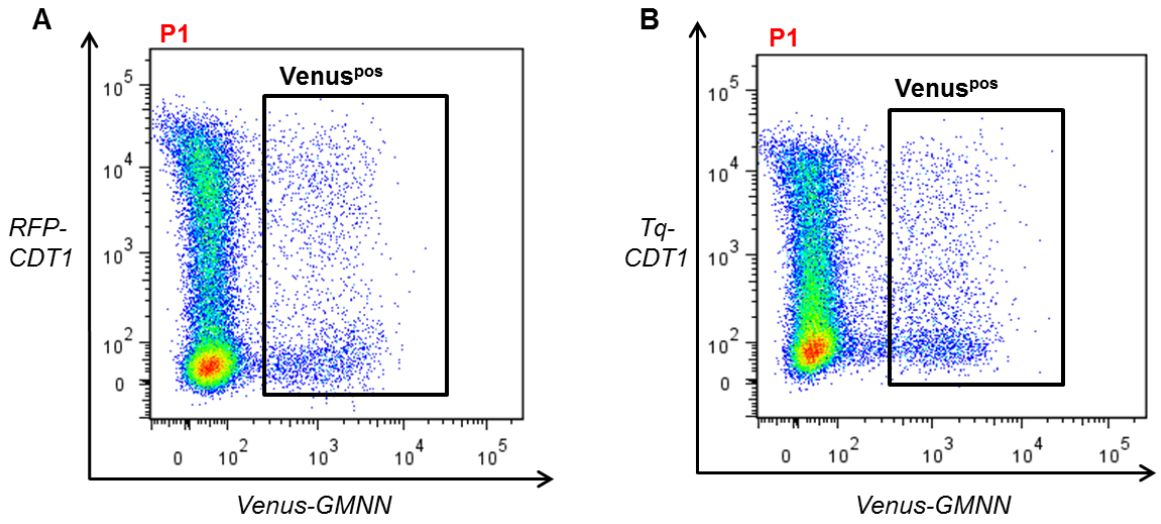

Figure 11: Flow cytometry analysis of OCI-AML2 RFP^{low} and Tq^{low} cells transduced with the vector encoding for Venus-$GMNN_{(1/110)}$ expression. (A) The gate for sorting $Venus^{pos}$ cells of the OCI-AML2 RFP^{low} cells. **(B)** The gate for sorting $Venus^{pos}$ cells of the OCI-AML2 Tq^{low} cells.

The cells transduced and sorted twice, stably expressing both cell cycle indicators were expanded in culture to test whether their fluorescence label would reflect the indicated cell cycle phase.

First, I analyzed the OCI-AML2 cells expressing RFP-$CDT1_{(30/120)}$ and Venus-$GMNN_{(1/110)}$ by flow cytometry. Again many cells were double-negative (40 %; Figure 12, A and B), similar to the results of the single vector strategy (3.1.2.1). As I had selected the transduced cells by FACS (Figure 10; Figure 11), the remaining double-negative cells indicated that the introduced vector cassettes might not lead to sufficient expression levels of the fusion proteins. In addition, the flow cytometric analysis showed that more cells were $RFP^{neg}/Venus^{pos}$ (28 %), representing the cells in the G2 phase, than $RFP^{pos}/Venus^{neg}$ (12 %), representing the cells in the G1 phase of the cell cycle (Figure 12, A and B, left panel). In contrast, PI-based re-analysis of these cells sorted for the "live gate" as a control showed more cells in the G1 phase than the G2 phase (Figure 12 B, control). This finding suggested that the expression of the cell cycle indicators did not label all cells according to their cell cycle phase. To test whether some cells were correctly labeled showing a cell cycle-dependent expression of the fusion proteins, I sorted different cell populations according to their fluorescence intensity. I sorted $RFP^{pos}/Venus^{neg}$ cells (Figure 12 A, P2) and two $Venus^{pos}$ cell populations, one showing a high RFP expression (Figure 12 A, P3), the other showing a low RFP expression (Figure 12 A, P4). As

anticipated the $RFP^{pos}/Venus^{neg}$ (Figure 12 A, P2) cells were exclusively in the G1 phase of the cell cycle when re-analyzed by PI-staining (Figure 12 A, P2). Re-analyzing the $Venus^{pos}/RFP^{high}$ (Figure 12 A, P3) and $Venus^{pos}/RFP^{low}$ (Figure 12 A, P4) cells, I expected both populations to be enriched in the S phase. As the RFP-$CDT1_{(30/120)}$ fusion protein is degraded during the onset of S phase, I anticipated to see an increasing amount of cells in the late S/G2 phase upon reduction in RFP fluorescence intensity. Surprisingly, both cell populations had almost the same cell cycle profile analyzed by PI-staining (FigureFigure 12 A, P3 and P4). Moreover, they both contained cells in all phases of the cell cycle. However, as RFP-$CDT1_{(30/120)}$ is degraded during the S phase and Venus-$GMNN_{(1/110)}$ quickly disappears after M phase, double positive cells ($RFP^{pos}/Venus^{pos}$) should be exclusively in the S phase. Thus, the analysis of the cells expressing RFP-$CDT1_{(30/120)}$ and Venus-$GMNN_{(1/110)}$ did not allow for a strict correlation between fluorescence and cell cycle phase. In contrast, the results of the experiment suggested that most cells either express RFP-$CDT1_{(30/120)}$ constantly or silenced its expression. To clarify this, I sorted RFP^{pos} and RFP^{neg} cells (Figure 12 B, upper left) expecting to see two identical cell cycle profiles by PI-based re-analysis. Indeed, both sorted cell populations showed an almost regular and identical cell cycle profile (Figure 12 B, bottom) as revealed by comparison to the PI-based re-analysis of the control consisting of cells sorted for the "live gate" (Figure 12 B, control). These results demonstrated that some cells were RFP^{pos} throughout the whole cell cycle, while others silenced the RFP-$CDT1_{(30/120)}$ expression and thus stayed RFP^{neg} in every cell cycle phase. Moreover, a selection in favor of the cells that silenced the RFP-$CDT1_{(30/120)}$ expression could explain the high amount of double-negative cells representing the G1 phase cells with a silenced RFP-$CDT1_{(30/120)}$ expression opposite to the small amount of $RFP^{pos}/Venus^{neg}$ cells representing the cells in the G1 phase that did not silence the RFP-$CDT1_{(30/120)}$ expression. Also, as the double-negative cells probably silenced only the RFP-$CDT1_{(30/120)}$ expression, they might still express Venus-$GMNN_{(1/110)}$ in a cell cycle-dependent manner, thus, label the G2 phase cells correctly. This could explain the unusual ratio of $RFP^{neg}/Venus^{pos}$ (G2 phase) to $RFP^{pos}/Venus^{neg}$ (G1 phase) cells initially noticed (Figure 12, A and B).

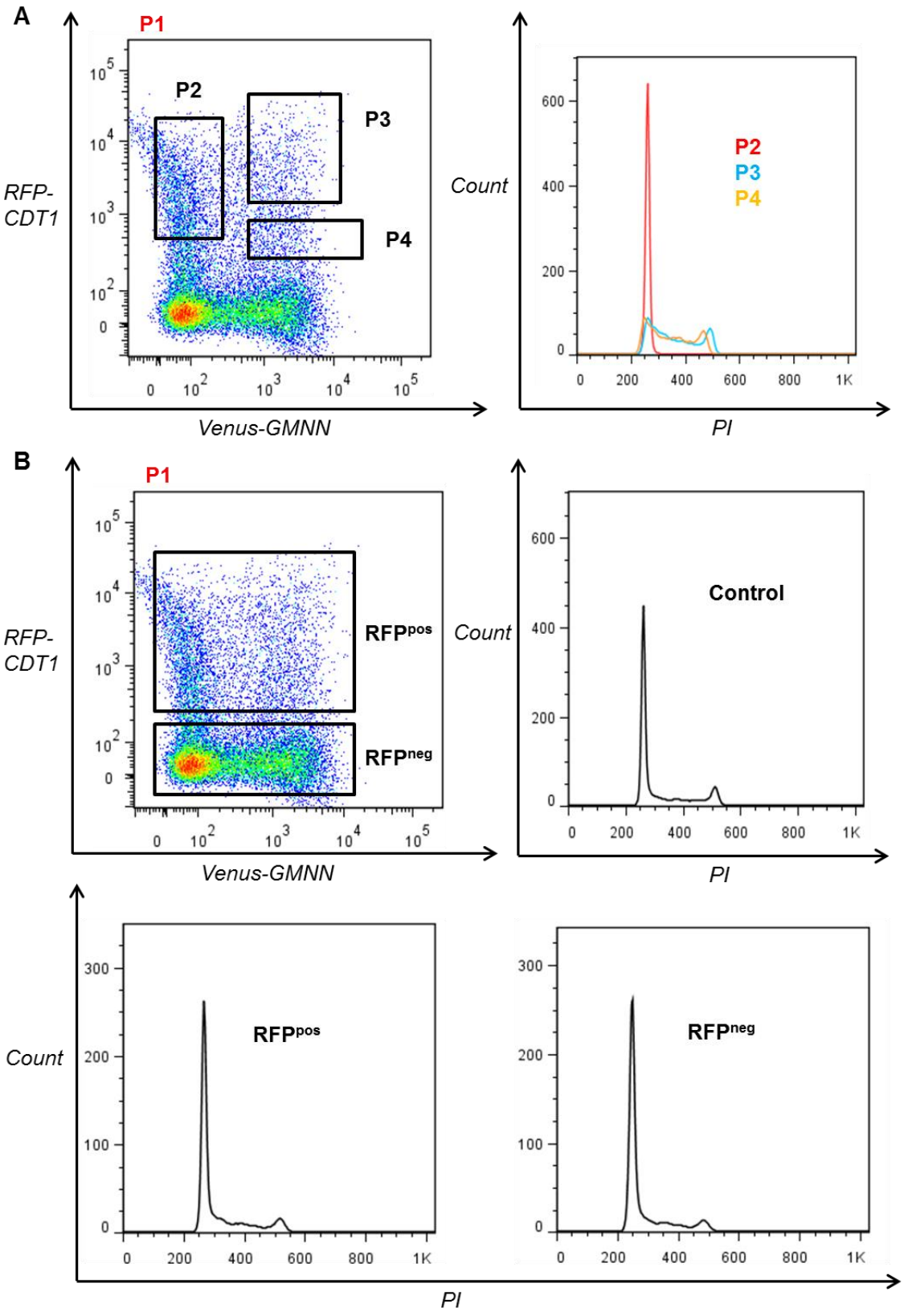

Figure 12: Using two separate vectors did not lead to a successful cell cycle phase separation. (A) Sort gates P2, P3 and P4 used to test the cell cycle-dependence of the cell cycle indicators and the corresponding PI-based re-analysis. **(B)** Sort gates RFP^{pos} and RFP^{neg} (upper left panel), the corresponding PI-based re-analysis (bottom panel) and as a control the PI-based analysis of cells sorted for the "live gate" (control, upper right panel).

These data showed that the separation of the different cell cycle phases by flow cytometry through the expression of RFP-CDT1$_{(30/120)}$ and Venus-GMNN$_{(1/110)}$ introduced by sequential transduction of OCI-AML2 cells was not feasible. However, RFP being a tetrameric protein might have led to the problems I faced introducing RFP-CDT1$_{(30/120)}$ as the G1 cell cycle indicator. Thus, I decided to test whether the dual vector strategy would work using Tq, which is a monomeric protein. Again, the flow cytometry analysis of OCI-AML2 cells expressing Tq-CDT1$_{(30/120)}$ and Venus-GMNN$_{(1/110)}$ showed a large number of Venus^{neg}/Tq^{neg} cells (30 %; e.g. Figure 13 A) although they had been previously enriched for cell stably expressing both vectors (Figure 10; Figure 11). Additionally, more cells were Venus^{pos}/Tq^{neg} (43 %) representing cells in the G2 phase compared to Tq^{pos}/Venus^{neg} cells (6 %) representing the G1 phase (e.g. Figure 13 A), consistent with the observation testing the dual vector strategy with RFP-CDT1$_{(30/120)}$ as the G1 phase indicator (Figure 12, A and B). This finding already indicated that the dual vector strategy using Tq-CDT1$_{(30/120)}$ might as well show an incorrect labeling of the cell cycle phases. To clarify this, I tested the cell cycle-dependence of the cell cycle indicator proteins by sorting five different cell populations. First, I sorted three cell populations similar to the ones I used for the analysis of the RFP-CDT1$_{(30/120)}$ and Venus-GMNN$_{(1/110)}$ expressing cells. Two Venus^{pos} cell populations, one showing a high Tq expression (Figure 13 A, P2), the other showing a low Tq expression (Figure 13 A, P3). Similar to the analysis of RFP-CDT1$_{(30/120)}$ and Venus-GMNN$_{(1/110)}$ expressing cells, PI-based re-analysis of these two populations – Tq^{high}/Venus^{pos} and Tq^{low}/Venus^{pos} – showed that both had almost the same cell cycle profile (Figure 13 A) and were not only enrichment in the S phase, but also in the G2 phase (Figure 13 A). This indicated that, although the Tq-CDT1$_{(30/120)}$ should be degraded towards the end of the S phase of the cell cycle, some cells show a constant Tq expression. To confirm this, I sorted a third cell population containing all cells that were Tq^{pos} (Figure 13 B) expecting to see a regular cell cycle profile instead of an enrichment of cells in the G1/S phase. Indeed, the PI-based re-analysis showed an almost regular cell cycle profile (Figure 13 B) similar to that of the RFP^{pos} cells analyzed earlier (Figure 12 B). Again, this led to the conclusion that some cells stay Tq^{pos} throughout the whole cell cycle, meaning the Tq-CDT1$_{(30/120)}$ is not degraded properly in the S phase.

While the G1 phase cell cycle indicators – the CDT1$_{(30/120)}$ fusion proteins – were either not degraded in a cell cycle-specific manner or their expression was silenced, Venus-GMNN$_{(1/110)}$ appeared to be accumulated and degraded cell cycle-dependently. Thus, to test whether the change in Venus-GMNN$_{(1/110)}$ fluorescence intensity did correlate with the cell cycle progression and might be used to separate a cell population into different cell cycle phases, I sorted two additional cell populations: Venus^{low}/Tq^{neg} cells

(Figure 13 C, P4) and Venus^{high}/Tq^{neg} cells (Figure 13 C, P5). As Venus-GMNN$_{(1/110)}$ accumulates over S/G2 phase, I expected the Venus fluorescence intensity to increase towards the G2 phase of the cell cycle. Consequently, I expected that the Venus^{low}/Tq^{neg} cell population (Figure 13 C, P4) would be enriched in the S phase and the Venus^{high}/Tq^{neg} cell population (Figure 13 C, P5) in late S/G2 phase. Indeed, the PI-based re-analysis of the sorted cells confirmed these predictions (Figure 13 C). Although the analysis of the OCI-AML2 cells expressing Tq-CDT1$_{(30/120)}$ and Venus-GMNN$_{(1/110)}$ did not lead to a successful cell cycle phase separation, the results strongly indicated the possibility to use Venus-GMNN$_{(1/110)}$ as a single cell cycle indicator allowing for a very precise and unperturbed cell cycle phase separation.

In summary, neither the dual vector strategy with RFP-CDT1$_{(30/120)}$ and Venus-GMNN$_{(1/110)}$ nor with Tq-CDT1$_{(30/120)}$ and Venus-GMNN$_{(1/110)}$ led to the desired result of an accurate cell cycle phase separation by flow cytometry. Both CDT1$_{(30/120)}$ fusion proteins were either expressed throughout the whole cell cycle or had been silenced. However, the Venus-GMNN$_{(1/110)}$ fusion protein seemed to be accumulated and degraded in a cell cycle dependent manner as I could separate two cell cycle phases by Venus fluorescence intensity, only (Figure 13 C). Thus, I decided to focus on establishing a cell cycle-readout relying on the Venus-GMNN$_{(1/110)}$ expression as a single cell cycle indicator.

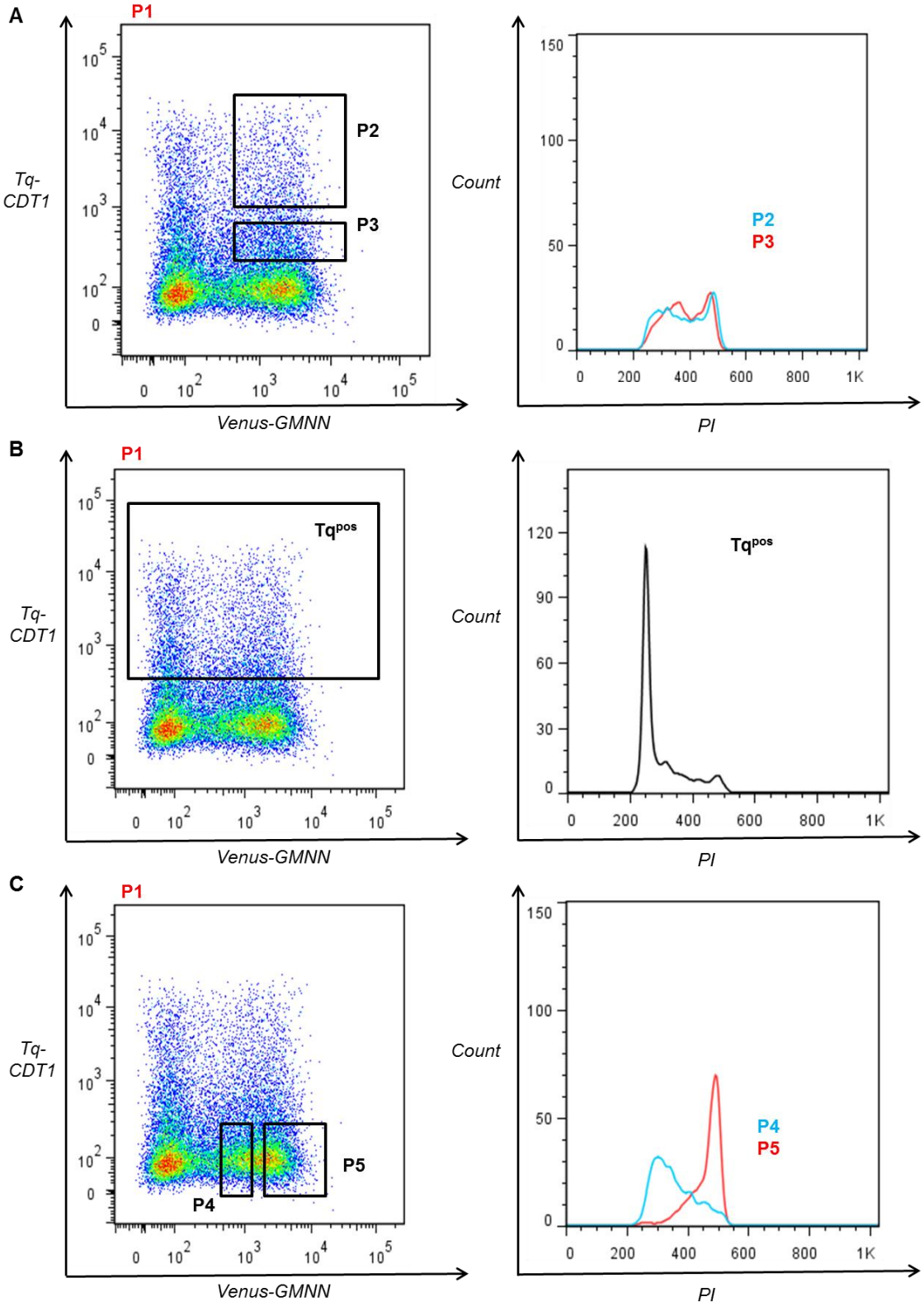

Figure 13: The expression of Tq-CDT1$_{(30/120)}$ and Venus-GMNN$_{(1/110)}$ in OCI-AML2 cells did not lead to a successful cell cycle phase separation but suggested that Venus-GMNN$_{(1/110)}$ could be useful as a single cell cycle phase indicator. (A) Sort gates P2 and P3 used to test the cell cycle dependent expression of Tq-CDT1$_{(30/120)}$ and Venus-GMNN$_{(1/110)}$ and the corresponding PI-based re-analysis. **(B)** Sort gate Tq^{pos} and the corresponding PI-based re-analysis. **(C)** Sort gates P4 and P5 used to test the cell cycle-dependent expression of Venus-GMNN$_{(1/110)}$ and the corresponding PI-based re-analysis.

3.1.3 Venus-GMNN$_{(1/110)}$ as single cell cycle indicator

As the Venus-GMNN$_{(1/110)}$ fusion protein degradation and accumulation within the cell cycle appeared to function properly, I proceeded in testing whether Venus-GMNN$_{(1/110)}$ as a single cell cycle indicator for the S/G2/M phase could be used to separate cells into all cell cycle phases. Aiming to work with murine HSPCs, I performed the experiments in murine hematopoietic cell lines, starting with 32D cells, a well-established murine cell line. I first transduced the cells with the vector encoding for the Venus-GMNN$_{(1/110)}$ expression only (Figure 8). The transduced cells were enriched by sorting the Venus^{pos} cells and after further expansion sorted into different cell populations according to the Venus fluorescence intensity. After sorting, I analyzed the cell cycle phase of the sorted cells by PI-based re-analysis. I expected an increase in mVenus fluorescence intensity with progression of the cells towards the G2 phase. Thus, the Venus^{neg} cells should be enriched in the G1 phase, the Venus^{low} cells in the S phase and the Venus^{high} cells in the G2 phase of the cell cycle.

3.1.3.1 Venus-GMNN$_{(1/110)}$-based cell cycle analysis in the 32D cell line

I transduced 32D cells with the pVG vector (Figure 8) to test whether the expression of Venus-GMNN$_{(1/110)}$ could be used as a single cell cycle indicator in a simple murine hematopoietic cell line. After transduction, I selected the cells for the expression of Venus-GMNN$_{(1/110)}$ by FACS. The analysis of an untransduced control of 32D cells (Figure 14 A) was used to set the correct gate for sorting the Venus^{pos} cells (Figure 14 B).

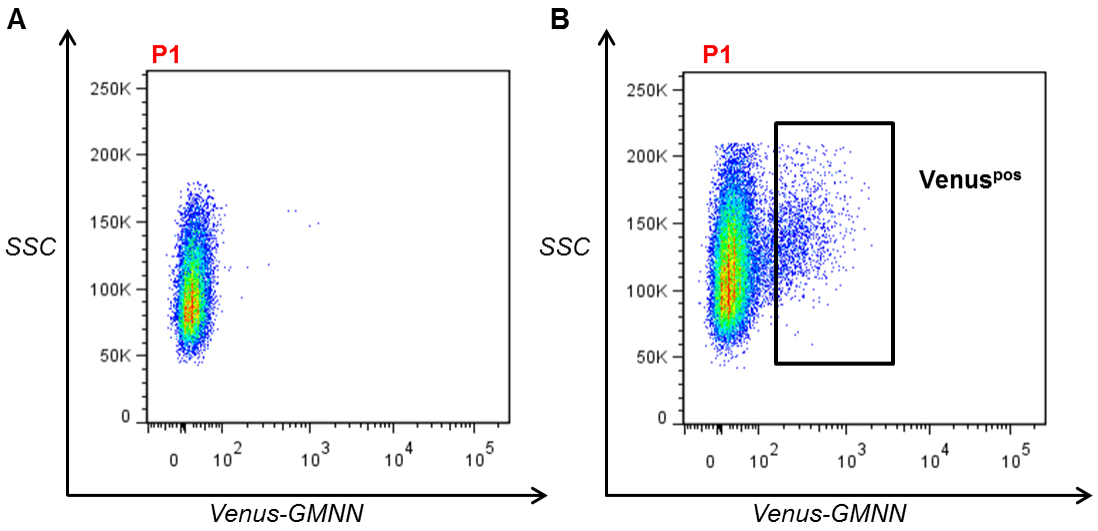

Figure 14: Flow cytometry analysis of 32D cells. (A) Untransduced 32D cells. **(B)** 32D cells expressing Venus-GMNN$_{(1/110)}$ and the sort gate for Venus^{pos} cells.

After further expansion, the sorted cells should stably express the Venus-GMNN$_{(1/110)}$ fusion protein (32D VG). Next, they were sorted into subpopulations by flow cytometry aiming to test the cell cycle-dependency of the Venus-GMNN$_{(1/110)}$ expression. Gaiting on the "live gate" (Figure 15 A, P1), I sorted five cell populations with increasing Venus fluorescence intensity (Figure 15 B, P2-6).

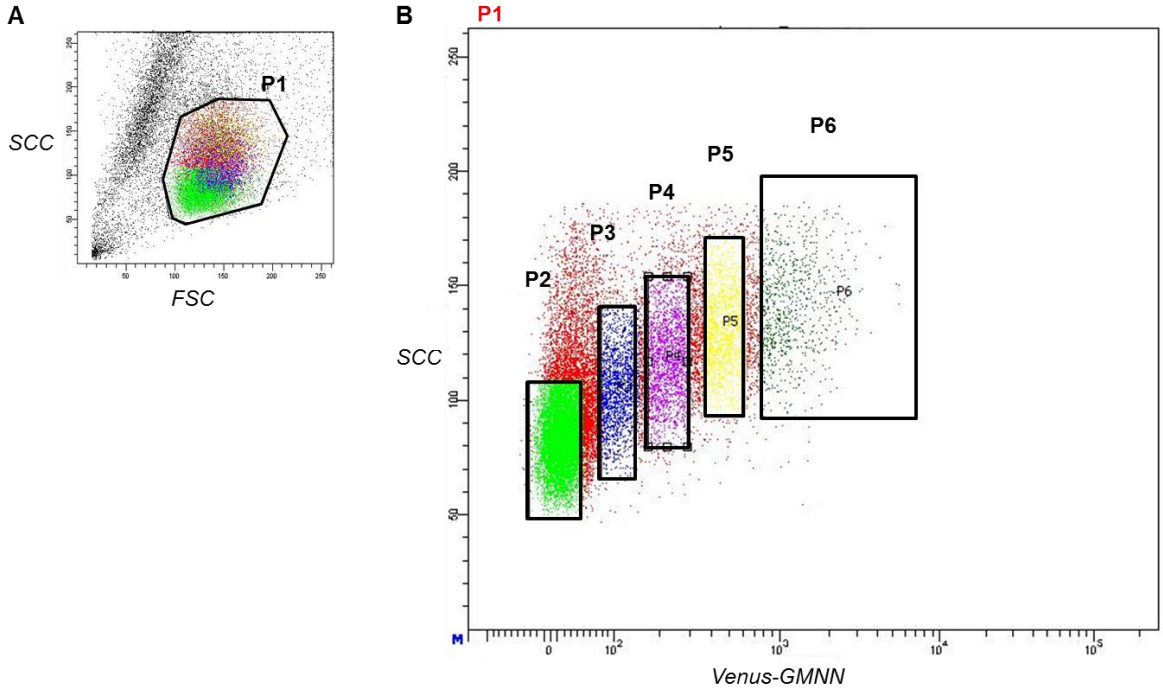

Figure 15: Flow cytometry sorting of 32D VG cells. (A) "Live gate" (P1). **(B)** Sort gates according to the Venus fluorescence intensity.

As Venus-GMNN$_{(1/110)}$ accumulates over S/G2, the Venus fluorescence intensity should increase, as well. I expected Venus^{neg} cells (Figure 15 B, P2) to be in the G1 phase of the cell cycle. Thus, I anticipated the cells with the lowest Venus intensity (Figure 15 B, P3) to be in the late G1/early S phase and the cells with the highest Venus intensity (Figure 15 B, P6) to be in the late S/G2 phase. Indeed, PI-based re-analysis of the sorted cells confirmed these expectations (Figure 16). The sorted Venus^{neg} cell population (Figure 15 B, P2) showed a pure G1 phase peak (Figure 16, P2), while the cells sorted for increasing Venus fluorescence intensity (Figure 15 B, P3-6) each were enriched in a different cell cycle phase displaying a progress from the G1 to the G2 phase: the P3 cell population (Figure 15 B) was enriched in the late G1/S phase (Figure 16, P3), the P4 cell population (Figure 15 B) in the S phase (Figure 16, P4), the P5 cell population (Figure 15 B) in the S/early G2 phase (Figure 16, P5) and the P6 cell population (Figure 15 B) in the late S/G2 phase (Figure 16, P6). Importantly, PI-based re-analysis of cells sorted for the "live gate" (Figure 15 A, P1) as a control showed a regular cell cycle profile (Figure 16,

P1) supporting that the Venus-GMNN$_{(1/110)}$ expression did not alter the typical distribution of cells in each cell cycle phase.

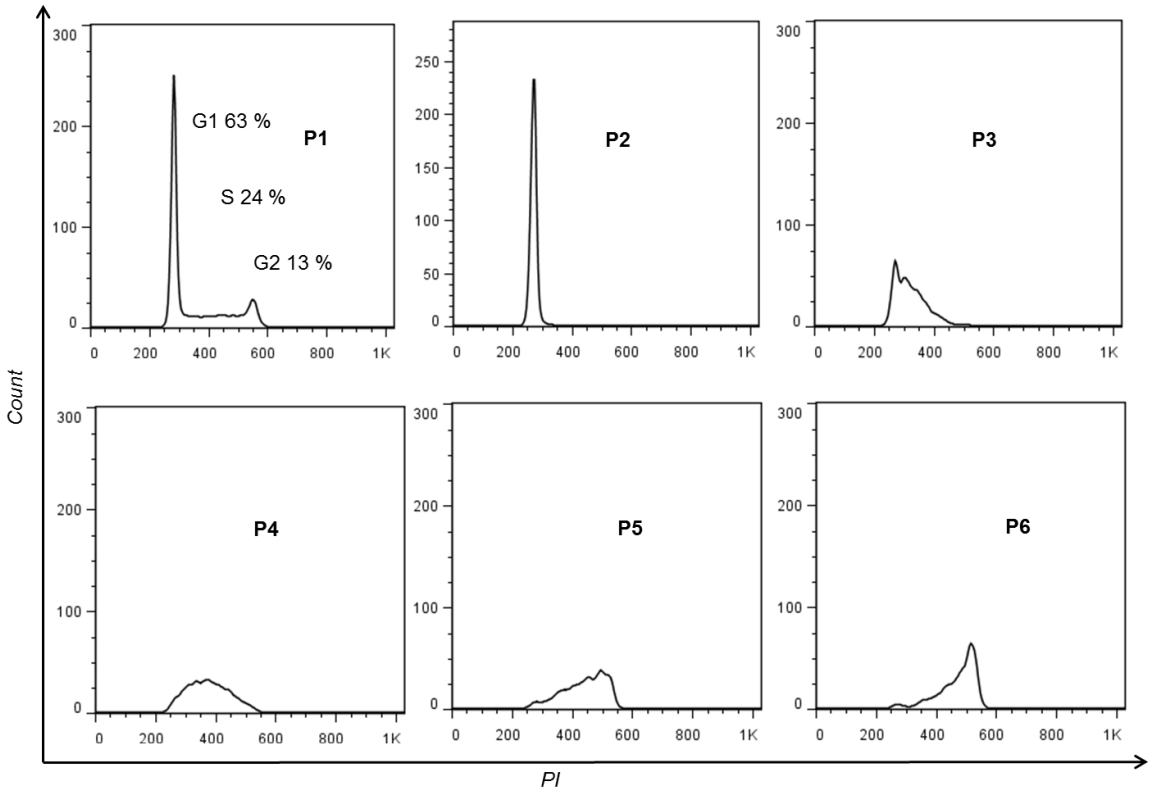

Figure 16: PI-based re-analysis of the 32D VG cells sorted according to the Venus-GMNN$_{(1/110)}$ fluorescence intensity revealed a distinct cell cycle phase separation. PI-based re-analysis of the cells sorted for the "live gate" and the gates sorted according to the Venus fluorescence intensity (Figure 15, A and B, P1-P6).

In conclusion, Venus-GMNN$_{(1/110)}$, as a single cell cycle indicator, allowed for a very distinct cell cycle phase separation of the 32D VG cells. The sorted populations were enriched without perturbation of the cell cycle progression and thus, this experimental design promised the possibility of a highly accurate gene expression analysis at the cell cycle phase level.

3.1.3.2 Venus-GMNN$_{(1/110)}$-based cell cycle analysis in the EML cell line

To confirm my findings, I tested the described setup using the EML cell line, as well. The EML cell line is a murine hematopoietic progenitor cell line immortalized by a retroviral vector encoding a dominant-negative version of the retinoic acid receptor (Tsai et al., 1994). This cell line has differentiation potential and, thus, is very close to primary murine HSPCs. I transduced the cells with the vector encoding for the Venus-GMNN$_{(1/110)}$ expression (Figure 8) and selected for the transduced cells by sorting the Venus^{pos} cells (EML VG), as described before (3.1.3.1). After 48 h of further cultivation, I analyzed the

sorted EML VG cells a second time for their Venus-GMNN$_{(1/110)}$ expression using flow cytometry (Figure 17, A and B).

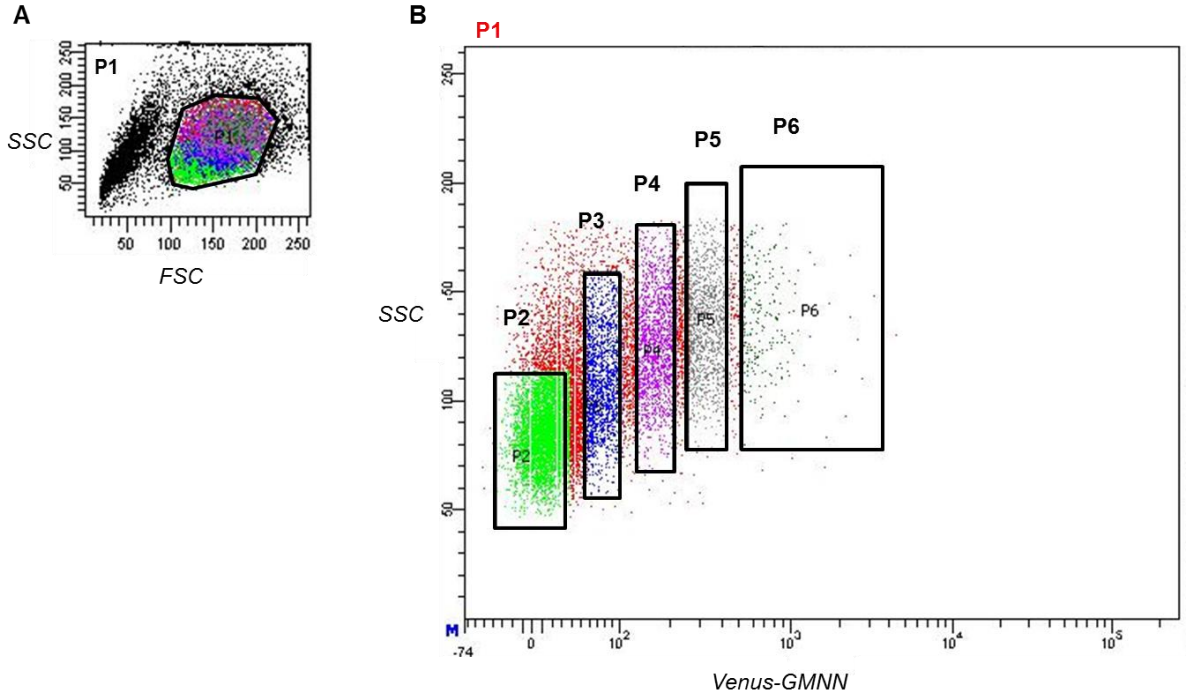

Figure 17: Flow cytometry sorting of EML VG cells. (A) "Live gate" (P1). **(B)** Sort gates according to the Venus fluorescence intensity.

To show that neither expression of Venus-GMNN$_{(1/110)}$ nor the FACS would alter the cell cycle profile of the EML cells, I used the following three controls: untransduced and unsorted EML cells, as a non-treated control, unsorted EML VG cells and EML VG cells sorted for the "live gate" (Figure 17 A, P1). Indeed, the PI-based re-analysis showed that all of the three analyzed controls had an almost identical and regular cell cycle profile (Figure 18) underlining that the Venus-GMNN$_{(1/110)}$ vector expression allowed for an unperturbed cell cycle phase progression.

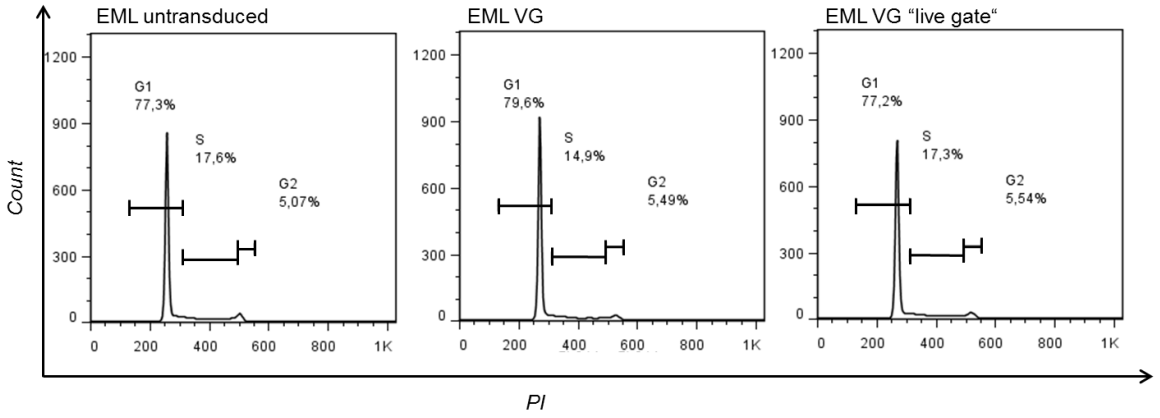

Figure 18: Comparison of the PI-based analysis of controls consisting of differentially treated EML cells underlined that expression of Venus-GMNN$_{(1/110)}$ did not alter the cell cycle progression. EML cells untransduced and unsorted, EML VG cells unsorted and EML VG cells sorted for the "live gate" were analyzed after PI-staining.

I anticipated that PI-based re-analysis of the five cell populations I sorted according to their Venus fluorescence intensity (Figure 17 B, P2-P6) would show a similar cell cycle phase separation compared to those obtained with 32D VG cells. Indeed, as expected the Venus^{neg} cells were enriched in the G1 phase (Figure 19, P2) while the cells with the highest Venus fluorescence intensity were enriched in the late S/G2 phase (Figure 19, P6). This analysis confirmed that the Venus fluorescence intensity can be used to separate the cell cycle phases.

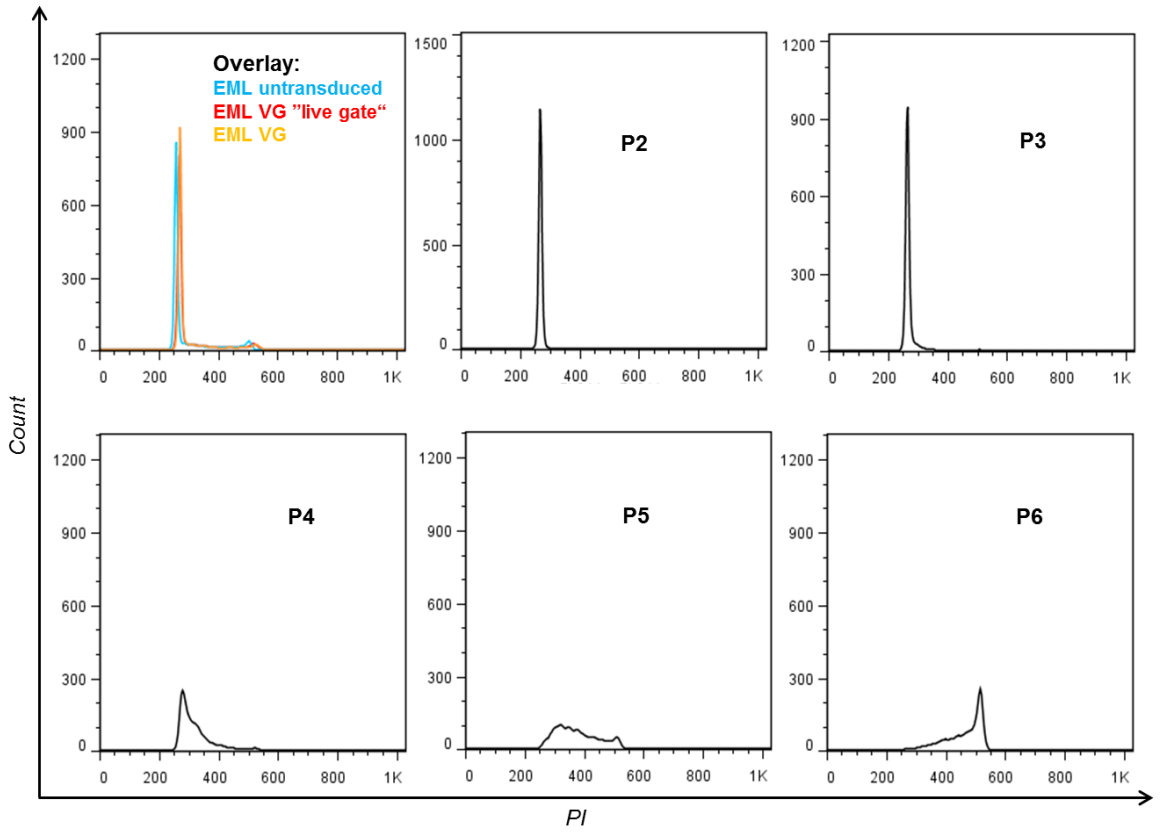

Figure 19: PI-based re-analysis of the EML VG cells sorted according to the Venus-GMNN$_{(1/110)}$ fluorescence intensity revealed a distinct cell cycle phase separation. Overlay of cell cycle profiles from EML control cells (Figure 18) and PI-based re-analysis of the gates sorted according to the Venus fluorescence intensity (Figure 17 B, P2-6).

3.1.3.3 Expression of cell cycle marker genes in EML VG cells

Next, to confirm that cells of each sorted cell cycle phase population indeed reflected their cell cycle stage by expression of specific marker genes, I performed gene expression analysis experiments for selected genes. I chose *E2f transcription factor 1* (E2f1) and *cyclin E1* (Ccne1) as indicators for the G1/S phase, *dihydrofolate reductase* (Dhfr) as indicator for the S phase and *forkhead box M1* (Foxm1) as indicator for the G2 phase. As controls, I used EML VG cells, unsorted (Figure 20, control) or sorted for the "live gate" (Figure 17, P1; Figure 20, P1).

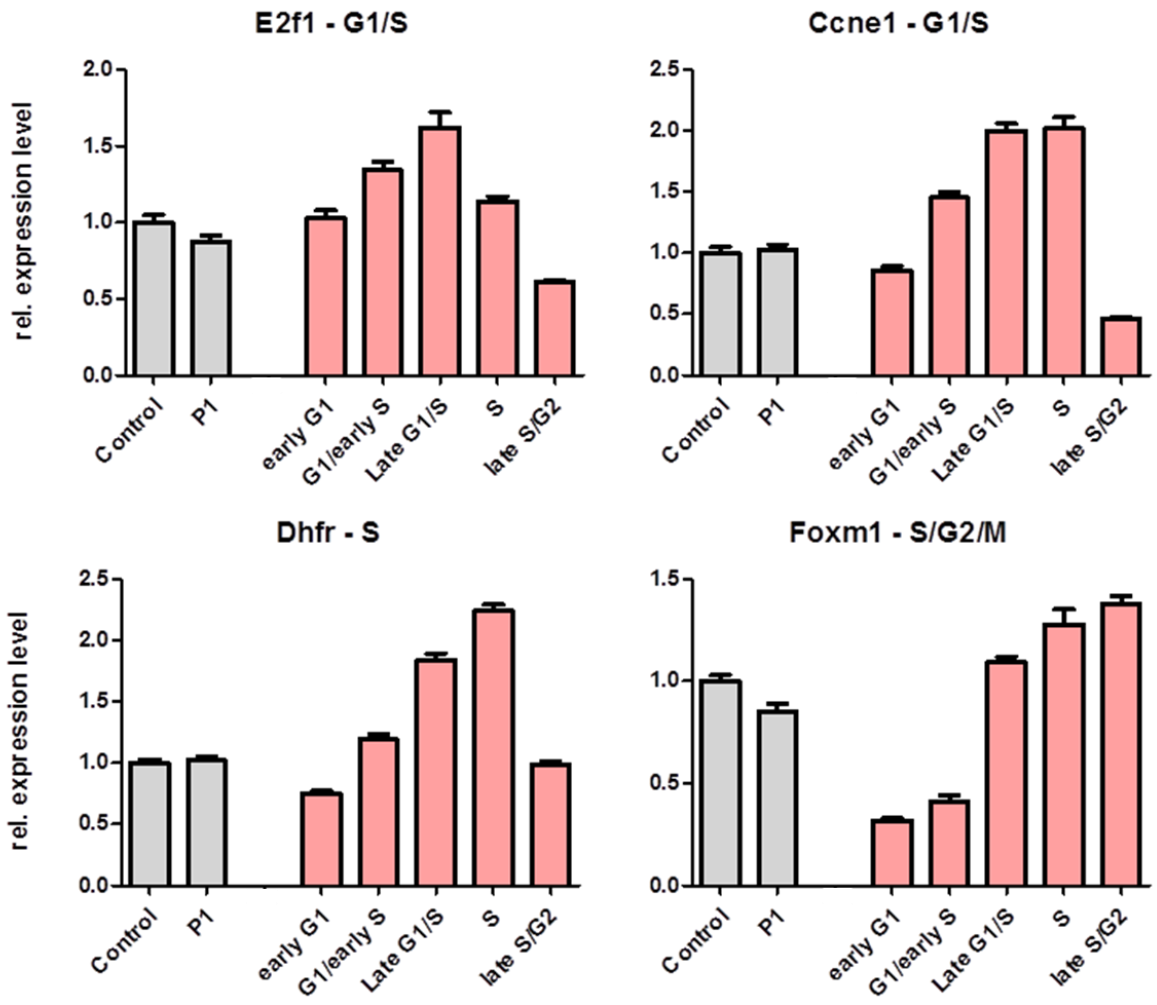

Figure 20: Gene expression in EML VG cells sorted according to the Venus-GMNN$_{(1/110)}$ fluorescence intensity showed known cell cycle phase distribution of the expression of the chosen cell cycle genes. QRT-PCR analysis was performed for known cell cycle genes in the EML VG cells sorted according to the Venus fluorescence intensity (Figure 17, P2-6;). Controls were EML VG cells unsorted (control) and sorted for the "live gate" (Figure 17, P1). *Measurements were performed in triplicates.*

The QRT-PCR results confirmed the known cell cycle phase dependence of expression levels for the chosen cell cycle genes (Figure 20). For example, Dhfr, a typical S phase gene, had its highest expression level within the S phase cell population (Figure 20). Also, the gene expression levels in the two controls did not show a significant difference compared to each other. This verified that the sorting of cells according to their cell cycle phase allowed for an accurate analysis of gene expression.

Taken together, the results of the gene expression analysis and the PI-based analyses underlined the fact that the separation of the cell cycle phases using Venus-GMNN$_{(1/110)}$ did not disturb the expression of known cell cycle genes or the progression of the cell cycle. Thus, the established method allowed for an unperturbed enrichment of

different cell cycle phases even in a cell line that is closely related to undifferentiated primary hematopoietic cells.

3.2 Clonal dominance of HSPCs mediated by sub-haploinsufficient Mybl2 expression levels

3.2.1 Clonal expansion of HSPCs *in vitro*

Recently, MYBL2 has been identified as a sub-haploinsufficient tumor suppressor in MDS, inducing myelodysplastic tumor growth in a gene dosage dependent manner at an expression level of 30 - 50 % (Heinrichs et al., 2013). In the mentioned study, a competitive bone marrow transplantation assay in mice showed that primary murine bone marrow cells with sub-haploinsufficient expression levels of Mybl2 – mediated by RNA interference (RNAi) – became clonally dominant and the mice developed myeloid disorders. To date, it had not been tested whether a sub-haploinsufficient expression level of Mybl2 would also have a clonal advantage for murine lineage-negative (lin.-neg.) enriched bone marrow cells *in vitro*.

Prior to testing whether HSPCs with reduced Mybl2 expression level would expand *in vitro*, the knockdown efficiency of the specific Mybl2 shRNA used in the study mentioned above was tested in EML cells and freshly isolated murine HSPCs from wild-type mice using QRT-PCR for Mybl2 expression analysis. A reduced Mybl2 expression level of 30 - 50 % was successfully reached after introduction of the constitutively expressed Mybl2 shRNA via lentiviral vector transduction (Figure 21).

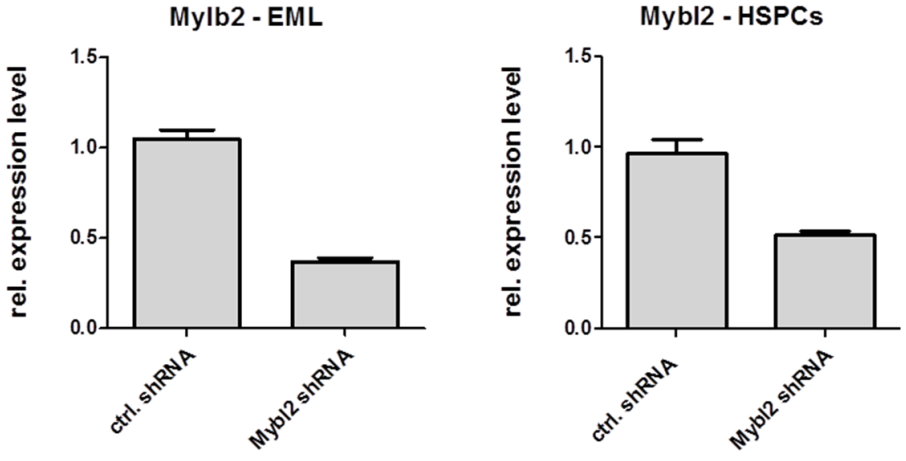

Figure 21: Knockdown verification in EML cells and HSPCs. The knockdown efficiency of the Mybl2 shRNA to a 30 - 50 % expression level of Mybl2 was successfully tested *in vitro*. Control cells were transduced with a lentiviral vector encoding an ill-defined shRNA (ctrl. shRNA). *Measurements were performed in triplicates.*

In order to test the expansion of murine HSPCs *in vitro* upon an RNAi mediated Mybl2 knockdown to levels of 30 - 50 % (Mybl2 shRNA), I first isolated lin.-neg. enriched murine bone marrow cells from wild type mice. 24 h later, one part of the isolated cells was transduced with a lentiviral vector encoding the tested Mybl2 shRNA. To have different controls in this experiment, I transduced another part of the isolated cells with one of two lentiviral vectors each encoding an ill-defined shRNA (ctrl. shRNA1 and ctrl. shRNA2). Additionally, some cells were left as untransduced controls. All lentiviral vectors carried a red fluorescent protein sequence (DsRed-Express2/RFP) (Strack et al., 2008) to enable monitoring of the frequency of transduced cells by flow cytometry. 48 h post transduction, I first measured the RFP frequency in each of the three transduced cell cultures. Subsequently, I adjusted the frequency of RFP positive cells by addition of non-transduced cells, in order to start monitoring cell growth and possible clonal dominance from the same level of transduced cells in each culture.

After the first week in culture, basically no difference in growth could be measured. However, during the course of the second week all control cell cultures lost their proliferative capacity, while cells with a reduced Mybl2 expression level kept expanding (Figure 22). This already indicated a proliferative advantage of cells, induced by reduced Mybl2 expression levels *in vitro*.

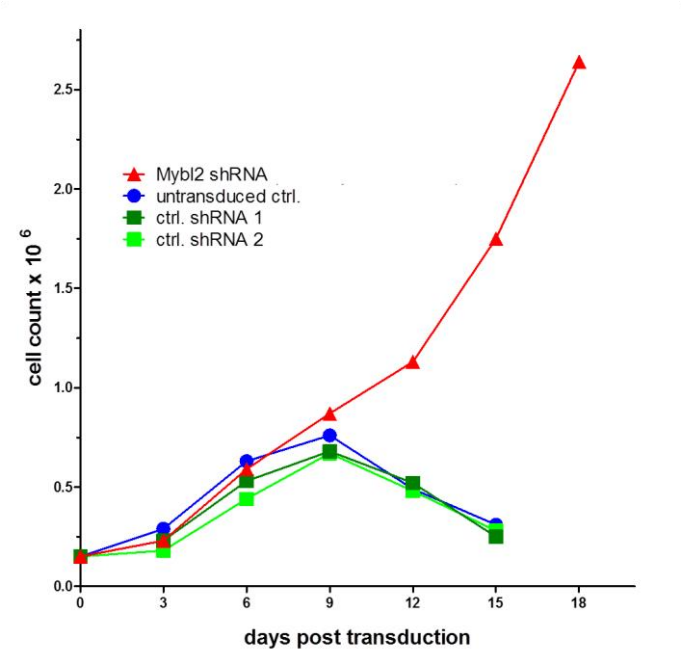

Figure 22: Clonal dominance *in vitro*. Growth of murine lineage-negative enriched bone marrow cells either untransduced, transduced with a control shRNA (ctrl. shRNA 1 or 2) or a specific Mybl2 shRNA encoding vector. *Cell count was performed using a Neubauer counting chamber.*

In a weekly interval, I measured the RFP frequency of each transduced cell culture. While the RFP frequency, thus the frequency of transduced cells, was stable in the control cells, the RFP frequency in the cell culture with a low Mybl2 expression level increased significantly over time (Figure 23 A). This supported the idea that low expression levels of Mybl2 result in a proliferative and clonal advantage of HSPCs *in vitro*. In addition to monitoring the RFP frequency, I analyzed the immunophenotype of the cell cultures using a standard immunophenotyping panel for HSPCs to determine the amount of lin.-neg., thus immature, cells within each culture. I anticipated that, while cells with low Mybl2 expression levels would stay rather immature over the monitored course of time, the control cells would differentiate. Indeed, while control cells were fully differentiated after two weeks, the cell culture with a reduced Mybl2 expression level kept increasing the amount of lineage negative cells over time reaching a frequency of almost 90 % after 30 days in culture (Figure 23, B and C). Morphologic analysis of cytospins performed with the same cultures after about two weeks of proliferation supported these findings (data not shown).

This demonstrated that freshly isolated lin.-neg. enriched murine bone marrow cells proliferate and differentiate in cell culture within two weeks. In contrast, cells with a low Mybl2 expression level gain a self-renewal potential, show clonal dominance and a proliferative advantage. Over time, the amount of lin.-neg. cells driven by reduced expression levels of Mybl2 increased and an immature cell population could be observed. In summary, a Mybl2 knockdown to expression levels between 30 - 50 % led to immortalization of hematopoietic stem and progenitor cells *in vitro*.

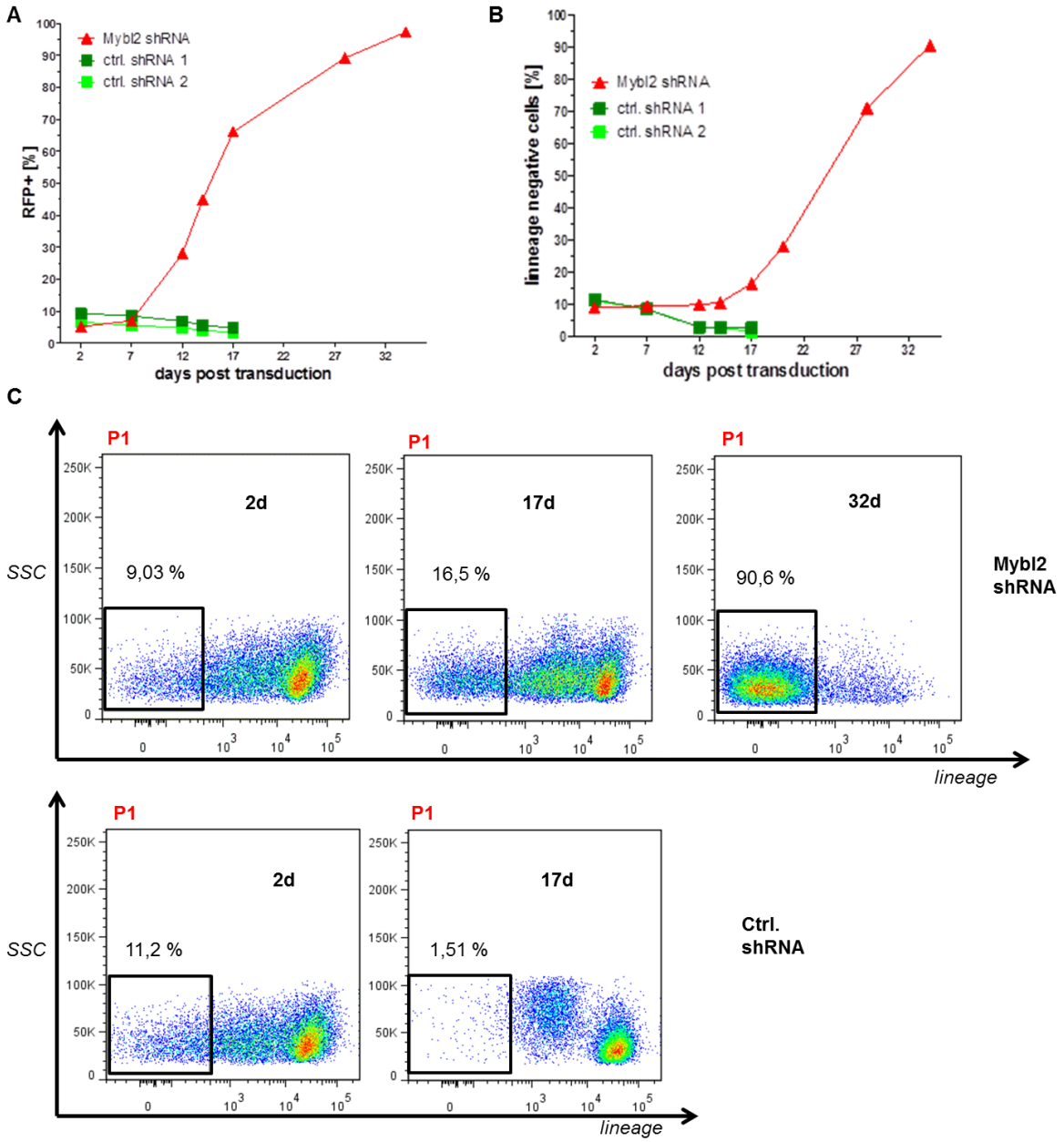

Figure 23: Immunophenotype of cells with a low Mybl2 expression level *in vitro*. **(A)** RFP frequency of the cells transduced with a control shRNA (ctrl. shRNA 1 or 2) or a specific Mybl2 shRNA encoding vector. **(B)** Frequency of lineage negative cells in cells transduced with a control shRNA (ctrl. shRNA 1 or 2) or a specific Mybl2 shRNA encoding vector. **(C)** Flow cytometry analysis of the cells transduced with the specific Mybl2 shRNA and one control shRNA at different time points post transduction. *(d = days). Cells were stained with a lineage detection cocktail containing antibodies against epitopes of murine CD11b, Ly6-G/C, CD45R, CD5, Terr119, 7-4.*

3.2.2 Establishment of an inducible ectopic Mybl2 expression

In order to address the question which genes are affected by the Mybl2 knockdown, I took advantage of a transgenic mouse line expressing a transcription factor with inducible transcriptional activity. This setup allowed reverting low levels of Mybl2, and possibly the proliferative phenotype seen in lin.-neg. enriched murine bone marrow cells *in vitro* (3.2.1). Meaning, re-expression of ectopic wild-type Mybl2 would ideally "rescue" the proliferative advantage and, consequently, stop cell growth.

3.2.2.1 Tetracycline controlled transcription

To control gene expression in an inducible and reversible manner, tetracycline controlled transcription has become very important for experimental setups. In this thesis, a transgenic mouse line (Rosa26 M2-rtTA, 2.1.8) expressing a reverse tetracycline-controlled transactivator protein, M2-rtTA (Gossen and Bujard, 1992; Urlinger et al., 2000), with inducible transcriptional activity, was used. All cells taken from these mice constitutively express a tetracycline-controlled transcription factor (rtTA) that is activated in presence of doxycycline. It binds to the TetOperator and activates transcription (Figure 24) (Hochedlinger et al., 2005). In my experiments Mybl2 was introduced as the downstream target to be inducible upon doxycycline treatment.

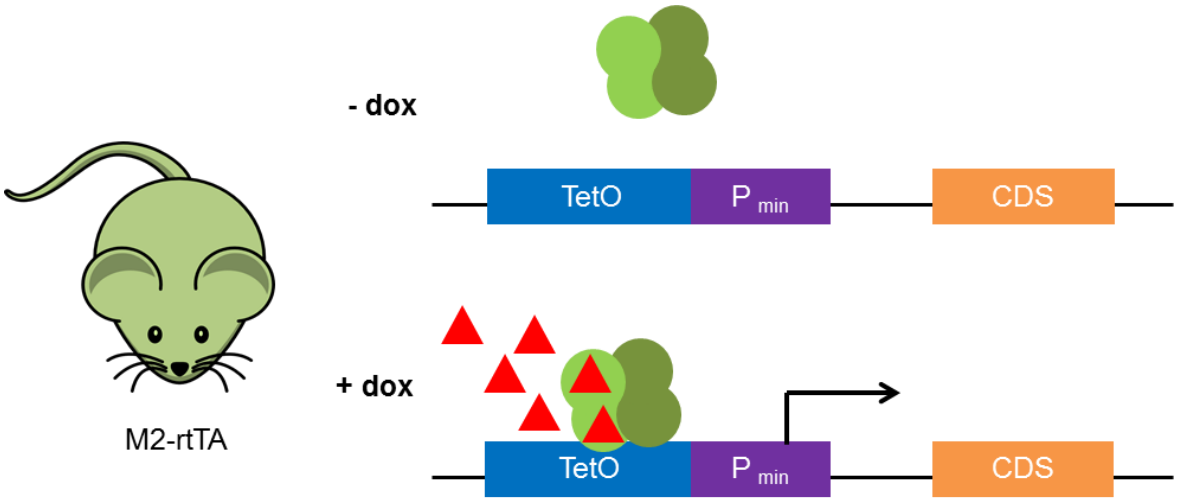

Figure 24: Tetracycline controlled gene transcription in cells from M2-rtTA mice (Hochedlinger et al., 2005). Upon addition of doxycycline (dox) the tetracycline responsive transcription factor is activated and binds to the TetOperator (TetO). Downstream target transcription of a coding DNA sequence (CDS) is then initiated. (P_{min} = minimal pormotor).

3.2.2.2 Vector design and experimental testing

In order to test the inducibility of ectopic Mybl2 expression using the tetracycline controlled gene transcription in cells from M2-rtTA mice, I designed a vector encoding for the inducible wild-type Mybl2 expression and, for selection purposes, a constitutive

blasticidin resistance (Figure 25 A, pT6B-Mybl2). A vector only encoding for the blasticidin resistance was used as a control (Figure 25 A, pLE11-Blast). To test for the inducibility of the ectopically introduced Mybl2, I decided to compare ectopic and endogenous Mybl2 expression levels using QRT-PCR in cells either transduced with the inducible Mybl2 expression vector or with the control vector, both in absence and presence of doxycycline. For the endogenous expression, I designed an oligonucleotide pair (primer pair) complementary to the 3'UTR of Mybl2 as this part is exclusive to the endogenous Mybl2 transcript. To measure expression levels of ectopic Mybl2 separately, I used a primer pair unique to the introduced lentiviral vector. The combined ectopic and endogenous Mybl2 expression levels were measured using a regular Mybl2 CDS primer pair.

After 24 h of cultivation, freshly isolated lin.-neg. bone marrow cells form M2-rtTA mice were transduced either with the vector encoding for the inducible Mybl2 expression or the control vector. After blasticidin selection, I supplemented half of each cell culture with doxycycline (1 µg/ml) for 48 h. All four cell culture groups were analyzed by QRT-PCR for endogenous, ectopic and the combined expression level of Mybl2 (Figure 25 B). I expected that endogenous Mybl2 expression would show a similar level in all analyzed cell cultures, while the ectopic and the combined Mybl2 expression levels would be increased only in the cells carrying the inducible Mybl2 cassette treated with doxycycline. Indeed, the analysis of the endogenous Mybl2 expression levels in cells with and without doxycycline treatment showed very similar expression levels (Figure 25 B, right panel). Thus, endogenous Mybl2 expression was not influenced by the induction of ectopic Mybl2 expression. Looking at the ectopic Mybl2 expression levels of all analyzed cell cultures, only the cells carrying the inducible Mybl2 vector had a significantly higher expression of Mybl2 upon doxycycline treatment (Figure 25 B, left panel, pT6B+). Measuring the combined ectopic and endogenous Mybl2 expression, again cells with the inducible Mybl2 expression showed an increased Mybl2 expression upon doxycycline treatment (Figure 24 B, middle, pT6B+). However, the combined Mybl2 expression level was also slightly elevated in cells with inducible Mybl2 expression but in absence of doxycycline (Figure 25 B, middle, pT6B-). This might indicate that in some cells Mybl2 was ectopically expressed independently from doxycycline treatment.

The experimental test showed that ectopic expression of Mybl2 did not alter endogenous Mybl2 expression, and an induction of ectopic Mybl2 was feasible upon doxycycline addition with a stable up-regulation of Mybl2 expression levels.

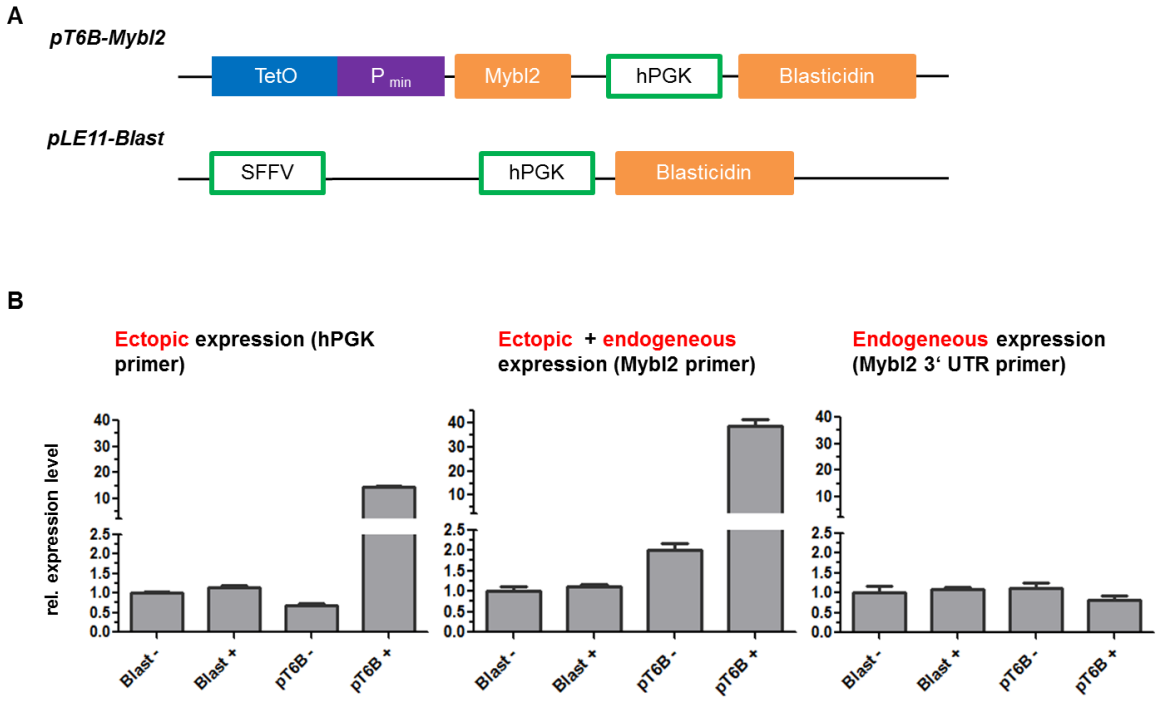

Figure 25: Test of the inducible system. (A) Vector design: pT6B-Mybl2 encoding for the inducible expression of Mybl2 and pLE11-Blast used as a control **(B)** Ectopic (left panel), endogenous (right panel) and the combined (middle) expression level of Mybl2 in lin.-neg. enriched murine bone marrow cells transduced with the inducible Mybl2 vector (pT6B) or the control vector (Blast), both either in absence (-) or presence (+) of doxycycline. *Measurements were performed in triplicates.*

3.2.3 Re-expression of Mybl2 abrogates proliferation

In order to test whether re-expression of ectopic Mybl2 would abrogate the phenotype by reduced Mybl2 expression levels in lin.-neg. enriched bone marrow cells (3.2.1), I designed a vector encoding both, the constitutive Mybl2 knockdown and the inducible Mybl2 expression (Figure 26 A). For selectional purposes a blasticidin resistance was included. As a control vector, I used one only encoding the inducible Mybl2 expression and a blasticidin resistance (Figure 26 B).

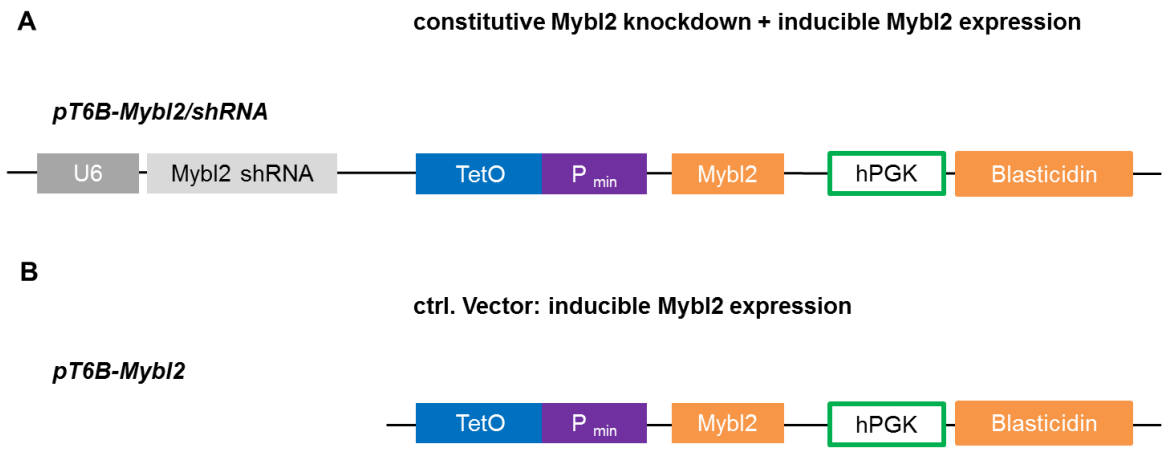

Figure 26: Vector design for inducible re-expression of wild-type Mybl2 in cells with reduced Mybl2 levels. (A) One vector encoding for the constitutive Mybl2 knockdown and the inducible Mybl2 expression, along with a constitutively expressed blasticidin resistance gene. **(B)** The control vector, only encoding for the inducible Mybl2 expression and the constitutively expressed blasticidin resistance gene.

To test whether ectopic expression of Mybl2 could “rescue” the growth phenotype induced by reduced Mybl2 expression levels, I set up an experiment recording growth of cells with low Mybl2 expression levels compared to cells with re-expressed Mybl2 using the inducible system (3.2.2). Again, 24 h after purification, I transduced lin.-neg. enriched bone marrow cells from M2-rtTA mice with the designed vectors, and blasticidin selection was performed. Yet again, cells with the constitutive Mybl2 knockdown and the inducible Mybl2 expression, as well as cells with the control vector, were cultured in presence and absence of doxycycline (1 µg/ml, 48 h). I anticipated that cells with a reduced Mybl2 expression level would show a clear proliferative advantage compared to the controls and continue expansion over the monitored time period. Further, I hypothesized that the ectopic re-expression of Mybl2 upon doxycycline addition would abrogate this phenotype within a certain time. In contrast, I expected that the cells transduced with the control vector, as well in absence as in presence of doxycycline, would stop proliferating after about two weeks in culture. Indeed, while cells with a reduced Mybl2 expression level kept proliferating, the re-expression of ectopic Mybl2 could prevent this phenotype (Figure 27 A, red and blue line). Also, both control cell cultures lost their proliferative capacity within two to three weeks of cultivation (Figure 27 A, dark and light green line). This result supported that the growth phenotype is caused by reduced Mybl2 expression levels, as it can be abrogated by re-expression of Mybl2. Of note, the ectopic expression of Mybl2 did not have an advantage for primary murine HSPCs *in vitro*, thus, did not seem to alter cell fate.

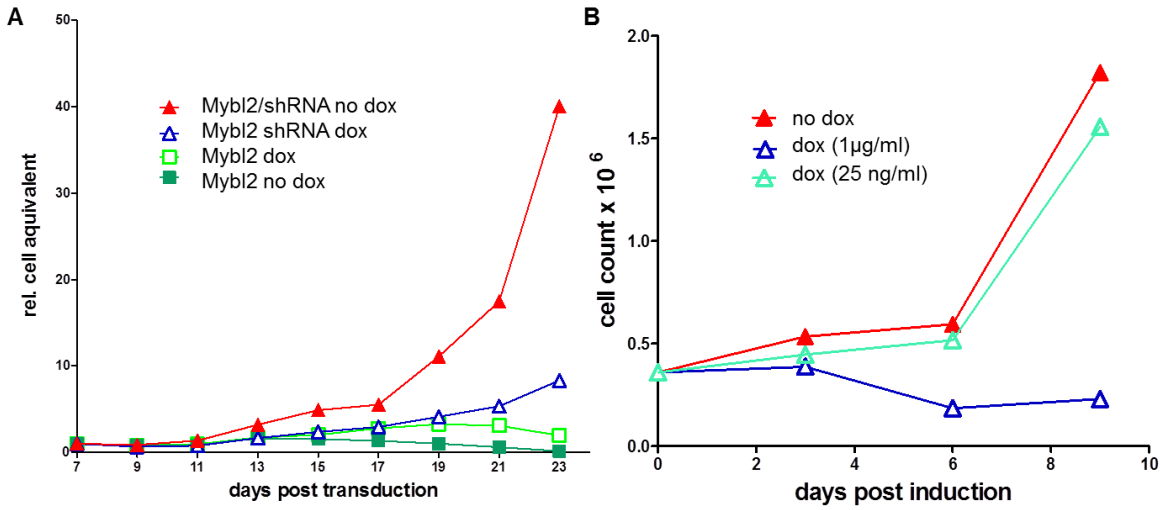

Figure 27: Re-expression of Mybl2 abrogates proliferation. (A) Growth of lineage negative enriched bone marrow cells form rtTA-M2 mice transduced with either a vector encoding for a specific Mybl2 shRNA and the inducible expression of Mybl2 (Mybl2/shRNA) or a vector only encoding for inducible expression of Mybl2 (Mybl2). The transduced cells were both cultured in presence (dox) and in absence (no dox) of doxycycline. *Cell count was measured using the Cell Titer Glo luminescent cell viability assay.* **(B)** Induced re-expression of Mybl2 in long term cultured cells with reduced Mybl2 levels (blue). *Cell counting was performed using a Neubauer chamber.*

Next, I asked whether long time cultured cells with reduced Mybl2 expression levels would also lose their proliferative capacity by induced re-expression of Mybl2. After about three weeks of cultivation, I took cells carrying the constitutive knockdown and the inducible Mybl2 cassette and induced ectopic Mybl2 expression. As the addition of 1 µg/ml doxycycline had induced a tenfold overexpression of ectopic Mybl2 (3.2.2.2), I decided to test in parallel whether the addition of 25 ng/ml doxycycline would have the same effects. Again, the growth phenotype could be abrogated within a few days by re-expression of Mybl2 using 1 µg/ml doxycycline (Figure 27 B, blue line). Although 25 ng/ml doxycycline were not enough to abrogate the growth phenotype, a slight inhibition of proliferation could be measured (Figure 27 B, turquoise line). This indicated that further testing for a dosage of doxycycline to induce a more physiological Mybl2 level would be necessary. Nevertheless, this experiment revealed the suitability of this system for gene expression analysis comparing cells with reduced levels of Mybl2 to cells where Mybl2 had been re-expressed. Unfortunately, this experiment could not be repeated with the same results (data not shown). Despite several tries, the reason could not be identified.

3.3 Cell cycle-dependent gene expression by Mybl2

As I could not confirm the reversion of the growth phenotype associated with reduced Mybl2 expression levels by ectopic re-expression of wild-type Mybl2, I used an inducible Mybl2 knockdown approach in primary murine HSPCs immortalized by dominant-negative RUNX1 (Tsuzuki and Seto, 2012) for gene expression analysis. Thus, only gene expression differences with cell cycle phase-resolution induced by changes of the Mybl2 expression level will be measured.

3.3.1 Venus-GMNN$_{(1/110)}$ in primary murine HSPCs immortalized by dominant-negative RUNX1

A polyclonal cell line, derived from primary murine HSPCs immortalized by dominant-negative RUNX1 was used for the following experiments. First, the established Venus-GMNN$_{(1/110)}$ vector (3.1.3) was introduced into these cells. To enable a selection for transduced cells without cell sorting, the pVG lentiviral vector was modified to additionally encode for the expression of a hygromycin resistance (Figure 28, pVG-Hygro). After lentiviral transduction with the pVG-Hygro vector, the cells were selected for 10 days by hygromycin. Subsequently, the cells were transduced with a lentiviral vector encoding an inducible Mybl2 shRNA (Figure 28, pT6B-shRNA Mybl2/BFP). The Mybl2 shRNA was designed and tested in the laboratory in parallel to my experiments. Taking advantage of the M2-rtTA system (3.2.2) a lentiviral vector encoding for the doxycycline-inducible expression of this Mybl2 shRNA was produced. In order to visualize the induction of the Mybl2 shRNA flow cytometrically, the expression of a blue fluorescent protein (BFP) (Subach et al., 2011) was additionally encoded by the vector, also under the control of the inducible promoter. For selection of transduced cells, the vector encodes for a blasticidin resistance (Figure 28).

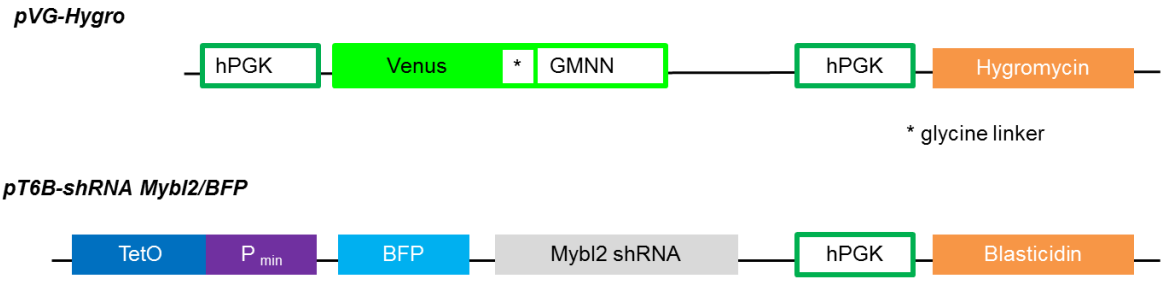

Figure 28: Vector design for gene expression analysis in immortalized HSPCs. The pVG-Hygro vector encoding for Venus-GMNN$_{(1/110)}$ and a hygromycin resistance gene, and the pT6B-shRNA Mybl2/BFP vector encoding the inducible Mybl2 shRNA along with BFP and a constitutively expressed blasticidin resistance gene.

In order to induce the expression of the Mybl2 shRNA resulting in a reduced Mybl2 expression level, doxycycline was added to one part of the described cell culture for 48 h (1 µg/ml). The cells without doxycycline treatment were used as control cells for the following PI-based re-analysis and gene expression analysis with cell cycle phase-resolution. First, both cell cultures, with and without doxycycline treatment, were analyzed for their Venus-GMNN$_{(1/110)}$ expression by flow cytometry. Gaiting on the "live gate" (Figure 29 A, P1), I determined four cell populations according to the Venus fluorescence intensity (Figure 29 B, P2-5) for cell sorting.

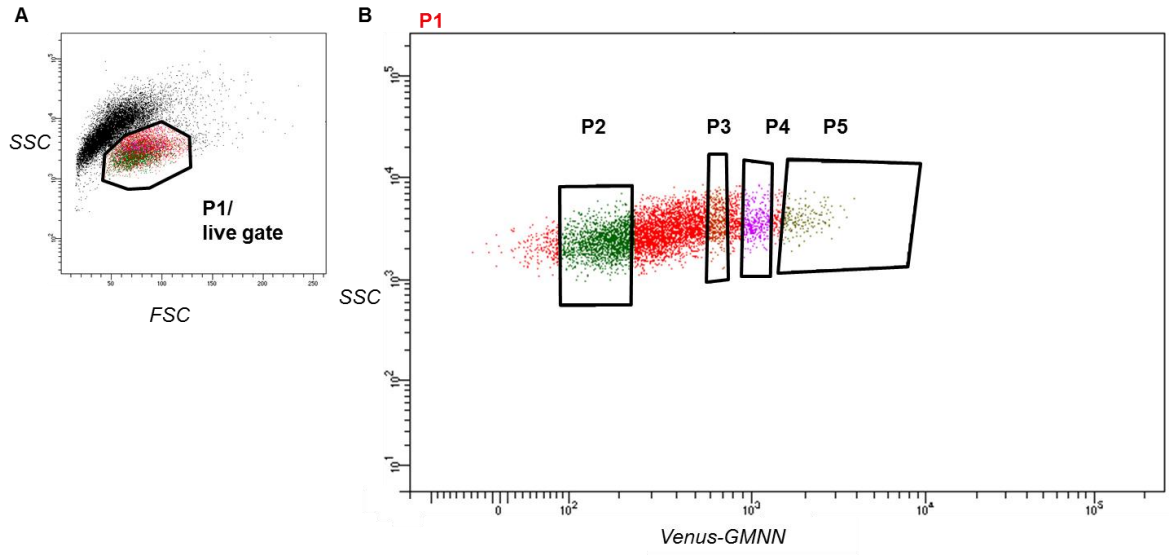

Figure 29: Flow cytometry sorting of immortalized HSPCs according to the Venus fluorescence intensity. (A) "Live gate" (P1). **(B)** Sort gates according to the Venus fluorescence intensity used for PI-based re-analysis and Mybl2-dependent gene expression analysis. *This figure shows the analysis of the immortalized HSPCs without doxycycline treatment (control cells).*

As in the experiments for the establishment of Venus-GMNN$_{(1/110)}$, the cell populations sorted for increased Venus fluorescence intensity (Figure 29 B, P2-5) each were enriched in a different cell cycle phase displaying a progress from the G1 to the G2 phase with increasing Venus fluorescence intensity (Figure 30, A and B). The PI re-analysis showed that the cells sorted for the P2 gate (Figure 29 B) were enriched in the G1 phase (Figure 30, A and B, P2 – G1) and cells sorted for the P3 gate (Figure 29 B) in the late G1/S phase (Figure 30, A and B, P3 – late G1/S). The P4 gate cell population (Figure 29 B) was mostly enriched in the S phase (Figure 30, A and B, P4 – S) and the P5 cell population (Figure 29 B) in the late S/G2 phase (Figure 30, A and B, P5 – lateS/G2). This was true for immortalized HSPCs with and without induced Mybl2 shRNA. For both of these HSPC cultures, cells were sorted for the "live gate" to generate a control cell cycle profile (Figure 29 A; Figure 30, A and B, P1).

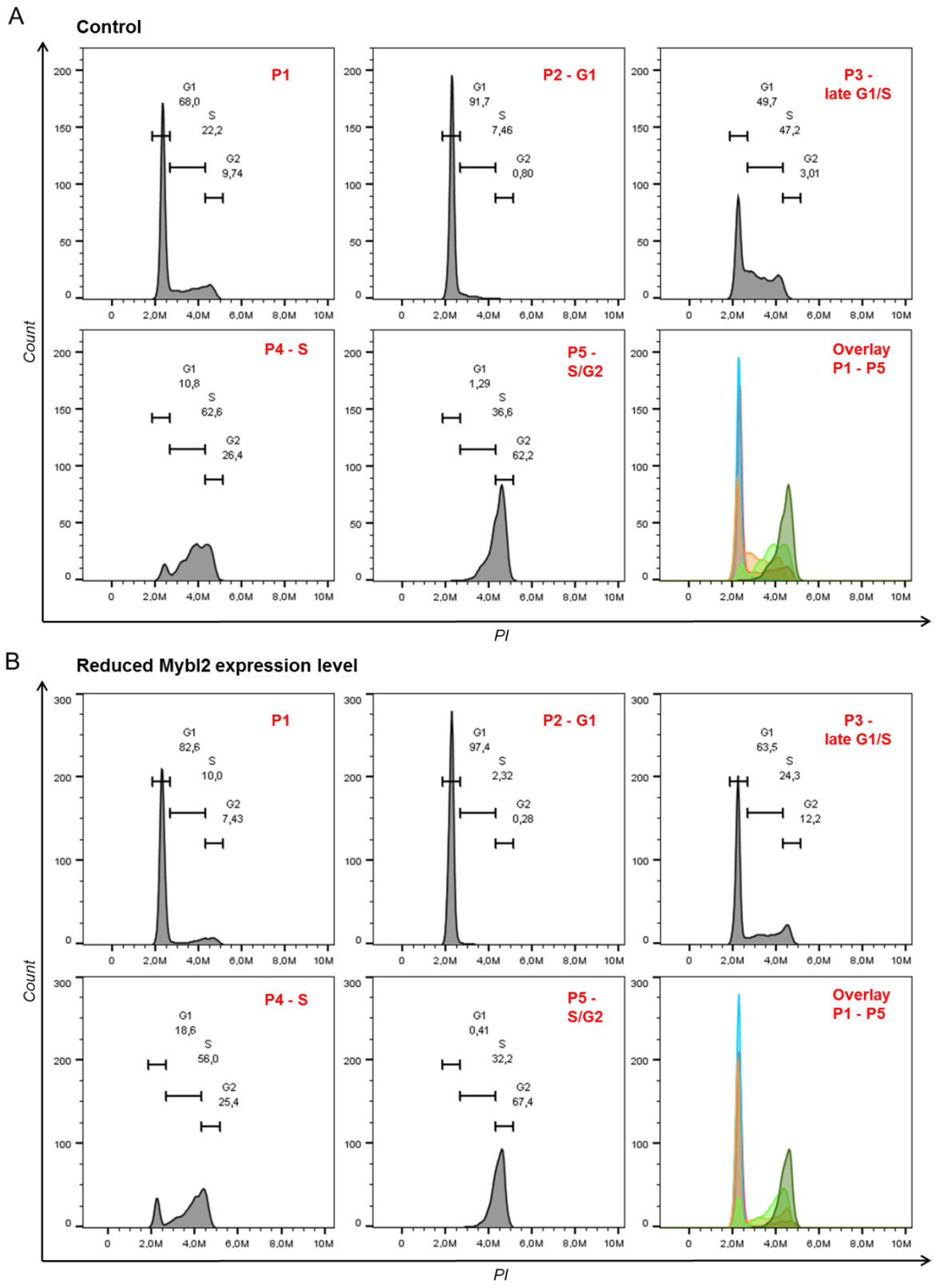

Figure 30: PI-based re-analysis of the immortalized HSPCs sorted according to the Venus-GMNN$_{(1/110)}$ fluorescence intensity revealed a distinct cell cycle phase separation. (A) PI-based re-analysis of the immortalized HSPCs without doxycycline treatment (control cells) sorted for the "live gate" and according to the Venus fluorescence intensity (Figure 29, A and B, P1-P5). **(B)** PI-based re-analysis of the immortalized HSPCs with reduced Mybl2 expression level sorted for the "live gate" and according to the Venus fluorescence intensity.

Importantly, PI-based re-analysis of the cells sorted for the “live gate” showed a regular cell cycle profile in both experimental groups (Figure 30, A and B, upper left, P1) demonstrating that the Venus-GMNN$_{(1/110)}$ expression did not alter the typical distribution of cells in each cell cycle phase. However, a difference in the cell cycle distribution between the two “live gate” cell populations (Figure 30, A and B, upper left, P1) had to be noted. While in the cell culture without doxycycline treatment about 70 % of cells were in the G1 phase and 22 % in the S phase (Figure 30 A, upper left), in the cells with reduced Mybl2 expression level 82 % were in the G1 phase and only 10 % in the S phase (Figure 30 B, upper left). This could be due to changes in the cell cycle by reduced Mybl2 expression levels, however, further measurements would be needed to support this finding. Also, the differences observed in the cell cycle distribution could be due to a day-to-day variation in machine-settings, as FACS and PI-based re-analysis of cells with induced Mybl2 shRNA and without were performed on different days. This could additionally explain that the cells enriched for the late G1/S phase (P3) and the S phase (P4) enriched cells also differ slightly comparing cells with reduced Mybl2 level to the cells without. Cells with induced expression of the Mybl2 shRNA showed more cells in the G1 and the G2 phase within the late G1/S phase enriched group, and more cells in G1 phase within the S phase enriched group compared to the control cells without doxycycline treatment. Gene expression analysis of typical cell cycle genes will reveal whether the enriched cell populations represent the correct cell cycle phase and can be compared to each other.

In conclusion, an enrichment of cells in each cell cycle phase of cells with reduced Mybl2 expression levels and control cells was successfully accomplished and the sorted cell populations were used for gene expression analysis.

3.3.2 Mybl2 dependent gene expression with cell cycle phase-resolution

Gene expression analysis was performed in the HSPCs immortalized by dominant-negative RUNX1 separated into the different cell cycle phases by FACS (3.3.1) comparing cells with reduced Mybl2 expression levels to cells with a physiological Mybl2 expression level (control). For this analysis, I decided to focus on a specific set of genes including the candidate genes for the gene dosage-dependent tumor suppressor function of Mybl2 from prior microarray data (Heinrichs et al., 2013) and unpublished data). I chose to measure the expression levels of Aspm and Nusap1, as both genes are known to be important for spindle formation in mitosis, and Aspm possibly influences stem cell maintenance (Capecchi and Pozner, 2015; Li et al., 2016). Changes in their expression level upon reduced Mybl2 expression levels could indicate that they are relevant for the tumor

suppressor function of Mybl2. In addition, I compared these candidate target genes to genes that are well-characterized key Mybl2 target genes within the cell cycle, e.g. Foxm1 and Ccnb1 (Sadasivam et al., 2012). I hypothesized that the key Mybl2 target genes important for cell cycle regulation would be less affected by reduced Mybl2 expression levels than the candidate genes that might be important for the tumor suppressor function of Mybl2. In addition, I expected that a cell cycle phase-resolution would reveal a more precise gene expression difference. Also, in order to ensure that the cell populations sorted according to the Venus fluorescence intensity reflected the correct cell cycle phase, I determined the expression level of the typical cell cycle marker genes used in establishing the Venus-$GMNN_{(1/110)}$ system: E2f1, Ccne1 and Dhfr.

First, I analyzed the Mybl2 expression level to validate that the induction of the expression of the Mybl2 shRNA had caused a Mybl2 knockdown in the immortalized HSPCs. Indeed, QRT-PCR analysis revealed a knockdown of Mybl2 to about 50 % expression level comparing cells sorted for the “live gate” with induced expression of the Mybl2 shRNA (Figure 31, P1, green bar) to the control (Figure 31, P1, grey bar). Further, evaluating the cell cycle distribution of the Mybl2 expression, it clearly showed a regulation within the cell cycle with an elevated expression in the S phase of cells with reduced expression level (Figure 31, green bars) as well as control cells (Figure 31, grey bars). The elevated expression in the S phase of the cell cycle is consistent with earlier reports about cell cycle phase distribution of Mybl2 expression (Lam et al., 1992). Interestingly, the Mybl2 expression level difference was greater between the cells enriched in the G1 and the late G1/S phase than in the S and late S/G2 phase comparing the cells with reduced Mybl2 to the control cells (Figure 31). This might indicate that in cells with reduced Mybl2 expression levels the cell cycle function of Mybl2 as a regulator of the transcription of genes required for the S/G2 phase progression is preserved. In contrast, genes regulated in the G1 phase could be strongly influenced by low levels of Mybl2.

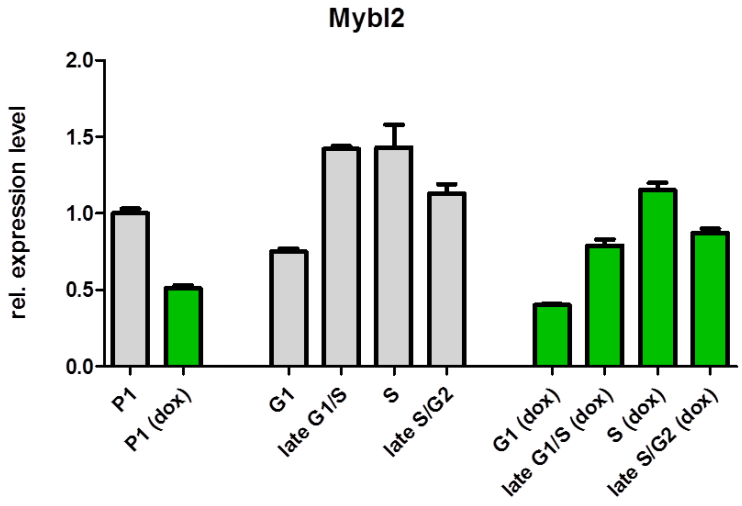

Figure 31: Gene expression analysis of Mybl2 showed a 50 % knockdown and an elevated expression level during S phase. Gene expression of Mybl2 in immortalized HSPCs with and without induced Mybl2 shRNA sorted according to the Venus-$GMNN_{(1/110)}$ fluorescence intensity. Green bars indicate cells with Mybl2 knockdown, grey bars indicate control cells. The analysis verified the Mybl2 knockdown to 50 % expression level in cells with induced expression of the Mybl2 shRNA and showed Mybl2 regulation within the cell cycle with a peaking expression in the S phase. The greatest expression level difference between cells with reduced Mybl2 level and the control was seen in the G1 and the late G1/S phase. *Measurements were performed in triplicates.*

Next, I analyzed whether the cell cycle marker genes (E2f1, Ccne1 and Dhfr) showed an elevated expression in their typical cell cycle phase. I expected that none of these genes would show expression differences upon Mybl2 gene-dosage changes. Surprisingly, E2f1 was the only typical cell cycle gene not affected by the reduced Mybl2 expression level showing its normal cell cycle phase distribution with a peak in the G1 to late G1/S phase (Figure 32, upper left). Dhfr and Ccne1, however, showed a reduced expression level in cells with reduced Mybl2 expression, both to about 50 % expression level compared to the “live gate” sorted cells from the control (Figure 32, P1(dox) and P1). While Dhfr was mainly downregulated in the G1 and the late G1/S phase with almost the same expression levels as the control in the S and the late S/G2 phase, Ccne1 was downregulated significantly in every cell cycle phase except for the late S/G2 phase (Figure 32, bottom). Of note, Dhfr, in contrast to E2f1 and Ccne1, did not show its typical cell cycle phase distribution with an elevated expression in the S phase. This could be due to the Mybl2 gene-dosage changes. However, the greatest difference in the Dhfr expression level was found comparing the G1 and the late G1/S phase enriched groups, the late G1/S phase also being the group with the greatest difference comparing enrichment in PI-based re-analysis of cells with reduced Mylb2 expression level to controls (Figure 30). Thus, this difference in enrichment might account for the atypical distribution of Dhfr. However, Mybl2, also known to be elevated in S phase, showed its

typical distribution (Figure 31) indicating that the enriched phases represent the correct cell cycle phase. Of note, it is possible that the Dhfr expression level might show minor changes in cell cycle phase enrichment more sensitively.

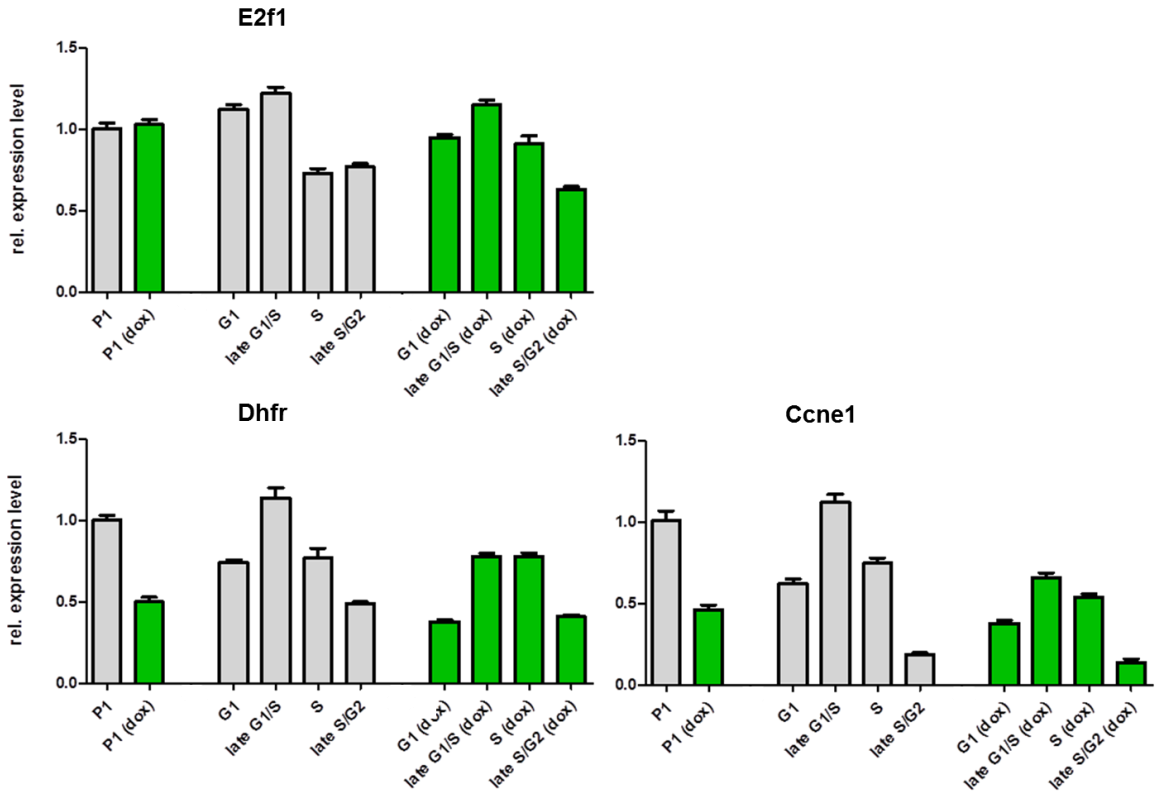

Figure 32: E2f1 expression is not affected by reduced Mybl2 expression levels, but Ccne1 and Dhfr show reduced expression levels. Gene expression of typical cell cycle genes in immortalized HSPCs with and without induced Mybl2 shRNA sorted according to the Venus-$GMNN_{(1/110)}$ fluorescence intensity. Green bars indicate cells with Mybl2 knockdown, grey bars indicate control cells. The analysis showed that only E2f1 is not affected by Mybl2 gene-dosage changes showing a regular distribution in the cell cycle phases. Ccne1 and Dhfr show reduced expression levels upon Mybl2 knockdown to 50 %. *Measurements were performed in triplicates.*

In addition, I measured the gene expression of the two known Mybl2 target genes, Ccnb1 and Foxm1, expecting both to be largely unaffected. Also, the two candidate target genes, Nusap1 and Aspm, were analyzed.

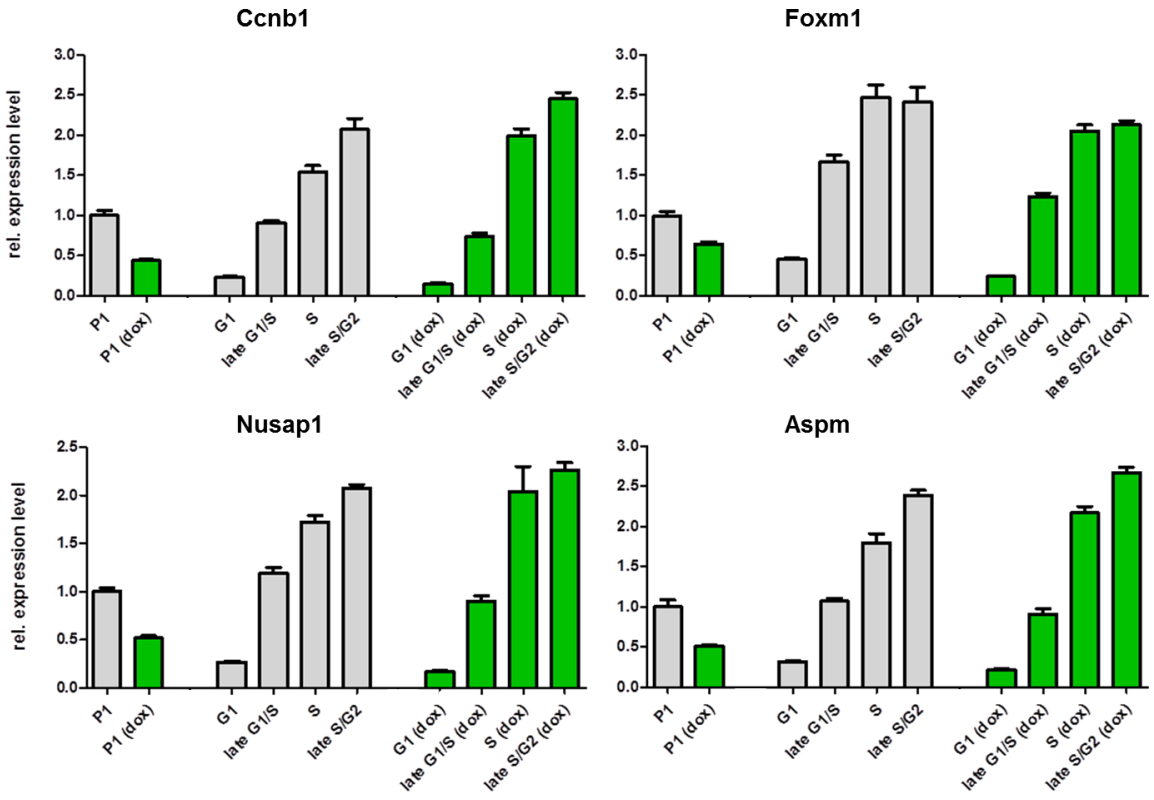

Figure 33: Ccnb1, Foxm1, Nusap1 and Aspm show reduced expression levels upon reduced Mybl2 levels. Gene expression of Mybl2 candidate target genes in immortalized HSPCs with and without induced Mybl2 shRNA sorted according to the Venus-GMNN$_{(1/110)}$ fluorescence intensity. Green bars indicate cells with Mybl2 knockdown, grey bars indicate control cells. Analysis showed that all four genes have reduced expression levels upon Mybl2 knockdown to an expression level of 50 %. The downregulation was most obvious in the G1 and the late G1/S phase, while in the S and late S/G2 phase expression levels were close to normal, and in case of Ccnb1, Aspm and Nusap1 even slightly upregulated. *Measurements were performed in triplicates.*

Surprisingly, Ccnb1 and Foxm1 clearly showed a downregulation to 40 % and 60 % expression level upon reduced Mybl2 expression. The cell cycle phase distribution of both genes with an elevated expression in the G2 phase, however, remained intact. While Foxm1 also showed slightly reduced expression levels in the S and G2 phase, Ccnb1 had slightly elevated levels in these phases in the cells with reduced Mybl2 levels. Both genes showed the greatest expression difference comparing the G1 phases of cells with reduced Mybl2 to controls. The candidate genes, Aspm and Nusap1, were equally reduced upon Mybl2 shRNA expression. They showed a similar distribution upon Mybl2 knockdown in the cell cycle as Ccnb1, meaning strongly reduced expression levels in the G1 phase and slightly elevated expression levels in S and G2 phase.

Interestingly, not only key Mybl2 target genes, Ccnb1 and Foxm1, but also classical cell cycle genes, Ccne1 and Dhfr, and the candidate target genes, Aspm and Nusap1, were strongly influenced by Mybl2 gene-dosage changes. These findings indicate that a

reduced Mybl2 expression level might equally affect its target genes. Of note, the typical distribution of the candidate target genes and the peak phase expression in the cell cycle were not altered by reduced Mybl2 expression. However, comparing the sorted cell cycle phases of cells with reduced Mybl2 expression level to controls an expression difference can be measured with an especially strong effect comparing the G1 phases. This demonstrates that a cell cycle phase-resolution is important to detect Mybl2 gene-dosage dependent expression differences. The strong regulation of all genes comparing their expression level in the G1 phase could also suggest that this phase might be important for the tumor suppressor function of Mybl2. Of note, the G1 phase is described to be very important for cell fate decision (Capecchi and Pozner, 2015). My results point towards a tumor suppressor function of Mybl2 closely related to the cell cycle. The tested genes are strong candidate genes for the tumor suppressor function of Mybl2. Further studies building on my findings will reveal the mechanistic pathway for the tumor suppressor function of Mybl2.

4. Discussion

In my thesis I aimed to establish a cell cycle-readout suitable for cell cycle phase-resolution of primary murine HSPCs with an RNAi-mediated Mybl2 knockdown to 30 - 50 % expression level *in vitro*. Gene expression analysis of surrogate Mybl2 target genes in these cells were sought to reveal a mechanistic insight into the recently discovered function of Mybl2 as a sub-haploinsufficient tumor suppressor in MDS (Heinrichs et al., 2013).

4.1 Establishment of a cell cycle-readout

The establishment of a cell cycle-readout allowing for an undisturbed cell cycle progression and an unperturbed enrichment of cells in the different cell cycle phases by flow cytometry was successfully accomplished in human and murine hematopoietic cells using Venus-GMNN$_{(1/110)}$ as a single cell cycle indicator. Notably, the originally planned implementation of the Fucci2 technique (Sakaue-Sawano et al., 2011) revealed several difficulties, especially concerning the use of the CDT1$_{(30/120)}$ fusion protein as the G1 phase indicator. Specifically, the replacement of mCherry in mCherry-CDT1$_{(30/120)}$ by DsRed-Express2 (RFP) (Strack et al., 2008) or mTurquoise2 (Tq) (Goedhart et al., 2012) resulted either in a continuous expression of the CDT1$_{(30/120)}$ fusion protein throughout the whole cell cycle or in the silencing of its expression (3.1.2).

To address the difficulties faced while establishing the Fucci2 technique, I focused on the modifications I had chosen to implement in order to create an improved version of Fucci2. In the first “Fucci” study, Hela cells had been cotransduced with two vectors, each encoding one cell cycle indicator (Sakaue-Sawano et al., 2008). I recorded the same difficulties with the CDT1$_{(30/120)}$ fusion protein in cells transduced with one vector encoding for both cell cycle indicators and cells sequentially transduced with two separate vectors, each encoding for one cell cycle indicator (3.1.2). Therefore, the differences in the transduction process are unlikely to account for the observed difficulties with the CDT1$_{(30/120)}$ fusion protein. Further, in parallel to my experiments, the Fucci technique has been established using only one vector suitable for cell culture and mice (Koh et al., 2017; Mort et al., 2014). Yet, another difference in my experiments was that I used the DNA sequences of mCherry-CDT1$_{(30/120)}$ and Venus-GMNN$_{(1/110)}$ from the original paper for the vectors, but exchanged the linker sequence designed to facilitate cloning steps by a glycine linker. Since the glycine linker did not alter the function of Venus-GMNN$_{(1/110)}$ as the G2 phase indicator, this change in sequence is also very unlikely to account for the difficulties faced with the CDT1$_{(30/120)}$ fusion protein. The most obvious modification, however, was the change of fluorochromes. The fluorochromes RFP and Tq allowing for

measurements on flow cytometers not equipped with a yellow-green laser might be unsuitable for a fusion to $CDT1_{(30/120)}$, a protein tightly regulated in the cell cycle by Ubiquitin-induced degradation (Nishitani et al., 2004). Especially the RFP-$CDT1_{(30/120)}$ fusion protein might predispose to accumulation in the cell due to the size of RFP as tetrameric protein inhibiting a quick and complete degradation after the G1 phase (Strack et al., 2008). However, the fusion protein of $CDT1_{(30/120)}$ and the monomeric Tq showed the same problem of continuous expression throughout the cell cycle. Further, the flow cytometric analysis of the fusion protein of $CDT1_{(30/120)}$ and another monomeric fluorochrome originating from a different structural fluorochrome background, mTagBFP (Subach et al., 2011), likewise suggested a continuous expression throughout the cell cycle (data not shown). In addition, I eventually tested the performance of the original fusion protein mCherry-$CDT1_{(30/120)}$ and the flow cytometric analysis confirmed the difficulties observed with the other fluorochromes (data not shown). Reassuringly, the original "Fucci" study already reported difficulties replacing mKO2 by fusing $CDT1_{(30/120)}$ to mRFP1 or mAG reporting a continuous expression throughout the cell cycle (Sakaue-Sawano et al., 2008). Interestingly, while this first Fucci study introducing mKO2-$CDT1_{(30/120)}$ remains unclear about the use of single cell clones in order to receive stable transformants, the improved version, Fucci2, successfully introducing mCherry for the $CDT1_{(30/120)}$ fusion protein established stable transformants by single cell cloning (Sakaue-Sawano et al., 2011). Most likely, observing that a high expression level of Tq-$CDT1_{(30/120)}$ or RFP-$CDT1_{(30/120)}$ led to cell death (3.1.2.2), a high expression level of CDT1 might be toxic for cells. Indeed, the experimental cancer drug MLN4924, inhibiting cullin-RING E3 ubiquitin ligases, was shown to induce DNA rereplication and cell apoptosis mediated by elevated levels of CDT1 (Lin et al., 2010). This is consistent with early reports about overexpression of CDT1 causing rereplication of DNA (Blow and Dutta, 2005; Vaziri et al., 2003). The high-expression levels of the G1 phase indicator probably exceeded the ubiquitination capability of the responsible E3 ligase resulting in the continuous expression observed. Thus, the cell cycle-dependent expression of the $CDT1_{(30/120)}$ fusion protein might only work in cells with a low expression level. In my experiments, the expression of the $CDT1_{(30/120)}$ fusion protein was under control of the SFFV promoter. This promoter might have been too potent especially used in hematopoietic cells. However, when exchanged for the less potent CMV promoter the expression of the $CDT1_{(30/120)}$ fusion proteins was still cell cycle phase-independent (data not shown).

These findings suggest that in a cell culture derived from a single cell clone having a tolerable expression level of the $CDT1_{(30/120)}$ fusion protein, the G1 phase indicator possibly labels cells correctly. A clonal selection of cells might also reveal single cells with

a cell cycle-dependent expression of RFP-CDT1$_{(30/120)}$ or Tq-CDT1$_{(30/120)}$. Of note, Venus-GMNN$_{(1/110)}$ did not need a single cell clone in order to be degraded in a cell cycle-dependent manner.

In the beginning of my experiments, Fucci had neither been used in hematopoietic cell lines nor in primary hematopoietic stem and progenitor cells. Although there are no *in vitro* implementations of Fucci in hematopoietic cells up to date, recently, transgenic mice expressing Fucci fluorescent cell cycle probes (Sakaue-Sawano et al., 2008) have been used to analyze the cell cycle in hematopoietic cells (Sakaue-Sawano et al., 2013; Shand et al., 2014; Tomura et al., 2013; Yo et al., 2014). Interestingly, already the selection of mice revealed difficulties, as only some mice expressed Fucci in hematopoietic cells at a sufficient level and often very low expression levels were faced. New mouse lines of Fucci have been created continuously as reports show problems with transgene inactivation and varying expression levels in several tissues (Abe et al., 2013; Mort et al., 2014), mirroring the problems I encountered during the implementation of the Fucci2 technique. Of note, while the GMNN$_{(1/110)}$ cell cycle indicator was interchangeable between species, different versions of the truncated CDT1 have been reported for zebrafish and fly, although cell cycle regulation is usually highly conserved among species. Again, the problem with the CDT1$_{(30/120)}$ fusion protein was a constant expression throughout the cell cycle (Sugiyama et al., 2009; Zielke et al., 2014). In addition, there have been different ways of interpreting the results of cells isolated from Fucci mice. Double-negative cells expressing Fucci are most often accounted to be in the very early G1 phase as cells lose expression of either marker right after division and need some time for the accumulation of mCherry-CDT1$_{(30/120)}$ (Jovic et al., 2013). Of note, in lymphocytes double-negative cells were interpreted as not expressing the indicators (Tomura et al., 2013). Indeed, the double-negative cells in my study could be cells in the early G1 phase due to a rapidly cycling cell population. However taking this into account, it is surprising that testing the RFP- and Tq-CDT1$_{(30/120)}$ fusion protein in the same OCI-AML2 cell line the amount of double-negative cells as well as RFP or Tq positive cells was not the same. Whether double-negative cells represent an early G1 phase could have been tested by sorting the double-negative cells and analyzing them again after a certain time in cell culture to see if they become RFP or Tq positive with progression of G1 phase. Importantly, even if the double-negative cells could be accounted as early G1 phase cells and were labeled correctly, the continuous expression of the CDT1$_{(30/120)}$ fusion protein in the G2 phase would still prohibit a correct cell cycle phase separation in my experiments.

In conclusion, the cell cycle separation of hematopoietic cells *in vitro* only using the GMNN$_{(1/110)}$ fusion protein is an easy and reproducible way of unperturbed cell cycle

phase separation for gene expression analysis. In need of two cell cycle indicators single cell clones or the use of hematopoietic cells from Fucci mice would offer a practical solution. Also, testing a murine version of CDT1 for separation of murine cell lines or search for a replacement of CDT1 would be reasonable. Most recently, a completely revised version, Fucci4, has been published (Bajar et al., 2016) introducing the first version visualizing every cell cycle phase and the transitions, additionally allowing to refrain from the $CDT1_{(30/120)}$ marker.

4.2 Clonal dominance of HSPCs in vitro by reduced Mybl2 expression levels

In my study, I could show that lin.-neg. enriched murine bone marrow cells with an RNAi-mediated Mybl2 knockdown show clonal dominance and a proliferative advantage *in vitro*. Thus, a Mybl2 expression level of 30 - 50 % immortalized primary murine HSPCs. The observed growth phenotype could be abrogated by re-expression of ectopic Mybl2 within a few days demonstrating the dependency of the immortalized cells on reduced Mybl2 levels. Unfortunately, this observation could not be reproduced in further experiments.

While *in vivo* two different Mybl2 shRNAs were successfully leading to clonal dominance of murine HSPCs (Heinrichs et al., 2013), only one of those shRNAs could be used to immortalize murine HSPCs *in vitro*. Also, the ectopic re-expression of Mybl2 could not consistently abrogate the growth phenotype by a reduced Mybl2 expression level. It is well known that the ectopic re-expression of a gene can be challenging. A key requirement for such a re-expression experiment is that the immortalized HSPCs *in vitro* constantly depend on reduced Mybl2 levels. Taking this into account, the time point of the re-expression in culture is most likely very important. While an early passage of cells might still be dependent on the on-target effect of the Mybl2 shRNA, thus, the reduced Mybl2 expression level, acquisition of further mutations may lead to growth advantages due to possible off-target effects of reduced Mybl2 level. In a genome wide analysis of the efficacy and specificity of siRNA-mediated gene silencing it has been shown that partial sequence identity of the siRNA sequence to a non-target sequence can mediate strong off-target effect (Jackson et al., 2003). These off-target effects are due to miRNA-like binding effects that lead to the simultaneous binding of one miRNA to various target mRNAs (Lim et al., 2005). Such effects are unpredictable, and most off-target effects are disadvantageous for cell growth and survival, thus, rarely lead to clonal expansion. In this study however, most likely, an advantageous combination of a positive on-target effect by the Mybl2 shRNA with a collaborating positive off-target effect is the reason for the Mybl2 independent expansion *in vitro*. This is supported by the fact that in parallel to my thesis,

experiments have shown that an inducible RNAi system for Mybl2 using a miRNA-derived shRNA expression vector could not immortalize primary HSPCs on its own (Heinrichs Lab, unpublished). To which extend, however, the off-target effect supports cell expansion *in vitro* remains to be determined. Also, although taking great care planning the experiments, experimental settings, integration problems with the vector or varying levels of reduced Mybl2 could have prohibited a successful reproduction of the Mybl2 re-expression experiment *in vitro*.

4.3 Cell cycle-dependent gene expression analysis

Cell cycle-dependent gene expression analysis in primary murine HSPCs immortalized by dominant-negative RUNX1 revealed reduced expression levels of Mybl2 and possible target genes upon a Mybl2 knockdown to about 50 % expression level. The classical Mybl2 target genes, Ccnb1 and Foxm1, as well as Aspm, Nusap1, Ccne1 and Dhfr were found to be regulated by Mybl2. The largest expression differences between cells with reduced Mybl2 expression and controls were observed in the G1 phase. The typical cell cycle phase distribution of the target genes and the peak phase expression in the cell cycle were not altered by reduced Mybl2 expression.

PI-based re-analysis of immortalized HSPCs after FACS according to the Venus-$GMNN_{(1/110)}$ fluorescence intensity revealed slight differences in data acquired on different days. This demonstrated that minor changes due to day-to-day variations in machine and staining parameters can have a significant impact on resolution and enrichment of cells in each phase. Performing the flow cytometric experiments used for gene expression analysis on the same day could improve the comparability between sorted cell populations. Further, a second dimension, ideally a different G1 phase indicator than $CDT1_{(30/120)}$ might strongly improve robustness of the demonstrated sorting approach. Recently, with the introduction of “Fucci4” an alternative G1 phase marker ($SLBP_{18-126}$) was published (Bajar et al., 2016). In addition, talking about comparability of gene expression between the cells sorted for different cell cycle phases, the type of housekeeping genes used have to be taken into account. As gene expression analysis is normalized to the expression of housekeeping genes, the stability of housekeeping gene expression in different phases is very important. To rule out expression level differences induced by instable housekeeping genes, I used 3 different ones, none of which is known to be cell cycle-regulated.

Originally, I hypothesized that target genes of Mybl2 could be divided into two groups: One set of target genes would have low affinity binding sites and would be possibly responsible for the tumor suppressor function, which is gene-dosage dependent.

In contrast, another set of target genes responsible for the cell cycle regulation would have high affinity binding sites. The target genes with high affinity binding sites were sought to be largely unaffected by reduced Mybl2 expression levels. However, the gene expression data suggests that at least the target genes analyzed here were equally affected pointing towards overall gradual effects on all target genes. Thus, a differential effect (core functionality vs. tumor suppressor activity of Mybl2) could result from reaching threshold expression levels of specific downstream target genes. This relies on the fact that small changes can have a strong biological impact if the gene expression level of a specific gene is close to the threshold level affecting its biological function. Thus, especially the cell cycle related gene expression changes are likely to result in proliferation or influence cell fate decision as most cell cycle genes are regulated very tightly within the cell cycle. It is important to notice that protein levels play a great role in the cell cycle and many pathways are regulated via protein ubiquitination rather than only gene expression. Western blots of Mybl2 and its target genes would further support the gene expression findings in this study on the protein level.

Interestingly, I could show that Mybl2 gene-dosage modification influences the expression of Aspm, Ccne1 and Nusap1. Aspm has been shown to be necessary for maintenance of symmetric progenitor cell division in mice. Further, it was recently found that Aspm protects Ccne1 from ubiquitination (Capecchi and Pozner, 2015). In the same study, in Aspm homozygous mutant mice, the cell cycle progression was found to be Ccne1-dependent, while mitotic cleavage orientation was Ccne1 independent. Ccne1 itself is described to be regulated by an E2f-dependent mechanism. My data suggests that Ccne1 is an important gene to follow-up as it might be regulated via an E2f1 induced Mybl2-Aspm pathway. Interestingly, Ccne1 downregulation provided HSCs with a competitive advantage in bone marrow transplantation experiments (Campaner et al., 2013). Further, Ccne1 is also described to have a function in S phase and mitotic progression (Capecchi and Pozner, 2015), just as Mybl2. These facts along with the finding that Mybl2 influences gene expression levels of Aspm and Ccne1 suggest a role for Mybl2 in symmetric versus asymmetric stem cell division. The Mybl2 induced regulation of Nusap1, known to regulate spindle formation in mitosis and microtubule oscillation (Li et al., 2016), further supports this notion.

4.4 Outlook

This work showed that Venus-GMNN$_{(1/110)}$ as a single cell cycle indicator could be used successfully for enrichment of cells in different cell cycle phases for Mybl2 gene-dosage dependent gene expression analysis in immortalized HSPCs. My data suggested

that all Mybl2 target genes were equally affected by downregulation of Mybl2 expression, depending on the cell cycle phase. This could be revealed for Ccnb1, Foxm1, Aspm, Nusap1, Dhfr and Ccne1. The Mybl2-dependent regulation of the cell cycle genes Foxm1, Ccnb1 and Ccne1 strongly suggests a central role of the tumor suppressor function of Mybl2 in the cell cycle. The newly discovered regulation of Aspm and Nusap1 possibly points towards an additional role of Mybl2 in cell fate decision in HSPCs. Further studies building on my findings on the cell cycle-dependency of Mybl2's transactivation function will support to define the Mybl2 driven tumor suppressor pathway. Improvements for following experiments should consider introducing a second dimension, i.e. a different G1 phase marker than $CDT1_{(30/120)}$, for robustness of the cell cycle phase separation. Additionally, analyzing the immunophenotype and the changes of distribution of cells in the cell cycle phases upon reduced Mybl2 levels would reveal an even better idea of Mybl2 induced changes in HSPCs. To gain a deeper understanding of Mybl2 regulation of the target genes, western blot analysis would demonstrate how changes in the gene expression analysis translate to the protein level. Microarray-based global gene expression analysis of the cells with reduced Mybl2 expression levels separated into the cell cycle phases will help to identify further target genes important for the tumor suppressor function of Mybl2. The implementation of my results and their advancement by the mentioned techniques will reveal a mechanistic insight into the tumor suppressor function of Mybl2, which will hopefully reveal new therapeutic targets for patients suffering from MDS.

.

5. Summary

MYBL2 has been identified as a dosage-dependent tumor suppressor in myelodysplastic syndromes (MDS). The gene is ubiquitously expressed and encodes a transcription factor which is strictly required for cell cycle progression. Of note, downregulation of Mybl2 expression levels to 30 - 50 % (sub-haploinsufficiency) provides a clonal advantage to hematopoietic stem and progenitor cells *in vivo*. Yet, the molecular mechanism of this phenotype is unknown. In this thesis, I aimed to identify Mybl2 candidate target genes responsible for its tumor suppressor function by analyzing Mybl2-dependent gene expression differences at the cell cycle phase level in murine hematopoietic stem and progenitor cells. Here I show that RNA interference-mediated knockdown of Mybl2 to sub-haploinsufficient levels allows freshly isolated hematopoietic stem and progenitor cells to proliferate and expand *in vitro*. The re-expression of wild type Mybl2 abrogated the growth of these cells within a few days. Unfortunately, the reversion of the growth phenotype could not be reproduced consistently. As a consequence, for gene expression analysis I used an inducible Mybl2 knockdown approach in murine hematopoietic stem and progenitor cells that were immortalized with dominant-negative RUNX1. Additionally, I established the expression of a cell cycle phase-dependent indicator protein (Venus-$GMNN_{(1/110)}$) that allowed the undisturbed separation of cells at the different cell cycle phases by flow cytometry. I exploited the combination of the inducible Mylb2 knockdown and the Venus-$GMNN_{(1/110)}$-based cell cycle phase separation to identify candidate target genes affected by reduced levels of Mybl2. The well-established Mybl2 target genes, Cyclin B1 (Ccnb1) and Foxm1, showed a significantly reduced expression upon Mybl2 downregulation even without cell cycle phase-resolution. In addition, my results demonstrated that the expression levels of Aspm and Nusap1, two genes important for spindle formation during mitosis, were influenced by Mybl2. I could also show that the expression levels of Cyclin E (Ccne1) and Dhfr, two classical cell cycle regulatory genes, were reduced upon low expression levels of Mybl2. Comparing the cells with reduced Mybl2 expression level and controls sorted for the different cell cycle phases the strongest expression differences were determined comparing the G1 phases. My data confirmed Cyclin B1 and Foxm1 as Mybl2 target genes and newly identified Aspm, Nusap1, Dhfr and Cyclin E as regulated upon Mybl2 gene-dosage changes. These findings point towards a role of these genes in a cell cycle-related tumor suppressor function of Mybl2 and, for instance the regulation of Aspm, towards a possible role of Mybl2 in cell fate decision.

6. Zusammenfassung

MYBL2 ist ein dosis-abhängiger Tumorsuppressor in Myelodysplastischen Syndromen. Dieses Gen ist ubiquitär exprimiert und kodiert einen Transkriptionsfaktor, der unabdingbar für den Ablauf des Zellzyklus ist. Die Verminderung der Mybl2 Expression auf 30 - 50 % des Normallevels führt jedoch zu einem klonalen Expansionsvorteil hämatopoetischer Stamm- und Vorläuferzellen *in vivo*. Die Komponenten des molekularen Mechanismus dieses Phänotyps sind bisher völlig unbekannt. Ziel dieser Arbeit war es Kandidatengene, die maßgeblich an der Tumorsuppressorfunktion von Mybl2 beteiligt sind, mittels zellzyklusaufgelöster Genexpressionsanalysen zu identifizieren. Zunächst konnte ich zeigen, dass frisch isolierte murine hämatopoetische Stamm- und Vorläuferzellen durch einen RNA-Interferenz-vermittelten Knockdown von Mybl2 auf 30 - 50 % auch *in vitro* einen Expansionsvorteil haben. Die ektopische Expression von Wildtyp Mybl2 konnte diesen Expansionsvorteil in kurzer Zeit aufheben. Leider ließ sich dieses Ergebnis nicht konstant reproduzieren. Für die geplanten Genexpressionsanalysen nutzte ich daher die Induzierbarkeit eines RNA-Interferenz vermittelten Mybl2 Knockdowns in murinen hämatopoetischen Stamm- und Vorläuferzellen, die mittels dominant-negativem RUNX1 immortalisiert wurden. Zusätzlich habe ich die Expression eines zellzyklusregulierten Indikatorproteins (Venus-$GMNN_{(1/110)}$) in hämatopoetischen Zellen etabliert, welche die durchflusszytometrische Trennung von Zellpopulationen entsprechend der einzelnen Zellzyklusphasen erlaubt. Die Kombination dieser beiden Systeme habe ich genutzt, um mittels Genexpressionsanalysen Targetgene von Mybl2 zu identifizieren, die durch Verminderung des Mybl2 Expressionslevels unterschiedlich reguliert werden. Die bereits etablierten Mybl2 Targetgene, Cyclin B1 (Ccnb1) und Foxm1, zeigten schon ohne Beachtung der Zellzyklusauflösung ein deutlich herabgesetztes Expressionslevel. Weiterhin war die Expression von Aspm und Nusap1, zwei Gene, die wichtig für die Formation der Mitosespindel sind, ebenfalls stark von reduzierten Mybl2 Expressionsleveln betroffen. Auch die Expression von Cyclin E und Dhfr, zwei klassischen Regulatoren des Zellzyklus, war in Zellen mit Verminderung des Mybl2 Expressionslevels deutlich erniedrigt. Die Genexpression im Vergleich der einzelnen Zellzyklusphasen zeigte, dass insbesondere die Expression in der G1 Phase bei allen Mybl2 Targetgenen vermindert ist. Meine Arbeit bestätigte Cyclin B und Foxm1 als Mybl2 Targetgene, zeigte aber auch, dass die Expression von Aspm, Nusap1, Dhfr und Cyclin E stark von Mybl2 Gendosisveränderungen betroffen war. Dies lässt zum einen eine Funktion dieser Gene in einer zellzyklusnahen Tumorsuppressorfunktion von Mybl2 vermuten, andererseits weist die Regulation, zum Beispiel von Aspm, auf eine mögliche Beteiligung von Mybl2 an der Zellschicksalsentscheidung hin.

Bibliography

1. Abe, T., Sakaue-Sawano, A., Kiyonari, H., Shioi, G., Inoue, K., Horiuchi, T., Nakao, K., Miyawaki, A., Aizawa, S., Fujimori, T. (2013). Visualization of cell cycle in mouse embryos with Fucci2 reporter directed by Rosa26 promoter. Development 140, 237-246.

2. Alimonti, A., Carracedo, A., Clohessy, J. G., Trotman, L. C., Nardella, C., Egia, A., Salmena, L., Sampieri, K., Haveman, W. J., Brogi, E., Richardson, A. L., Zhang, J.,Pandolfi, P. P. (2010). Subtle variations in Pten dose determine cancer susceptibility. Nat Genet 42, 454-458.

3. Amos-Landgraf, J. M., Irving, A. A., Hartman, C., Hunter, A., Laube, B., Chen, X., Clipson, L., Newton, M. A., Dove, W. F. (2012). Monoallelic silencing and haploinsufficiency in early murine intestinal neoplasms. Proc Natl Acad Sci U S A 109, 2060-2065.

4. Aoki, K., Komatsu, N., Hirata, E., Kamioka, Y., Matsuda, M. (2012). Stable expression of FRET biosensors: a new light in cancer research. Cancer Sci 103, 614-619.

5. Arber, D. A., Orazi, A., Hasserjian, R., Thiele, J., Borowitz, M. J., Le Beau, M. M., Bloomfield, C. D., Cazzola, M., Vardiman, J. W. (2016). The 2016 revision to the World Health Organization (WHO) classification of myeloid neoplasms and acute leukemia. Blood, blood-2016-2003-643544.

6. Aul, C., Giagounidis, A., Germing, U. (2001). Epidemiological features of myelodysplastic syndromes: results from regional cancer surveys and hospital-based statistics. Int J Hematol 73, 405-410.

7. Bajar, B. T., Lam, A. J., Badiee, R. K., Oh, Y.-H., Chu, J., Zhou, X. X., Kim, N., Kim, B. B., Chung, M., Yablonovitch, A. L., Cruz, B. F., Kulalert, K., Tao, J. J., Meyer, T., Su, X.-D., Lin, M. Z. (2016). Fluorescent indicators for simultaneous reporting of all four cell cycle phases. Nat Meth 13, 993-996.

8. Baum, C., Hegewisch-Becker, S., Eckert, H. G., Stocking, C., Ostertag, W. (1995). Novel retroviral vectors for efficient expression of the multidrug resistance (mdr-1) gene in early hematopoietic cells. J Virol 69, 7541-7547.

9. Bellacosa, A., Godwin, A. K., Peri, S., Devarajan, K., Caretti, E., Vanderveer, L., Bove, B., Slater, C., Zhou, Y., Daly, M., Howard, S., Campbell, K. S., Nicolas, E., Yeung, A. T., Clapper, M. L., Crowell, J. A., Lynch, H. T., Ross, E., Kopelovich, L., Knudson, A. G. (2010). Altered gene expression in morphologically normal epithelial cells from heterozygous carriers of BRCA1 or BRCA2 mutations. Cancer Prev Res (Phila) 3, 48-61.

10. Bench, A. J., Nacheva, E. P., Hood, T. L., Holden, J. L., French, L., Swanton, S., Champion, K. M., Li, J., Whittaker, P., Stavrides, G., Hunt, A. R., Huntly, B. J., Campbell, L. J., Bentley, D. R., Deloukas, P., Green, A. R. (2000). Chromosome 20 deletions in myeloid malignancies: reduction of the common deleted region, generation of a PAC/BAC contig and identification of candidate genes. UK Cancer Cytogenetics Group (UKCCG). Oncogene 19, 3902-3913.

11. Bennett, J. M., Catovsky, D., Daniel, M. T., Flandrin, G., Galton, D. A., Gralnick, H. R., Sultan, C. (1982). Proposals for the classification of the myelodysplastic syndromes. Br J Haematol 51, 189-199.

12. Berger, A. H., Knudson, A. G., Pandolfi, P. P. (2011). A continuum model for tumour suppression. Nature 476, 163-169.

13. Birnboim, H. C., Doly, J. (1979). A rapid alkaline extraction procedure for screening recombinant plasmid DNA. Nucleic Acids Res 7, 1513-1523.

14. Blow, J. J., Dutta, A. (2005). Preventing re-replication of chromosomal DNA. Nat Rev Mol Cell Biol 6, 476-486.

15. Braun, T., de Botton, S., Taksin, A. L., Park, S., Beyne-Rauzy, O., Coiteux, V., Sapena, R., Lazareth, A., Leroux, G., Guenda, K., Cassinat, B., Fontenay, M., Vey, N., Guerci, A., Dreyfus, F., Bordessoule, D., Stamatoullas, A., Castaigne, S., Terre, C., Eclache, V., Fenaux, P., Ades, L. (2011). Characteristics and outcome of myelodysplastic syndromes (MDS) with isolated 20q deletion: a report on 62 cases. Leuk Res 35, 863-867.

16. Campaner, S., Viale, A., De Fazio, S., Doni, M., De Franco, F., D'Artista, L., Sardella, D., Pelicci, P. G., Amati, B. (2013). A non-redundant function of cyclin E1 in hematopoietic stem cells. Cell Cycle 12, 3663-3672.

17. Capecchi, M. R., Pozner, A. (2015). ASPM regulates symmetric stem cell division by tuning Cyclin E ubiquitination. Nat Commun 6, 8763.

18. Charrasse, S., Carena, I., Brondani, V., Klempnauer, K. H., Ferrari, S. (2000). Degradation of B-Myb by ubiquitin-mediated proteolysis: involvement of the Cdc34-SCF(p45Skp2) pathway. Oncogene 19, 2986-2995.

19. Chomczynski, P., Sacchi, N. (1987). Single-step method of RNA isolation by acid guanidinium thiocyanate-phenol-chloroform extraction. Anal Biochem 162, 156-159.

20. Clarke, M., Dumon, S., Ward, C., Jager, R., Freeman, S., Dawood, B., Sheriff, L., Lorvellec, M., Kralovics, R., Frampton, J., Garcia, P. (2013). MYBL2 haploinsufficiency increases susceptibility to age-related haematopoietic neoplasia. Leukemia 27, 661-670.

21. Cogle, C. R. (2015). Incidence and Burden of the Myelodysplastic Syndromes. Curr Hematol Malig Rep 10, 272-281.

22. Corey, S. J., Minden, M. D., Barber, D. L., Kantarjian, H., Wang, J. C., Schimmer, A. D. (2007). Myelodysplastic syndromes: the complexity of stem-cell diseases. Nature Reviews Cancer 7, 118-129.

23. Davis, P. K., Ho, A., Dowdy, S. F. (2001). Biological methods for cell-cycle synchronization of mammalian cells. Biotechniques 30, 1322-1326, 1328, 1330-1321.

24. Eckert, H. G., Stockschlader, M., Just, U., Hegewisch-Becker, S., Grez, M., Uhde, A., Zander, A., Ostertag, W., Baum, C. (1996). High-dose multidrug resistance in primary human hematopoietic progenitor cells transduced with optimized retroviral vectors. Blood 88, 3407-3415.

25. Friend, S. H., Bernards, R., Rogelj, S., Weinberg, R. A., Rapaport, J. M., Albert, D. M., Dryja, T. P. (1986). A human DNA segment with properties of the gene that predisposes to retinoblastoma and osteosarcoma. Nature 323, 643-646.

26. Gangat, N., Patnaik, M. M., Tefferi, A. (2016). Myelodysplastic syndromes: Contemporary review and how we treat. Am J Hematol 91, 76-89.

27. Germing, U., Kobbe, G., Haas, R., Gattermann, N. (2013). Myelodysplastic syndromes: diagnosis, prognosis, and treatment. Deutsches Ärzteblatt International 110, 783.

28. Goedhart, J., von Stetten, D., Noirclerc-Savoye, M., Lelimousin, M., Joosen, L., Hink, M. A., van Weeren, L., Gadella, T. W., Jr., Royant, A. (2012). Structure-guided evolution of cyan fluorescent proteins towards a quantum yield of 93%. Nat Commun 3, 751.

29. Gossen, M., Bujard, H. (1992). Tight control of gene expression in mammalian cells by tetracycline-responsive promoters. Proc Natl Acad Sci U S A 89, 5547-5551.

30. Graf, T., Beug, H. (1978). Avian leukemia viruses: interaction with their target cells in vivo and in vitro. Biochim Biophys Acta 516, 269-299.

31. Greenberg, P., Cox, C., LeBeau, M. M., Fenaux, P., Morel, P., Sanz, G., Sanz, M., Vallespi, T., Hamblin, T., Oscier, D., Ohyashiki, K., Toyama, K., Aul, C., Mufti, G., Bennett, J. (1997). International scoring system for evaluating prognosis in myelodysplastic syndromes. Blood 89, 2079-2088.

32. Greenberg, P., Tuechler, H., Schanz, J., Sanz, G., Garcia-Manero, G., Sole, F., Bennett, J. M., Bowen, D., Fenaux, P., Dreyfus, F., Kantarjian, H., Kuendgen, A., Levis, A., Malcovati, L., Cazzola, M., Cermak, J., Fonatsch, C., Le Beau, M. M., Slovak, M. L., Krieger, O., Luebbert, M., Maciejewski, J., Magalhaes, S. M., Miyazaki, Y., Pfeilstocker, M., Sekeres, M., Sperr, W. R., Stauder, R., Tauro, S., Valent, P., Vallespi, T., van de Loosdrecht, A. A., Germing, U., Haase, D. (2012). Revised international prognostic scoring system for myelodysplastic syndromes. Blood 120, 2454-2465.

33. Haase, D., Germing, U., Schanz, J., Pfeilstocker, M., Nosslinger, T., Hildebrandt, B., Kundgen, A., Lubbert, M., Kunzmann, R., Giagounidis, A. A., Aul, C., Trumper, L., Krieger, O., Stauder, R., Muller, T. H., Wimazal, F., Valent, P., Fonatsch, C., Steidl, C. (2007). New insights into the prognostic impact of the karyotype in MDS and correlation with subtypes: evidence from a core dataset of 2124 patients. Blood 110, 4385-4395.

34. Haferlach, T., Nagata, Y., Grossmann, V., Okuno, Y., Bacher, U., Nagae, G., Schnittger, S., Sanada, M., Kon, A., Alpermann, T., Yoshida, K., Roller, A., Nadarajah, N., Shiraishi, Y., Shiozawa, Y., Chiba, K., Tanaka, H., Koeffler, H. P., Klein, H. U., Dugas, M., Aburatani, H., Kohlmann, A., Miyano, S., Haferlach, C., Kern, W., Ogawa, S. (2014). Landscape of genetic lesions in 944 patients with myelodysplastic syndromes. Leukemia 28, 241-247.

35. Heinrichs, S., Conover, L. F., Bueso-Ramos, C. E., Kilpivaara, O., Stevenson, K., Neuberg, D., Loh, M. L., Wu, W. S., Rodig, S. J., Garcia-Manero, G., Kantarjian, H. M., Look, A. T. (2013). MYBL2 is a sub-haploinsufficient tumor suppressor gene in myeloid malignancy. Elife 2, e00825.

36. Heinrichs, S., Kulkarni, R. V., Bueso-Ramos, C. E., Levine, R. L., Loh, M. L., Li, C., Neuberg, D., Kornblau, S. M., Issa, J. P., Gilliland, D. G., Garcia-Manero, G., Kantarjian, H. M., Estey, E. H., Look, A. T. (2009). Accurate detection of uniparental disomy and microdeletions by SNP array analysis in myelodysplastic syndromes with normal cytogenetics. Leukemia 23, 1605-1613.

37. Hochedlinger, K., Yamada, Y., Beard, C., Jaenisch, R. (2005). Ectopic expression of Oct-4 blocks progenitor-cell differentiation and causes dysplasia in epithelial tissues. Cell 121, 465-477.

38. Huh, J., Tiu, R. V., Gondek, L. P., O'Keefe, C. L., Jasek, M., Makishima, H., Jankowska, A. M., Jiang, Y., Verma, A., Theil, K. S., McDevitt, M. A., Maciejewski, J. P. (2010). Characterization of chromosome arm 20q abnormalities in myeloid malignancies using genome-wide single nucleotide polymorphism array analysis. Genes Chromosomes Cancer 49, 390-399.

39. Jackson, A. L., Bartz, S. R., Schelter, J., Kobayashi, S. V., Burchard, J., Mao, M., Li, B., Cavet, G., Linsley, P. S. (2003). Expression profiling reveals off-target gene regulation by RNAi. Nat Biotechnol 21, 635-637.

40. Joaquin, M., Watson, R. J. (2003). Cell cycle regulation by the B-Myb transcription factor. Cell Mol Life Sci 60, 2389-2401.

41. Jovic, D., Sakaue-Sawano, A., Abe, T., Cho, C. S., Nagaoka, M., Miyawaki, A., Akaike, T. (2013). Direct observation of cell cycle progression in living mouse embryonic stem cells on an extracellular matrix of E-cadherin. Springerplus 2, 585.

42. Karasawa, S., Araki, T., Yamamoto-Hino, M.,Miyawaki, A. (2003). A green-emitting fluorescent protein from Galaxeidae coral and its monomeric version for use in fluorescent labeling. J Biol Chem 278, 34167-34171.

43. Knudson, A. G., Jr. (1971). Mutation and cancer: statistical study of retinoblastoma. Proc Natl Acad Sci U S A 68, 820-823.

44. Koh, S. B., Mascalchi, P., Rodriguez, E., Lin, Y., Jodrell, D. I., Richards, F. M., Lyons, S. K. (2017). A quantitative FastFUCCI assay defines cell cycle dynamics at a single-cell level. J Cell Sci 130, 512-520.

45. Kronke, J., Fink, E. C., Hollenbach, P. W., MacBeth, K. J., Hurst, S. N., Udeshi, N. D., Chamberlain, P. P., Mani, D. R., Man, H. W., Gandhi, A. K., Svinkina, T., Schneider, R. K., McConkey, M., Jaras, M., Griffiths, E., Wetzler, M., Bullinger, L., Cathers, B. E., Carr, S. A., Chopra, R., Ebert, B. L. (2015). Lenalidomide induces ubiquitination and degradation of CK1alpha in del(5q) MDS. Nature 523, 183-188.

46. Lam, E. W., Bennett, J. D., Watson, R. J. (1995). Cell-cycle regulation of human B-myb transcription. Gene 160, 277-281.

47. Lam, E. W., Robinson, C., Watson, R. J. (1992). Characterization and cell cycle-regulated expression of mouse B-myb. Oncogene 7, 1885-1890.

48. Li, C., Zhang, Y., Yang, Q., Ye, F., Sun, S. Y., Chen, E. S., Liou, Y. C. (2016). NuSAP modulates the dynamics of kinetochore microtubules by attenuating MCAK depolymerisation activity. Sci Rep 6, 18773.

49. Liew, E., Owen, C. (2011). Familial myelodysplastic syndromes: a review of the literature. Haematologica 96, 1536-1542.

50. Lim, L. P., Lau, N. C., Garrett-Engele, P., Grimson, A., Schelter, J. M., Castle, J., Bartel, D. P., Linsley, P. S., Johnson, J. M. (2005). Microarray analysis shows that some microRNAs downregulate large numbers of target mRNAs. Nature 433, 769-773.

51. Lin, J. J., Milhollen, M. A., Smith, P. G., Narayanan, U., Dutta, A. (2010). NEDD8-targeting drug MLN4924 elicits DNA rereplication by stabilizing Cdt1 in S phase, triggering checkpoint activation, apoptosis, and senescence in cancer cells. Cancer Res 70, 10310-10320.

52. Lindsley, R. C., Ebert, B. L. (2013). Molecular pathophysiology of myelodysplastic syndromes. Annu Rev Pathol 8, 21-47.

53. List, A., Dewald, G., Bennett, J., Giagounidis, A., Raza, A., Feldman, E., Powell, B., Greenberg, P., Thomas, D., Stone, R., Reeder, C., Wride, K., Patin, J., Schmidt, M., Zeldis, J., Knight, R. (2006). Lenalidomide in the myelodysplastic syndrome with chromosome 5q deletion. N Engl J Med 355, 1456-1465.

54. Litovchick, L., Sadasivam, S., Florens, L., Zhu, X., Swanson, S. K., Velmurugan, S., Chen, R., Washburn, M. P., Liu, X. S., DeCaprio, J. A. (2007). Evolutionarily conserved multisubunit RBL2/p130 and E2F4 protein complex represses human cell cycle-dependent genes in quiescence. Mol Cell 26, 539-551.

55. Lynch, C. J., Milner, J. (2006). Loss of one p53 allele results in four-fold reduction of p53 mRNA and protein: a basis for p53 haplo-insufficiency. Oncogene 25, 3463-3470.

56. Ma, X., Does, M., Raza, A., Mayne, S. T. (2007). Myelodysplastic syndromes: incidence and survival in the United States. Cancer 109, 1536-1542.

57. Malcovati, L., Papaemmanuil, E., Bowen, D. T., Boultwood, J., Della Porta, M. G., Pascutto, C., Travaglino, E., Groves, M. J., Godfrey, A. L., Ambaglio, I., Galli, A., Da Via, M. C., Conte, S., Tauro, S., Keenan, N., Hyslop, A., Hinton, J., Mudie, L. J., Wainscoat, J. S., Futreal, P. A., Stratton, M. R., Campbell, P. J., Hellstrom-Lindberg, E., Cazzola, M. (2011). Clinical significance of SF3B1 mutations in myelodysplastic syndromes and myelodysplastic/myeloproliferative neoplasms. Blood 118, 6239-6246.

58. Mort, R. L., Ford, M. J., Sakaue-Sawano, A., Lindstrom, N. O., Casadio, A., Douglas, A. T., Keighren, M. A., Hohenstein, P., Miyawaki, A., Jackson, I. J. (2014). Fucci2a: a bicistronic cell cycle reporter that allows Cre mediated tissue specific expression in mice. Cell Cycle 13, 2681-2696.

59. Mullighan, C. G., Goorha, S., Radtke, I., Miller, C. B., Coustan-Smith, E., Dalton, J. D., Girtman, K., Mathew, S., Ma, J., Pounds, S. B., Su, X., Pui, C. H., Relling, M. V., Evans, W. E., Shurtleff, S. A., Downing, J. R. (2007). Genome-wide analysis of genetic alterations in acute lymphoblastic leukaemia. Nature 446, 758-764.

60. Nagai, T., Ibata, K., Park, E. S., Kubota, M., Mikoshiba, K., Miyawaki, A. (2002). A variant of yellow fluorescent protein with fast and efficient maturation for cell-biological applications. Nat Biotechnol 20, 87-90.

61. Nakayama, K. I., Nakayama, K. (2006). Ubiquitin ligases: cell-cycle control and cancer. Nat Rev Cancer 6, 369-381.

62. Neukirchen, J., Schoonen, W. M., Strupp, C., Gattermann, N., Aul, C., Haas, R., Germing, U. (2011). Incidence and prevalence of myelodysplastic syndromes: data from the Dusseldorf MDS-registry. Leuk Res 35, 1591-1596.

63. Nishitani, H., Lygerou, Z., Nishimoto, T. (2004). Proteolysis of DNA replication licensing factor Cdt1 in S-phase is performed independently of geminin through its N-terminal region. J Biol Chem 279, 30807-30816.

64. Nishitani, H., Lygerou, Z., Nishimoto, T., Nurse, P. (2000). The Cdt1 protein is required to license DNA for replication in fission yeast. Nature 404, 625-628.

65. Nomura, N., Takahashi, M., Matsui, M., Ishii, S., Date, T., Sasamoto, S., Ishizaki, R. (1988). Isolation of human cDNA clones of myb-related genes, A-myb and B-myb. Nucleic Acids Res 16, 11075-11089.

66. Papaemmanuil, E., Gerstung, M., Malcovati, L., Tauro, S., Gundem, G., Van Loo, P., Yoon, C. J., Ellis, P., Wedge, D. C., Pellagatti, A., Shlien, A., Groves, M. J., Forbes, S. A., Raine, K., Hinton, J., Mudie, L. J., McLaren, S., Hardy, C., Latimer, C., Della Porta, M. G., O'Meara, S., Ambaglio, I., Galli, A., Butler, A. P., Walldin, G., Teague, J. W., Quek, L., Sternberg, A., Gambacorti-Passerini, C., Cross, N. C., Green, A. R., Boultwood, J., Vyas, P., Hellstrom-Lindberg, E., Bowen, D., Cazzola, M., Stratton, M. R., Campbell, P. J. (2013). Clinical and biological implications of driver mutations in myelodysplastic syndromes. Blood 122, 3616-3627; quiz 3699.

67. Robinson, C., Light, Y., Groves, R., Mann, D., Marias, R., Watson, R. (1996). Cell-cycle regulation of B-Myb protein expression: specific phosphorylation during the S phase of the cell cycle. Oncogene 12, 1855-1864.

68. Rosenbauer, F., Wagner, K., Kutok, J. L., Iwasaki, H., Le Beau, M. M., Okuno, Y., Akashi, K., Fiering, S., Tenen, D. G. (2004). Acute myeloid leukemia induced by graded reduction of a lineage-specific transcription factor, PU.1. Nat Genet 36, 624-630.

69. Sadasivam, S., Duan, S., DeCaprio, J. A. (2012). The MuvB complex sequentially recruits B-Myb and FoxM1 to promote mitotic gene expression. Genes Dev 26, 474-489.

70. Sakaue-Sawano, A., Hoshida, T., Yo, M., Takahashi, R., Ohtawa, K., Arai, T., Takahashi, E., Noda, S., Miyoshi, H., Miyawaki, A. (2013). Visualizing developmentally programmed endoreplication in mammals using ubiquitin oscillators. Development 140, 4624-4632.

71. Sakaue-Sawano, A., Kobayashi, T., Ohtawa, K., Miyawaki, A. (2011). Drug-induced cell cycle modulation leading to cell-cycle arrest, nuclear mis-segregation, or endoreplication. BMC Cell Biol 12, 2.

72. Sakaue-Sawano, A., Kurokawa, H., Morimura, T., Hanyu, A., Hama, H., Osawa, H., Kashiwagi, S., Fukami, K., Miyata, T., Miyoshi, H., Imamura, T., Ogawa, M., Masai, H., Miyawaki, A. (2008). Visualizing spatiotemporal dynamics of multicellular cell-cycle progression. Cell 132, 487-498.

73. Schanz, J., Tuchler, H., Sole, F., Mallo, M., Luno, E., Cervera, J., Granada, I., Hildebrandt, B., Slovak, M. L., Ohyashiki, K., Steidl, C., Fonatsch, C., Pfeilstocker, M., Nosslinger, T., Valent, P., Giagounidis, A., Aul, C., Lubbert, M., Stauder, R., Krieger, O., Garcia-Manero, G., Faderl, S., Pierce, S., Le Beau, M. M., Bennett, J. M., Greenberg, P., Germing, U., Haase, D. (2012). New comprehensive cytogenetic scoring system for primary myelodysplastic syndromes (MDS) and oligoblastic acute myeloid leukemia after MDS derived from an international database merge. J Clin Oncol 30, 820-829.

74. Shand, F. H., Ueha, S., Otsuji, M., Koid, S. S., Shichino, S., Tsukui, T., Kosugi-Kanaya, M., Abe, J., Tomura, M., Ziogas, J., Matsushima, K. (2014). Tracking of intertissue migration reveals the origins of tumor-infiltrating monocytes. Proc Natl Acad Sci U S A 111, 7771-7776.

75. Shaner, N. C., Campbell, R. E., Steinbach, P. A., Giepmans, B. N., Palmer, A. E., Tsien, R. Y. (2004). Improved monomeric red, orange and yellow fluorescent proteins derived from Discosoma sp. red fluorescent protein. Nat Biotechnol 22, 1567-1572.

76. Shepard, J. L., Amatruda, J. F., Stern, H. M., Subramanian, A., Finkelstein, D., Ziai, J., Finley, K. R., Pfaff, K. L., Hersey, C., Zhou, Y., Barut, B., Freedman, M., Lee, C., Spitsbergen, J., Neuberg, D., Weber, G., Golub, T. R., Glickman, J. N., Kutok, J. L., Aster, J. C., Zon, L. I. (2005). A zebrafish bmyb mutation causes genome instability and increased cancer susceptibility. Proc Natl Acad Sci U S A 102, 13194-13199.

77. Song, W. J., Sullivan, M. G., Legare, R. D., Hutchings, S., Tan, X., Kufrin, D., Ratajczak, J., Resende, I. C., Haworth, C., Hock, R., Loh, M., Felix, C., Roy, D. C., Busque, L., Kurnit, D., Willman, C., Gewirtz, A. M., Speck, N. A., Bushweller, J. H., Li, F. P., Gardiner, K., Poncz, M., Maris, J. M., Gilliland, D. G. (1999). Haploinsufficiency of CBFA2 causes familial thrombocytopenia with propensity to develop acute myelogenous leukaemia. Nat Genet 23, 166-175.

78. Sperling, A. S., Gibson, C. J., Ebert, B. L. (2016). The genetics of myelodysplastic syndrome: from clonal haematopoiesis to secondary leukaemia. Nat Rev Cancer

79. Steensma, D. P., Bejar, R., Jaiswal, S., Lindsley, R. C., Sekeres, M. A., Hasserjian, R. P., Ebert, B. L. (2015). Clonal hematopoiesis of indeterminate potential and its distinction from myelodysplastic syndromes. Blood 126, 9-16.

80. Strack, R. L., Strongin, D. E., Bhattacharyya, D., Tao, W., Berman, A., Broxmeyer, H. E., Keenan, R. J., Glick, B. S. (2008). A noncytotoxic DsRed variant for whole-cell labeling. Nat Methods 5, 955-957.

81. Subach, O. M., Cranfill, P. J., Davidson, M. W., Verkhusha, V. V. (2011). An enhanced monomeric blue fluorescent protein with the high chemical stability of the chromophore. PLoS One 6, e28674.

82. Sugiyama, M., Sakaue-Sawano, A., Iimura, T., Fukami, K., Kitaguchi, T., Kawakami, K., Okamoto, H., Higashijima, S., Miyawaki, A. (2009). Illuminating cell-cycle progression in the developing zebrafish embryo. Proc Natl Acad Sci U S A 106, 20812-20817.

83. Takahashi, Y., Rayman, J. B., Dynlacht, B. D. (2000). Analysis of promoter binding by the E2F and pRB families in vivo: distinct E2F proteins mediate activation and repression. Genes Dev 14, 804-816.

84. Tanaka, Y., Patestos, N. P., Maekawa, T., Ishii, S. (1999). B-myb is required for inner cell mass formation at an early stage of development. J Biol Chem 274, 28067-28070.

85. Thorner, A. R., Hoadley, K. A., Parker, J. S., Winkel, S., Millikan, R. C., Perou, C. M. (2009). In vitro and in vivo analysis of B-Myb in basal-like breast cancer. Oncogene 28, 742-751.

86. Tiu, R. V., Gondek, L. P., O'Keefe, C. L., Elson, P., Huh, J., Mohamedali, A., Kulasekararaj, A., Advani, A. S., Paquette, R., List, A. F., Sekeres, M. A., McDevitt, M. A., Mufti, G. J., Maciejewski, J. P. (2011). Prognostic impact of SNP array karyotyping in myelodysplastic syndromes and related myeloid malignancies. Blood 117, 4552-4560.

87. Tomura, M., Sakaue-Sawano, A., Mori, Y., Takase-Utsugi, M., Hata, A., Ohtawa, K., Kanagawa, O., Miyawaki, A. (2013). Contrasting quiescent G0 phase with mitotic cell cycling in the mouse immune system. PLoS One 8, e73801.

88. Trauth, K., Mutschler, B., Jenkins, N. A., Gilbert, D. J., Copeland, N. G., Klempnauer, K. H. (1994). Mouse A-myb encodes a trans-activator and is expressed in mitotically active cells of the developing central nervous system, adult testis and B lymphocytes. Embo j 13, 5994-6005.

89. Tsai, S., Bartelmez, S., Sitnicka, E., Collins, S. (1994). Lymphohematopoietic progenitors immortalized by a retroviral vector harboring a dominant-negative retinoic acid receptor can recapitulate lymphoid, myeloid, and erythroid development. Genes Dev 8, 2831-2841.

90. Tsuzuki, S., Seto, M. (2012). Expansion of functionally defined mouse hematopoietic stem and progenitor cells by a short isoform of RUNX1/AML1. Blood 119, 727-735.

91. Urlinger, S., Baron, U., Thellmann, M., Hasan, M. T., Bujard, H., Hillen, W. (2000). Exploring the sequence space for tetracycline-dependent transcriptional activators: novel mutations yield expanded range and sensitivity. Proc Natl Acad Sci U S A 97, 7963-7968.

92. Van den Berghe, H., Cassiman, J. J., David, G., Fryns, J. P., Michaux, J. L., Sokal, G. (1974). Distinct haematological disorder with deletion of long arm of no. 5 chromosome. Nature 251, 437-438.

93. Vardiman, J. W., Thiele, J., Arber, D. A., Brunning, R. D., Borowitz, M. J., Porwit, A., Harris, N. L., Le Beau, M. M., Hellstrom-Lindberg, E., Tefferi, A., Bloomfield, C. D. (2009). The 2008 revision of the World Health Organization (WHO) classification of myeloid neoplasms and acute leukemia: rationale and important changes. Blood 114, 937-951.

94. Vaziri, C., Saxena, S., Jeon, Y., Lee, C., Murata, K., Machida, Y., Wagle, N., Hwang, D. S., Dutta, A. (2003). A p53-dependent checkpoint pathway prevents rereplication. Mol Cell 11, 997-1008.

95. Werwein, E., Schmedt, T., Hoffmann, H., Usadel, C., Obermann, N., Singer, J. D., Klempnauer, K. H. (2012). B-Myb promotes S-phase independently of its sequence-specific DNA binding activity and interacts with polymerase delta-interacting protein 1 (Pdip1). Cell Cycle 11, 4047-4058.

96. Westin, E. H., Gallo, R. C., Arya, S. K., Eva, A., Souza, L. M., Baluda, M. A., Aaronson, S. A., Wong-Staal, F. (1982). Differential expression of the amv gene in human hematopoietic cells. Proc Natl Acad Sci U S A 79, 2194-2198.

97. Yamauchi, T., Ishidao, T., Nomura, T., Shinagawa, T., Tanaka, Y., Yonemura, S., Ishii, S. (2008). A B-Myb complex containing clathrin and filamin is required for mitotic spindle function. Embo j 27, 1852-1862.

98. Yo, M., Sakaue-Sawano, A., Noda, S., Miyawaki, A., Miyoshi, H. (2014). Fucci-guided purification of hematopoietic stem cells with high repopulating activity. Biochem Biophys Res Commun

99. Zhu, W., Giangrande, P. H., Nevins, J. R. (2004). E2Fs link the control of G1/S and G2/M transcription. The EMBO journal 23, 4615-4626.

100. Zielke, N., Korzelius, J., van Straaten, M., Bender, K., Schuhknecht, G. F., Dutta, D., Xiang, J., Edgar, B. A. (2014). Fly-FUCCI: A versatile tool for studying cell proliferation in complex tissues. Cell Rep 7, 588-598.

Appendix

Table of Figures

Oligonucleotides

QRT-PCR oligonucleotides:

Oligoname	Sequence (5' to 3')
Ccnb1-FW1	TGCAGTGAGTGACGTAGACGCAGAT
Ccnb1-RV1	CCAGTCACTTCACGACCCTGTAGGT
Ccne1-FW1	AGGAAGGCAAATGTGGCCGTGTT
Ccne1-RV1	TGAAAGAGCAGGGGTCCACGCAT
Dhfr-FW1	ACCAGGCCACCTCAGACTCTTTGT
Dhfr-RV1	ACCTCAGAGAGGACGCCTGGGTAT
E2f1-FW1	GATGCCCACCTGTCTGCAGCTTT
E2f1-RV1	ATGTGGCAGCAACCAAACCCCAG
Foxm1-FW1	AGCTAAGGGTGTGCCTGTTCCCA
Foxm1-RV1	TGGTTAAGCTGTTGTCCAGCGTGC
hPGKpro-FW1	GCACATTCTTCACGTCCGTTC
hPGKpro-RV1	CAAGGAACCTTCCCGACTTAGG
Mybl2-FW1	ATCCACTCCAGTGTGTAGCCAAA
Mybl2-RV1	CCATGGAGTACTTCTGATCTGGG
Mybl2-FW6	TGGGTACAGCTTTGCCCTGTGAGT
Mybl2-RV6	GGCCCAAGCCAAGTGCGTTATGA
Ubql1-FW1	GCACCTAGCACTGCACCTAGTGA
Ubql1-RV1	TGAAATCTGACTTCTGGACTCTGC
Vps39-FW1	GAGGAGAAGGTGTGCATGGTATG
Vps39-RV1	GGTGTCGGCTGAGTTTACCTCTT
Ywhaz-FW1	TGAAGAGTCGTACAAAGACAGCACGC
Ywhaz-RV1	CAGACAAAGGTTGGAAGGCCGGT

PCR oligonucleotides:

Oligoname	Sequence (5‘ to 3‘)
C-CDT1-FW1	TCCATCACACTGGCGGCCGCTCGAGCCCAGCCCCGCCAGGCCCG
C-CDT1-FW2	GGACGAGCTGTACAAGGGCGGAGGACCCAGCCCCGCCAGGCCC
C-CDT1-FW3	CCACCACCTGTTCCAGGGCGGAGGACCCAGCCCCGCCAGGCCCG
C-CDT1-FW4	GGATCTAGGGGCGGAGGACCCAGCCCCGCCAGGCCCG
C-CDT1-RV1	CCGATACGCGTTTAGATGGTGTCCTGGTCCTGC
C-Fucci2-FW1	GGCATGGACGAGCTGTACAAGGGATATCCATCACACTGGCGGCC
C-GMNN-FW1	TCCATCACACTGGCGGCCGCTCGAGATGAATCCCAGTATGAAGCAG AAACAA
C-GMNN-FW2	GGACGAGCTGTACAAGGGCGGAGGAAATCCCAGTATGAAGCAGAA ACAAGAA
C-GMNN-RV1	CCGATGGTACCTTACAGCGCCTTTCTCCGTTTTTCTGC
C-mCherry-FW1	CGCTGGAATTCGCCACCATGGTGAGCAAGGGCGAGGA
C-mCherry-RV1	CTTGTACAGCTCGTCCATGC
C-RFP-FW1	CGCTGGAATTCGCCACCATGGATAGCACTGAGAACGTCAT
C-RFP-RV1	CCCGCCACCACCTGTTCCAG
C-Venus-FW1	CGCTGGGATCCGCCACCATGGTGAGCAAGGGCGAGGA
C-Venus-RV1	CTTGTACAGCTCGTCCATGCC
mTurquoise2 FW1	CGCTGTCTAGAGCCACCATGGTGAGCAAGGGCGAGGA
mTurquoise2 RV1	GGGATCCACCGGATCTAGGGGCGGAGGA

Abbreviations

ACK	Ammonium-Chloride-Potassium
AML	Acute myeloid leukemia
Aspm	Abnormal spindle microtubule assembly
ATP	Adenosine triphosphate
BFP	Blue fluorescent protein
bp	base pair
BSA	Bovine serum albumin
CA	California
$CaCl_2$	Calcium chloride
Ccnb1	Cyclin B1
Ccne1	Cyclin E1
CD	Cluster of differentiation
CDK	Cyclin-dependent kinase
cDNA	Complementary desoxyribonucleic acid
CDR	Common deleted region
CDS	Coding sequence
Cdt1	Chromatin licensing and DNA replication factor 1
CHIP	Clonal hematopoiesis of indeterminate potential
CK1α	Casein kinase 1α
CKI	Cyclin-dependent kinase inhibitor
cm	centimeter
CMV	Cytomegalovirus
CRBN	Cereblon
Ctrl.	Control

d	days
del	deletion
Dhfr	dihydrofolate reductase
DMEM	Dulbecco's modified Eagle medium
DMSO	Dimethylsulfoxide
DNA	Desoxyribonecleic acid
dNTP	Desoxyribonukleosidtriphosphates
Dox	Doxycycline
DPBS	Dulbecco’s Phosphate-Buffered Saline
e.g.	exempli gratia
E2f1	E2F transcription factor 1
EDTA	Ethylenediaminetetraacetic acid
et al.	et alia
etc.	et cetera
FAB	French-American-British
FACS	Fluorescence activated cell sorting
FBS	Fetal bovine serum
FITC	Fluoreszeinisothiocyanat
Foxm1	Forkhead box M1
FSC	forward scatter
FW	Forward (primer)
g	gravity/gramms
GFP	green fluorescent protein
Gmnn/GMNN	Geminin
h	hours
HCl	Hydrogen chloride
HEPES	4-(2-hydroxyethyl)-1-piperazineethanesulfnic acid
HIV-1	Human immunodeficiency Virus-1
hPGK	human phosphoglycerate kinase (promoter)
HSC	hematopoietic stem cell
HSCT	hematopoietic stem cell transplantation
HSPC	hematopoietic stem and progenitor cell
i.e.	id est
IL-3	Interleukin 3
IMDM	Iscove’s modified Dulbecco’s Medium
Inc.	Incorporated
IPSS	International prognostic scoring system
IPSS-R	Revised International prognostic scoring system
kb	kilobase
LB	Lysogeny broth
lin.- neg.	lineage - negative
M/mM	Molar/millimolar
MA	Massachusetts
MACS	Magnetic activated cell sorting
MDS	Myelodysplastic syndromes
mFlt3 ligand	murine Fms-like tyrosine kinase 3 ligand
mg	milligram
Mg^{2+}	Magnesium
MgCl	Magnesium chloride
MGUS	monoclonal gammopathy of undetermined
min	minute
miRNA	microRNA
ml	milliliter
MO	Missouri
MPN	Myeloproliferative neoplasm
mRNA	messenger ribonucleic acid
MSC	Myelodysplastic stem cell
mScf	murine stem cell factor

mTpo	murine thrombopoietin
Myb	myeloblastosis oncogene
Mybl1	MYB like 1
Mybl2	MYB like 2
NaCl	Sodium chloride
ng/nm	nanogram/ nanometer
Nusap1	Nucleolar and spindle associated protein 1
O_2	Oxygen
PBS	Phosphate-bufered saline
PCR	Polymerase chain reaction
PE	R-Phycoerythrin
Pen/Strep	Penicillin/Streptomycin
PI	Propidium iodide
Pmin	minimal promoter
QPCR	Quantitative PCR
QRT-PCR	Quantitative Reverse Transcription PCR
RB1	RB transcriptional corepressor 1
rel.	relative
RFP	Red fluorescent protein
RNA	Ribonucleic acid
RNAi	RNA interference
rpm	rounds per minute
RPMI	Roswell Park Memorial Institute (medium)
RT	Reverse transcriptase
rtTA	reverse tetracycline-controlled transactivator
RUNX1	Runt related transcription factor 1
RV	reverse (primer)
sAML	secondary AML
Scf	Stem cell factor
SDS	Sodium Dodecyl Sulfate
sec	seconds
SFFV	Speen focus-forming virus
shRNA	short hairpin RNA
siRNA	small interfering RNA
SNP	Single Nucleotide Polymorphism
SSC	side scatter
St.	Saint
TAE	Tris-Acetat-EDTA
TBS-T	Tris-Buffered Saline-Tween 20
Tet	Tetracycline
TetO	Tet Operator
tMDS	therapy-related MDS
TP53	Tumor protein 53
Tq	mTurquoise2
Tris	Tris(hydroxymethyl)aminomethane
Tris-Cl	Tris-Chloride
U	Unit
Ubqln1	Ubiquilin1
USA	United States of America
UTR	untranslated region
UV	Ultra violet
V	Volt
WHO	World Health Organization
WI	Wisconsin
°C	Degree Celsius
µg/µm/µM/µl	microgram/ micrometer/micromolar/ microliter/
%	Percent
3‘/ 5‘	3 prime/ 5 prime (UTR)

Note of thanks

Foremost, I owe great thanks to my supervisor Dr. Stefan Heinrichs for his constant support, his patience and the knowledge he shared through the past 4 years. Stefan is one of the best teachers I know and I am thankful for his advice and encouragement through all issues in research and writing. I am sure to remember what I learned from his experience in research for life.

Also, I want to thank Prof. Dr. Horn for giving me the opportunity to perform my project at his institute. I am very grateful for his constant interest, encouragement and feedback in my work.

My participation in the ELAN graduation college and the BIOME graduation college has been of great value to my personal development as a researcher. Thus, here is the place to say thank you to all the persons involved and to the Else-Kröner Fresenius Stiftung for their highly appreciated financial support of ELAN enabling me to take off time from studying to focus on my experiments in the laboratory.

I want to say “Thank you!” to all the current and former members of the Heinrichs Lab that participated in and supported my work through the past years. A special thank you goes to Antje for being an encouraging laboratory companion with great advice, and for becoming a friend.

In addition, I want to thank all the other current and former members of the Institute for Transfusion Medicine at the University Hospital Essen. You were wonderful to me. There was always a helping hand and mental support when needed.

A very important “Thank you!” goes to my family. My boyfriend, Patrick, was the rock I could lean on constantly. He encouraged me when I most needed it and gave me some free time in between to get my mind off the thesis. The same is true for my parents. Their unwavering support and advice was and still is of great value to me. If it was not for those three, I would not be where I am today. I love you all. At last, but not least, I want to acknowledge my grandparents for their constant support, as well. All of them just knew I could achieve what I aimed for.
It is more than I could ever dream of, to have a loving family that always has my back. Without doubt, I would not have been able to achieve this without any of you.

Curriculum Vitae

„Der Lebenslauf ist in der Online-Version aus Gründen des Datenschutzes nicht enthalten.**"**